Characterization of the Interactions of the Bacterial Cell Division Regulator MinE

Fatima Hafizi

Thesis Submitted to
The Faculty of Graduate and Postdoctoral Studies
In partial fulfillment of the requirements for the degree of
M.Sc. in Biochemistry

uOttawa

Department of Biochemistry, Microbiology and Immunology
Faculty of Medicine
University of Ottawa

Drop by drop you will have a sea….

Abstract

Symmetric cell division in gram-negative bacteria is essential for generating two equal-sized daughter cells, each containing cellular material crucial for growth and future replication. The Min system, comprised of proteins MinC, MinD and MinE, is particularly important for this process since its deletion leads to minicells incapable of further replication. This thesis focuses on the interactions involving MinE that are important for allowing cell division at the mid-cell and for directing the dynamic localization of MinD that is observed in vivo. Previous experiments have shown that the MinE protein contains an N-terminal region that is required to stimulate MinD-catalyzed ATP hydrolysis in the Min protein interaction cycle. However, MinD-binding residues in MinE identified by in vitro MinD ATPase assays were subsequently found to be buried in the hydrophobic dimeric interface in the MinE structure, raising the possibility that these residues are not directly involved in the interaction. To address this issue, the ability of N-terminal MinE peptides to stimulate MinD activity was studied to determine the role of these residues in MinD activation. Our results implied that MinE likely undergoes a change in conformation or oligomerization state before binding MinD. In addition we performed circular dichroism spectroscopy of MinE. The data suggest that direct interactions between MinE and the lipid membrane can lead to conformational changes in MinE. Using NMR spectroscopy in an attempt to observe this structure change, different membrane-mimetic environments were tested. However the results strongly suggest that structural studies on the membrane-bound state of MinE will pose significant challenges. Taken together, the results in this thesis open the door for further exploration of the interactions involving MinE in order to gain a better understanding of the dynamic localization patterns formed by these proteins in vivo.

Acknowledgements

First and foremost I would like to thank Dr.Natalie Goto for her constant support and advice. It has been an honour working with her and having her guidance and encouragement throughout the years. There has been much I have learned which would not have been possible without her. Thank you for all your help in making the completion of this thesis possible. Your efforts and feedback are greatly appreciated.

It has been an enjoyable experience working in the Goto lab and having the opportunity to meet such wonderful people. I would like to thank Dr.Allison Sherrat, Dr.Houman Ghasriani, and Cheryl Mcdowell for all their help and suggestions. Thank you, Saud Ayed and Laura Mcleod for sharing your thoughts on Min and being such amazing colleagues. I would also like to thank Christopher Hart for his contribution in generating the ATPase assays which made this thesis possible. As well, I would like to acknowledge Saud for the improvements he made which have made the procedure less stressful. A special thanks goes to Tabussom Qureshi who helped me when I first started in the lab and has continued to be a support throughout the years. What can I say Tabs, the lab just wouldn't be complete without you!

Last but not least, a very special thanks to my family who have been a great source of support and encouragement always. Thank you, Mom and Dad for keeping my spirits up during the writing of this thesis. It is a long process, but much has been gained from it.

Table of Contents

List of Abbreviations

BCA	bicinchoninic acid
CHAPS	3-[(3-cholamidopropyl)dimethylammonio]-1-propanesulfonate
CD	circular dichroism
CMC	critical micelle concentration
DHPC(C6)	1,2-dihexanoyl-*sn*-glycero-3-phosphocholine
DHPC(C7)	1,2-diheptanoyl-*sn*-glycero-3-phosphocholine
DMPC	1,2-dimyristoyl-*sn*-glycero-3-phosphocholine
DOPC	1,2-dioleoyl-*sn*-glycero-3-phosphocholine
DOPG	1,2-dioleoyl-*sn*-glycero-3-[phosphor-*rac*-(1-glycerol)]
Ec	*Escherichia coli*
Fos-12	N-dodecylphosphocholine
Fos-16	N-hexadecylphosphocholine
Hp	*Helicobacter pylori*
HSQC	heteronuclear single quantum coherence
LB	luria-bertani
LMPC	1-myristoyl-2-hydroxy-*sn*-glycero-3-phosphocholine
LMPG	1-myristoyl-2-hydroxy-*sn*-glycero-3-[phopho-*rac*-(1-glycerol)]
Ng	*Neisseria gonorrhoeae*
NMR	nuclear magnetic resonance
OD	optical density
PAGE	polyacrylamide gel electrophoresis
SDS	sodium dodecyl sulfate

List of Figures

List of Tables

Chapter 1: Introduction

1.1 Bacterial Cell Division

Cytokinesis is a crucial phase of the cell cycle responsible for the partitioning of replicated cellular material to the two daughter cells through the action of the cell division septum (1). During septum formation, the cell membrane invaginates at mid-cell as new cell walls are formed to separate the daughter cells. The formation of the division septum is initiated on the surface of the bacterial inner membrane by the polymerization of a distant homologue of tubulin called FtsZ (2). This gives rise to a polymer that forms an annulus around the circumference of the cell, called the Z-ring, which also recruits other division proteins such as FtsK and ZapA (3,4). This polymer causes constriction of the cell membrane while new cell walls are built, until the daughter cells are pinched off to complete the process (1-4).

In bacteria, symmetric division of the parental cell is necessary to generate viable daughter cells that are also capable of replication. In gram-negative bacteria, the nucleoid occlusion system (5,6) as well as the Min system (7,8) are responsible for ensuring that cell division occurs only in the middle of the cell. In the nucleoid occlusion system, Z-ring assembly is blocked in the vicinity of the nucleoid. The nucleoid occlusion factor in *Escherichia coli* is SlmA, identified using fluorescence microscopy (9). It causes cell filamentation when overexpressed in vivo by preventing cell division through inhibition of FtsZ polymerization (9-11). However, even though the nucleoid occlusion factors can affect the positioning of the division septum, they do not seem to be as important in the control of symmetric cell division. In particular, *E.coli* cells with a *slmA* deletion (9) show similar morphology to wild type cells,

although SlmA may become important when DNA replication or segregation is abnormally regulated (9,12). Nonetheless, the Min system seems to be more crucial for symmetric division under regular growth conditions. Its deletion allows cell division to also occur in the polar regions, forming minicells which jeopardize the propagation of the population (6,12,13). Thus, knowledge regarding the mechanism through which the Min system allows symmetric cell division to occur is likely to be more important for future development of antibacterial drugs that could prevent cell division.

The Min system is composed of three proteins coded by the *minB* operon: MinC, MinD and MinE (14). While much is known about how MinC can inhibit cell division through interactions with MinD, with MinE counteracting this action (14-16), the molecular mechanism by which the Min system restricts localization of the cell division septum to the midcell region is not well understood. The research done in this thesis attempts to shed light on this question by characterizing interactions made by MinE that underpin Min system function.

1.2: Min Protein Interactions

Originally, it was thought that the localization of Min proteins was static (17,18), with MinE being concentrated at midcell and MinC and MinD at the cell poles to prevent cell division from occurring at these sites. However, subsequent experiments looking at the localization of Min proteins labeled with fluorescent tags showed that this model was incorrect (5,15,16,19). In fact, the Min proteins undergo a cycle of interactions on and off the membrane as outlined in Figure 1.1. In this cycle MinD is thought to exist in an ADP-bound form in the cytosol (20). Nucleotide exchange with ATP causes MinD to dimerize (21-23) and bind to the cell membrane

through its C-terminal amphipathic helix (24-26). In this form, MinD-ATP dimers can recruit MinC to the membrane to form the MinCD complex. MinC binds to the MinD dimer through its C-terminal domain and antagonizes FtsZ polymerization by inhibiting its assembly through the N-terminal domain of MinC (4,27-29). Counteracting this inhibition of cell division is the displacement of MinC by MinE binding to an overlapping site on MinD (30). MinE binding stimulates the hydrolysis of ATP by MinD, leading to dissociation of the complex from the membrane (30). This regenerates cytoplasmic MinE and ADP-bound MinD, allowing the cycle to begin again (31).

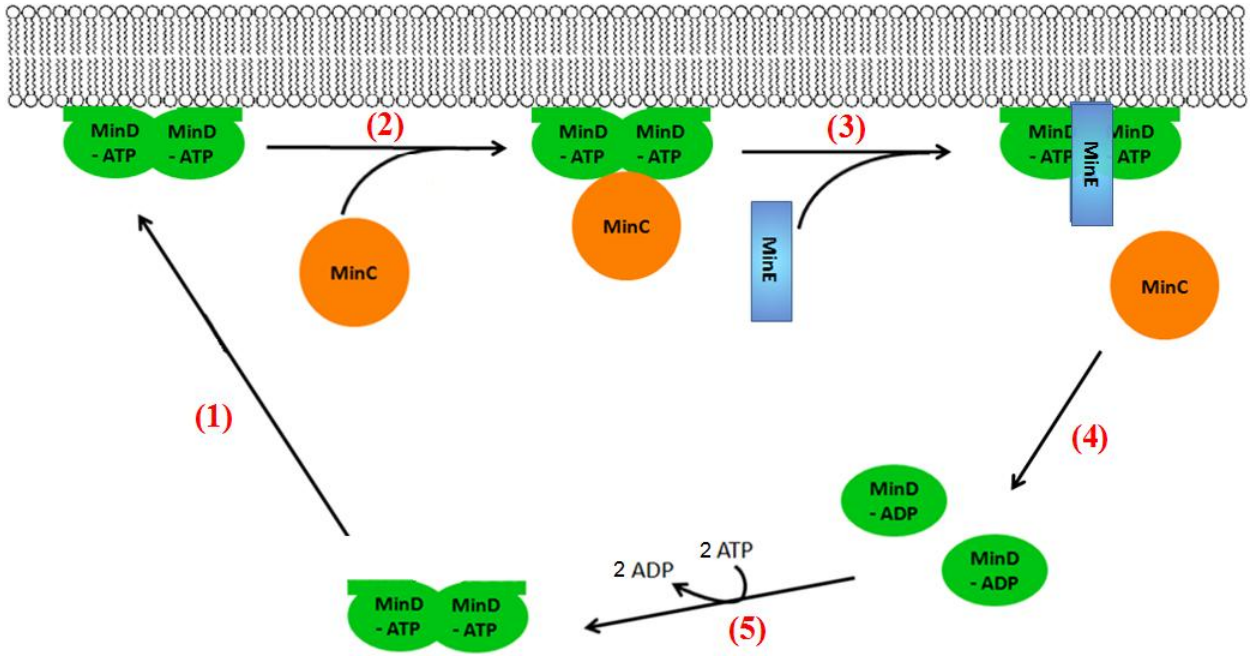

Figure 1.1: The Min Cycle of Interactions. (1) MinD-ATP dimers localize to the cell membrane. (2) In this state, it can recruit MinC, which then interferes with FtsZ polymerization, inhibiting formation of the cell division septum. (3) MinE displaces MinC and stimulates ATP hydrolysis by MinD. (4) This leads to dissociation of MinE from MinD, dissociation of the complex from the membrane, and regeneration of monomeric ADP-bound MinD. (5) Monomeric MinD-ADP then undergoes nucleotide exchange, whereupon it dimerizes and follows the cycle again.

Not only do the Min proteins cycle on and off the membrane, but they also oscillate between the cell poles. According to fluorescence microscopy studies of MinD in *E. coli*, the concentration of membrane-bound MinD increases at one cell pole, creating a region rich in MinCD complex that grows towards midcell (32). Subsequent deconvolution of these images showed that MinD actually forms coiled subcellular structures at the cell membrane (33). When followed over time, it was found that these structures tend to initiate at one cell pole, with the coil growing towards midcell. To counteract this, a high concentration of MinE adds onto the leading edge of this MinD subcellular structure, creating an annular structure called the E-ring (32,34). This E-ring seems to move along the Min polymer structure towards the cell pole, displacing MinC and causing the disassembly of MinD from the membrane (2,35). The liberated MinD can accumulate at the opposite side of the cell to form a new MinCD-rich zone on the membrane and allow the process to repeat itself at the new pole. The overall effect is an oscillation of Min proteins from pole to pole, giving rise to a higher time-averaged concentration of MinE in the mid-cell region, creating a zone that is permissive for cell division. Meanwhile a high time-averaged concentration of MinC and MinD at the cell poles is created, inhibiting cell division at these sites (36).

This dynamic self-organization of Min proteins has led many to wonder how these oscillations are controlled. Some of the first attempts to reconstruct oscillation *in silico* relied on simple reaction diffusion models (37-39). In this approach, variations in bulk diffusion properties caused by some molecular event (e.g. membrane binding), give rise to spatial heterogeneities in protein concentrations that follow defined patterns such as those seen in Min oscillation. However, more recent experiments with Min proteins labeled with fluorescent tags on a planar lipid bilayer in a flow cell showed dynamic pattern formation even when the concentration of

buffer components was maintained at a constant level (40,41). This suggested that Min protein oscillation is not a result of local heterogeneity in Min protein concentrations, but rather that a biochemical timing mechanism must be responsible for the patterns observed. Although no details regarding the nature of this putative biochemical timing mechanism have yet been described, potential candidates include Min protein polymerization, or ATP hydrolysis by MinD.

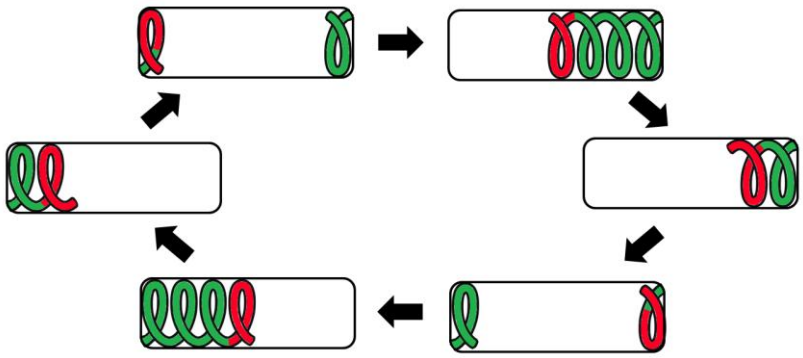

Figure 1.2: Schematic View of the Min Protein Oscillation Cycle in Rod-Shaped Bacteria. The MinCD complex forms a subcellular helical superstructure (green) that originates at the cell pole and grows toward the mid-cell. At this point, the E-ring forms along this structure, and drives disassembly of the MinCD complex from the membrane. The E-ring remains associated with the subcellular structure until it reaches the cell pole. A new subcellular structure can then grow at the opposite pole of the cell, allowing the cycle to repeat.

1.3: MinD Structure and Interactions with MinE

Structural and mutagenesis experiments have been performed in order to gain insight into the mechanism of interaction between MinE and MinD (42-45). Specifically, in order to understand how MinE binds MinD and stimulates the ATP hydrolysis event that drives the Min oscillation cycle, crystal structures had been resolved for MinD from some archaeal species, and more recently from *E. coli* (42-45). As expected from sequence homology, these structures show a high degree of similarity, with an α-β-α layered sandwich characteristic of all species of MinD

analyzed. Although most of the crystal structures were of the monomer form of MinD even when acquired in the presence of non-hydrolysable analogues of ATP (34), it was possible to obtain a structure for the dimer of *E. coli* MinD. This structure was obtained from a hydrolysis-deficient mutant of Ec-MinD (D40A) with the C-terminal amphipathic helix responsible for membrane binding also being omitted (45). Although ATPase activity was knocked out by elimination of the aspartic acid responsible for coordinating the incoming nucleophile (46), vesicle sedimentation studies on the full-length MinD mutant showed that interactions with both MinC and MinE were preserved (45), confirming the functional relevance of this structure.

The Ec-MinD crystal structure revealed the importance of ATP-binding for the dimerization of MinD. One molecule of ATP is bound to each subunit in a cleft located in the middle of the MinD dimeric interface, with each molecule of ATP participating in interactions involving both subunits of the dimer. For example, the side chain of Lys11 and backbone amide proton from Gly 12 interact with phosphate moieties of ATP bound to the cleft in the other subunit of the dimer (45). This is consistent with the observation that the K11A mutant of MinD was not able to self interact in yeast two-hybrid experiments, likely due to impaired ATP interactions across the dimer interface (47). This lysine residue is in fact part of the deviant Walker A motif (Fig.1.4) that characterizes the ParA family of ATPases to which MinD belongs (21,34). In this family, the side chain from the deviant lysine residue (K11 in Ec-MinD) interacts with ATP across the dimer interface, while the remainder of the Walker A motif forms a loop that interacts with phosphate groups from the ATP molecule bound within the same subunit. Dimer structures of other members of the ParA family, such as the NifH component of a bacterial nitrogen fixation system (48) and the plasmid portioning component Soj (46) have also shown similar interactions.

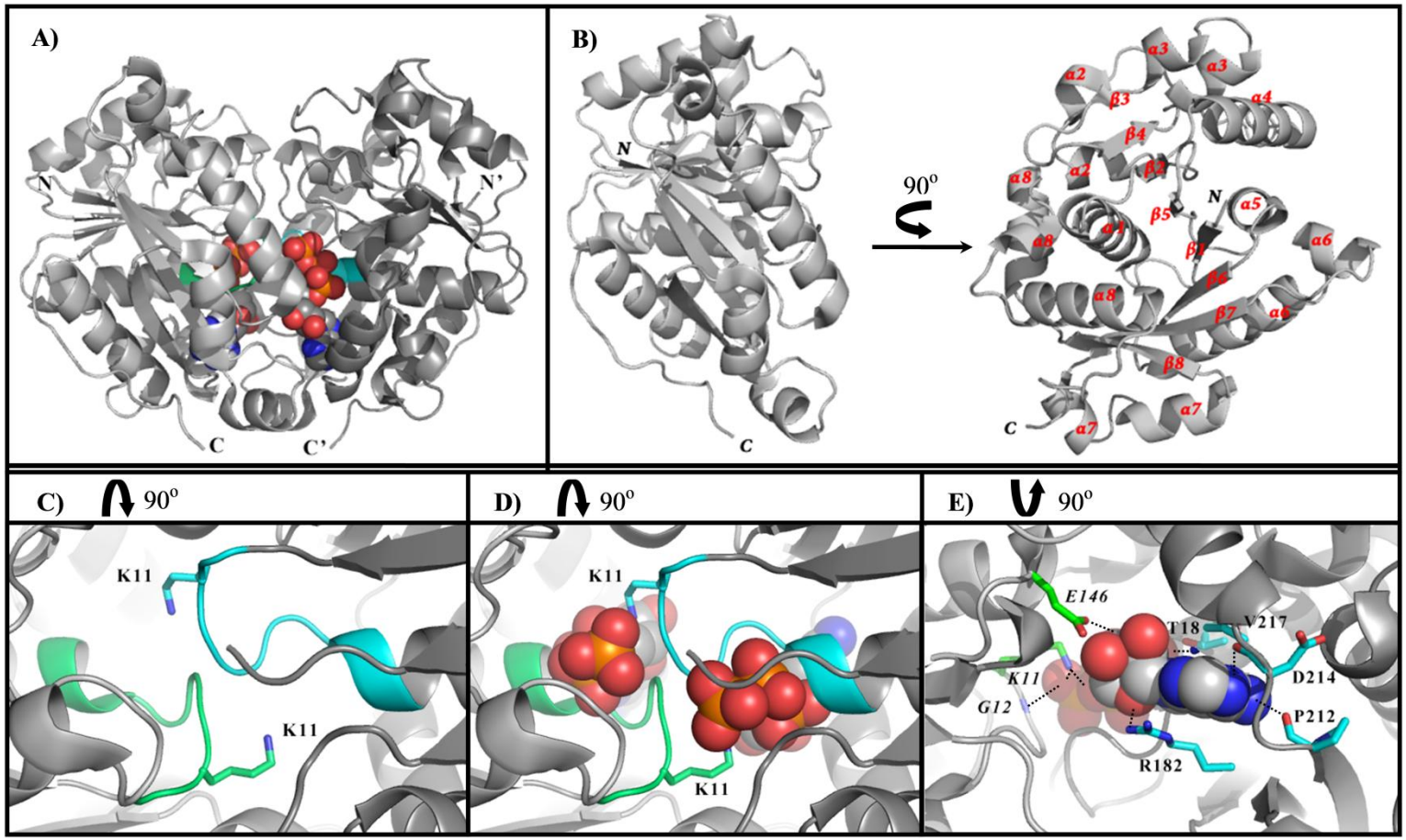

Figure 1.3: X-ray Structure of MinD from *Escherichia coli*. Structures are obtained from PDB ID: 3Q9L of an ATP-bound MinDΔ10-D40A dimer (45). A) The MinD dimer is shown with bound ATP in CPK representation and the deviant Walker A motif from different monomers in green and cyan. B) One subunit from A is rotated by 90° for better visualization of the β-sheets and α-helices (sequentially labeled in red). C) Expanded view of the deviant Walker A motif (green and cyan) with the K11 side chain highlighted. The structure from A) was rotated to give the view from top of this structure. D) The same as shown in C, with ATP included in CPK representation (red for oxygen, orange for phosphate, grey for carbon and blue for nitrogen). E) Residues important for interactions with ATP are shown for one of the binding sites, with interactions involving residues from the same (cyan) and opposite (green) subunits indicated. The structure from A was rotated to provide a view of the binding pocket from bottom of this structure.

G X X G X G K T/S Walker A motif

X K G G X X K T/S Deviant Walker A motif

Figure 1.4: Conventional versus Deviant Walker A Motif Characteristic of the ParA Family. The first lysine residue in the deviant Walker A motif (red) participates in intermolecular interactions with nucleotide phosphate groups bound to the cleft in the other subunit of the dimer.

Based on the location of solvent-exposed residues in the Ec-MinD dimer structure, mutagenesis experiments were performed to identify residues important for interactions with MinC and MinE (30,45,49). These studies identified a number of residues in close proximity to the MinD dimerization interface that were important for binding to MinC, MinE or both. These residues mapped to two contiguous surfaces located in clefts formed by the two subunits, one on either side of the MinD dimer (Fig. 1.5), illustrating the need for MinD dimerization for its interaction with MinE. Another important feature of this structure is that the residues important for MinE-binding are not near the ATP catalytic site of MinD. This raises the possibility that MinE does not directly participate in stimulating ATP hydrolysis, but its interaction with MinD may instead cause subtle conformational changes that would stabilize a catalytically competent MinD structure (45). Identifying the residues on MinE that are important for MinD interaction can improve our understanding of how these subtle changes may occur.

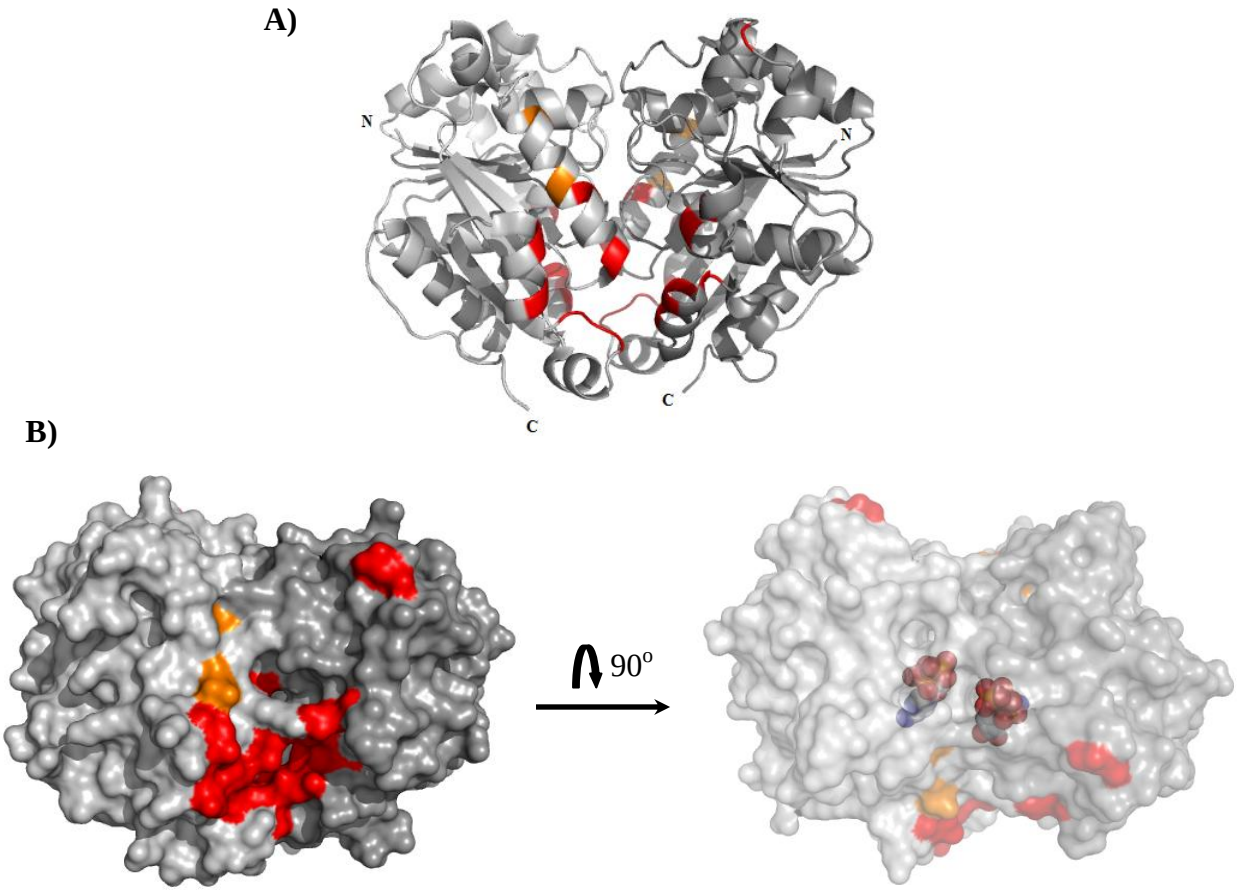

Figure 1.5: Localization of Potential MinE-Binding Residues on Ec-MinD. A) The structure of the Ec-MinD dimer is shown with colors identifying regions important for binding MinE (red), and both MinE and MinC (orange) as determined by bacterial two-hybrid assays with MinD mutants (45). B) Surface representation of MinD is shown with the MinE and MinE/C-binding regions coloured as in A (*left*), highlighting the cleft that comprises the MinE-binding site and rotated (*right*) to show a transparent top-view. ATP bound in the central region of the complex is shown in CPK representation.

1.4: MinE Residues Required for MinD Binding

Prior to structural studies on MinE, various experiments had been performed to identify the residues important for MinD-binding and stimulation of its ATPase activity. Truncations of MinE used in yeast two hybrid studies showed that MinE with an N-terminal 11 amino acid truncation retains interactions with MinD while an N-terminal 26 amino acid truncated MinE

does not (50). Phase contrast microscopy also showed that when the first 22 residues of MinE are expressed in a *minB* knockout overexpressing MinC and MinD, it inhibits the filamentation that is caused by the accumulation of the inhibitory MinCD complex on the membrane throughout the cell (51), while the C-terminal MinE fragment (residues 30-88) could not (18). As well, yeast two hybrid analyses showed that MinE(1-31) was sufficient for the interaction with MinD (52). Based on these results, the N-terminal region of MinE was assigned as the anti-MinCD domain.

Residues within the anti-MinCD domain that are required for MinD binding were subsequently identified in yeast three-hybrid experiments measuring the disruption of the MinCD complex by mutants of Ec-MinE(1-31). These results indicated that residues A18, L22, and I25 are vital for the interaction with MinD (52). Cells expressing full-length MinE with one of these mutations in place of the WT protein also showed an absence of oscillation of both fluorescently labelled MinE and MinD (52). Mutations at residues A15, K19, V26, and R30 of Ec-MinE(1-31) similarly showed some reduction in the strength of the MinD interaction in the same type of yeast three hybrid experiments (50,52).

MinD ATPase assays have also been used to pinpoint residues involved in anti-MinCD activity, since MinE interactions with MinD give rise to a 10-fold increase in ATP hydrolysis rates (29,31,53). The double MinE mutant I17A/A18R neither showed stimulation of MinD ATPase activity, nor support of GFP-MinD oscillation in vivo. Furthermore, K19A/E20A and K19Q MinE showed 50% stimulation with respect to wildtype MinE. The oscillation of GFP-MinD also took twice as long in the presence of these two mutants in bacterial cells, indicating that stimulation of MinD ATPase activity was correlated with MinD oscillation (31). Likewise ATPase assays have been used in the Goto lab to identify MinD-binding residues in MinE. The first N-terminal 22 residues of MinE were examined by alanine scanning and only mutations of

A18, R19, R21, and L22 affected stimulation of MinD activity by the full-length protein (54) in agreement with yeast three-hybrid results with MinE(1-31) (52).

In these mutational studies of the anti-MinCD domain, the results were always interpreted with the assumption that this domain was largely unstructured, and could be considered as a separate structural domain from the remainder of the protein. Experimental evidence for this assumption came from limited proteolysis of MinE by trypsin, which led to complete loss of the first 31 residues while the remaining sequence showed protection from cleavage (55). Since peptide bond cleavage occurs more rapidly at unstructured sites, this suggested that the N-terminal 31 residues were unstructured. Support for this was provided by solution NMR studies on a peptide comprised of the first ~22 residues, with shift and NOE patterns that suggested a largely unfolded state for this region of MinE, with some tendency to sample helical conformations (55). These results indicated that the anti-MinCD domain may exist in a solvent-exposed state, primed for interactions with dimeric MinD.

1.5: Topological Specificity Function in MinE

In addition to the assignment of MinE residues 1-31 as the anti-MinCD domain, early studies suggested that the remaining C-terminal part of the MinE sequence also had a distinct biological function. This was proposed based on the observation that deletion of these residues produced a minicell morphology, indicating that placement of the cell division septum was no longer regulated (55). Moreover, when the C-terminal portion of MinE (residues 36-88) was overexpressed in cells containing endogenous MinE, minicell formation was also observed (18,56). This suggested that these residues formed a functional domain that was responsible for

conferring topological specificity to the anti-MinCD function of MinE (51), leading to assignment of this region as the topological specificity domain (TSD). Mutations in this domain have also been identified, such as D45A and V49A, that disrupt the spatial and temporal localization of MinE during oscillation, and inhibit E-ring formation. In the double mutant D45A/V49A, the MinD polar zones were found to extend past the mid-cell during some cycles, with general irregularity in the dynamic oscillation cycle in vivo that also resulted in minicells (57).

The functional domain identified in these studies also appeared to correspond to a structural domain, as identified in limited proteolysis experiments on MinE (55). The stable C-terminal fragment that was isolated from this process contained the complete TSD, and formed a stable dimer with micromolar dimerization affinity (58). The stability of this fragment allowed its structure to be determined by solution NMR (58). As shown in Figure 1.6, the symmetric dimer is comprised of 4 β-strands, with a long α-helix contributed by each subunit to form one part of the dimeric interface. There are numerous hydrophobic interactions between the α-helices forming a coiled coil structure that is then packed against the β-strands at an angle of 30^{o} through additional hydrophobic interactions. Moreover, residues shown to be important for topological specificity mapped onto solvent-exposed regions of the TSD.

Given that the isolated TSD forms a distinct and stable structure (58), and that the isolated N-terminal anti-MinCD domain has some tendency to sample helical conformations as suggested by NOESY data in solution NMR spectra of this peptide (59), it was proposed that MinE binds to MinD through a coiled-coil type of interaction. Consistent with this, residues 31-35 in the TSD structure formed an α-helical structure that was proposed to continue for the remainder of the anti-MinCD domain. Moreover, residues important for anti-MinCD activity

were found to map to one side of an α-helix (52). This evidence, combined with sequence-based coiled coil predictions for the anti-MinCD domain, all suggested that the anti-MinCD domain of MinE might interact with an α-helix of MinD to form an intermolecular coiled coil. However, subsequent studies on MinE gave rise to structural data that provided a significant challenge to this theory.

1.6: A Surprising Structure For Full-length MinE

A major breakthrough in our understanding of MinE function came from the first structure of a full-length MinE protein, revealing some surprising insights that were in apparent contradiction to previous structural studies (54). This structure, obtained by solution NMR of MinE from *Neisseria gonorrhoeae* (Ng) with the solubility-enhancing mutation E46A, showed a dimeric structure with each subunit being comprised of a sheet made up of three β-strands and two α-helices. Unexpectedly, residues 19-31 from the anti-MinCD domain make up the first β-strand and form an integral part of the dimeric interface. This is in stark contrast to the MinE TSD structure which lacks the anti-MinCD domain and shows β3 forming hydrophobic interactions at the dimeric interface. In the full-length structure, there are extensive van der Waals interactions between side chains from β1 across the dimeric interface, as well as between α2 from the two subunits. Although unexpected, similar interactions were also observed in a crystal structure of *Helicobacter pylori* (Hp) MinE that was released at approximately the same time (56). Meanwhile, residues 3-8 in the Ng-MinE structure were found to form a short α-helix interacting with the other subunit in the dimer.

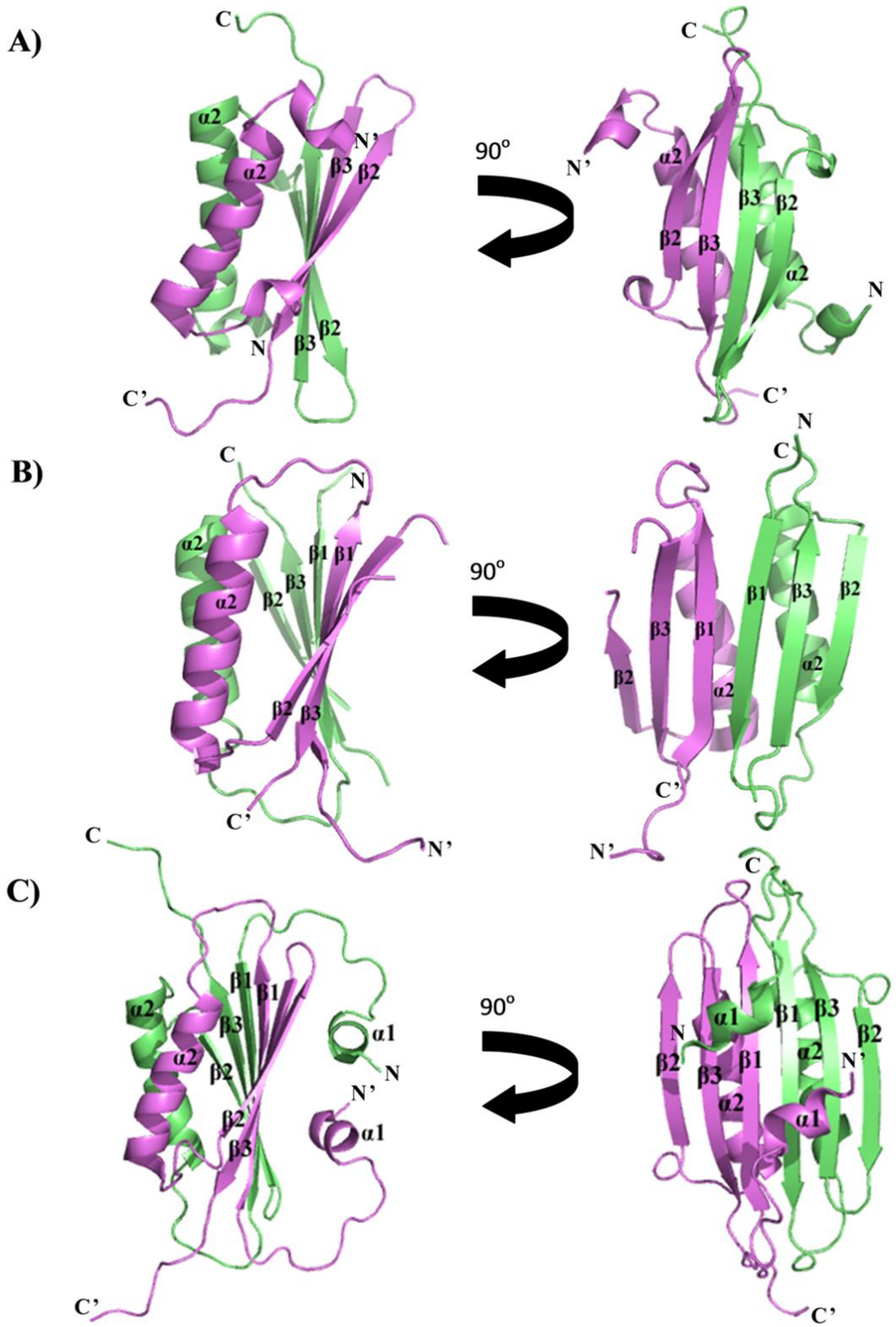

Figure 1.6: Comparison of MinE Structures Obtained for the Topological Specificity Domain versus the Full Length Protein. Subunits are indicated in different colours A) residues 30-87 from *Escherichia coli* B) residues 13-76 from *Helicobacter pylori* C) residues 1-88 from *Neisseria gonorrhoeae* MinE.

Examination of the location of MinD-binding residues identified using MinD ATPase assays (31,54) in the structure of the full-length MinE dimer shows that A18 and R19 are located in a loop that is well exposed for an intermolecular interaction with MinD. However, interactions involving residue R21 would be hindered in this structure due to the presence of the short N-terminal amphipathic helix that binds to the other subunit, forcing the intervening loop to partly reduce the solvent accessibility of this residue. Even more problematic is L22, since it is completely buried in the hydrophobic core of the dimer interface, making it unavailable for interaction (Fig. 1.7).

One of the potential explanations that buried residues such as L22 and R21 were identified as MinD-binding residues is that mutations made at these sites could have altered the structure of MinE, giving rise to an indirect effect on MinD binding. This should be particularly relevant for residues such as L22 that are located in structurally critical regions of MinE. In fact, it has already been shown by CD and solution NMR that the mutant L22D has an altered secondary structure compared to wild type MinE (60). Thus, it is not known if L22 is directly involved in stimulating MinD ATPase activity, or if the structural impact of its mutation prevents interaction with MinD. Therefore one of the aims of this thesis is to determine if these residues play a direct or indirect role in MinD interaction.

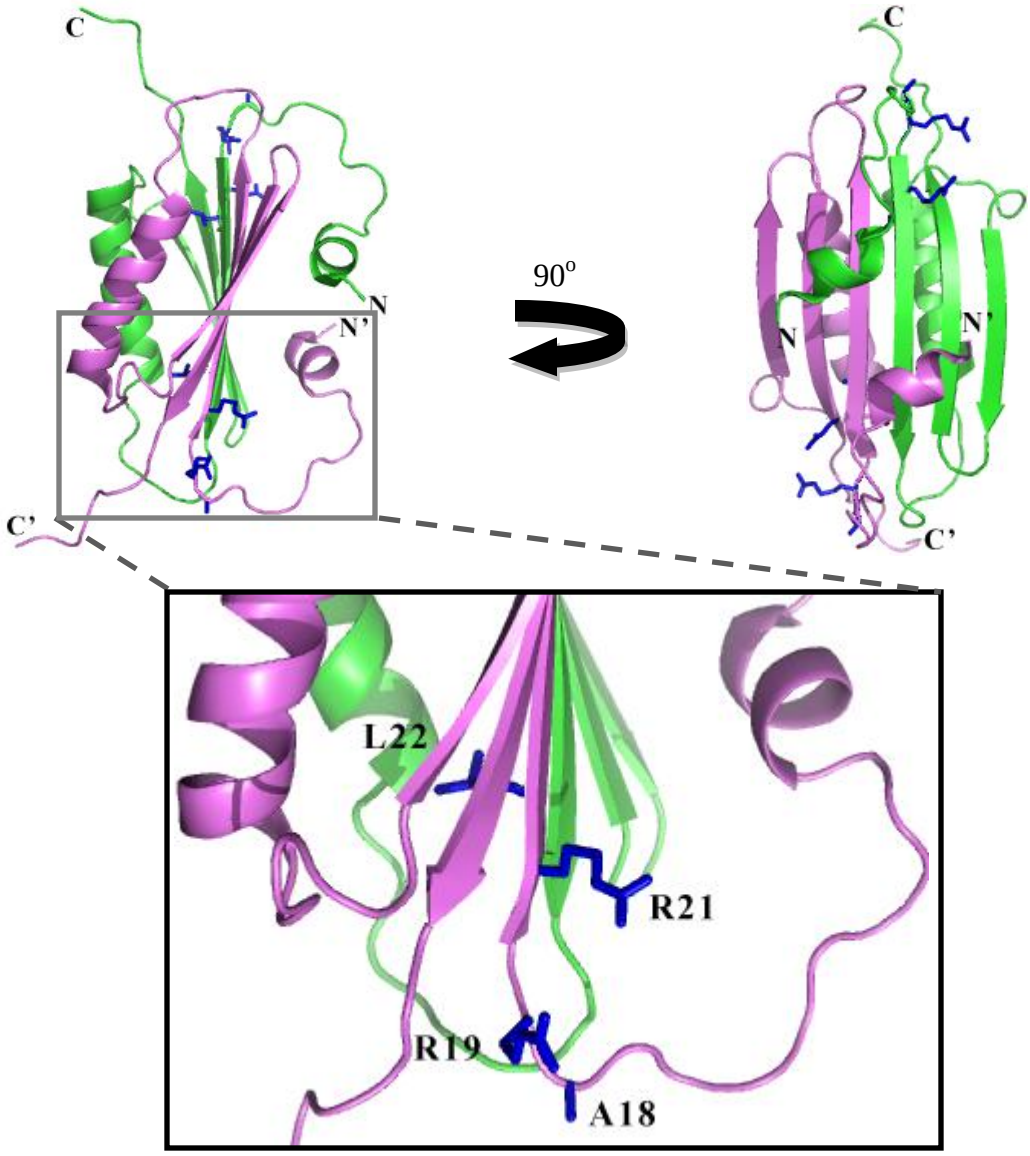

Figure 1.7: Residues on MinE that Have Been Shown to be Important for Stimulation of MinD ATPase Activity.

1.7: MinE Interaction with Lipids

In addition to these interactions with MinD, recent electron microscopy data has provided strong evidence that MinE can make direct interactions with the lipid membrane, even in the absence of MinD (61). In particular, it was shown that MinE can cause liposome deformation

and tubulation when present at high protein:lipid ratios. This effect could be achieved using just the N-terminal MinE(1-31) peptide alone, suggesting that the anti-MinCD domain is responsible for this effect. Meanwhile, sedimentation assays of MinE with liposomes at different salt concentrations indicated that the interaction was largely electrostatic in nature, since the interaction with it was inhibited by higher salt concentrations. The cluster of basic residues R10, K11 and K12 from the anti-MinCD domain, was found to be important for this interaction since the mutant R10E/K11E/K12E did not co-sediment with liposomes (61). These residues could be involved in interactions with the phosphate headgroups of the lipid molecules. The results were the first to demonstrate that MinE is capable of making direct interactions with the lipid membrane. We hypothesize that this interaction could have a profound effect on MinE structure and MinD-binding capability, raising interesting questions regarding the role of this lipid-binding interaction on MinE function.

1.8: Thesis Objectives

Previous studies in our lab performed to identify the residues in MinE important for stimulating MinD ATPase activity used mutants of the full length protein (54). However, the impact of these mutations on the conformation of MinE was not factored into these analyses, with mutants showing disrupted function that could have been a result of structural changes caused by the mutation. In some cases no structural change was incurred by a mutation that had lost MinD binding activity (e.g. A18D) as shown using CD spectroscopy (60), making it possible to unequivocally identify these residues as MinD binding residues. However, in the case of L22D, CD spectroscopy showed a large change in secondary structure relative to the WT protein

(60). Consequently, it is not clear if the loss of MinD binding activity in this mutant was caused by the elimination of a side-chain that directly participates in the interaction, or the structural change in MinE caused the inactivation. Therefore the first aim of this thesis is to determine whether residues in MinE identified as important for anti-MinCD activity that are also important for maintaining the structure of the dimer might also be involved in direct interactions with MinD.

In order to remove the influence of the MinE structure in our study of the interaction with MinD, we chose to use peptides from the anti-MinCD domain. MinE(1-22) has already been shown to interact with MinD, since MinE(1-22) can rescue cell division inhibition by MinC and MinD in vivo (51). In addition, solution NMR of this peptide shows that it is largely unstructured and highly dynamic (58); consequently, the structural tendencies of the peptide are not likely to be affected by the introduction of a mutation, even if it is non-conservative.

Moreover, a new facet of the MinE-MinD interaction that has not been well characterized is the possibility that direct interactions between MinE and the lipid bilayer could alter the structure of MinE and therefore influence its MinD-binding properties. For this reason, the second aim of this thesis is to determine how the MinE structure might change upon interaction with the lipid bilayer, and whether this change might give rise to a conformation that exposes more residues in MinE for MinD binding.

The tools that will be employed to pursue these aims are; 1) kinetic measurements of MinE peptide-stimulated MinD ATPase activity for the identification of residues directly involved in MinD binding; 2) circular dichroism (CD), for the study of conformational changes incurred upon lipid binding, and; 3) NMR spectroscopy for structure determination of the lipid-bound state. A brief description of the theoretical and practical aspects of these techniques is

provided at the end of this Chapter. Together these tools have been applied in this thesis to pursue the following objectives:

- Clarify the role of residues R21 and L22 in the stimulation of MinD ATPase activity
- Investigate the impact of interactions with the lipid bilayer on the structure of MinE using CD spectroscopy
- Investigate the role of R10 in lipid membrane interactions by MinE
- Investigate the role of MinE-lipid interactions on MinD ATPase activity
- Determine if solution conditions can be found that would allow the study of the membrane-bound conformation of MinE by solution NMR

Gaining insight into the interactions involving MinE will help pave the way for understanding the mechanism of MinE-MinD binding and stimulation of MinD ATP hydrolysis. Ultimately this knowledge should provide the basis to understand the molecular events that give rise to Min protein oscillation to regulate cell division.

1.9: *Neisseria gonorrhoeae* versus *Escherichia coli* Min Proteins

Although much research has been done with Min proteins from the rod-shaped bacteria *Escherichia coli*, the studies that have been performed in the Goto lab have used Min proteins from the coccus bacterium *Neisseria gonorrhoeae*, the causative agent of the sexually transmitted disease gonorrhea. This disease can lead to epididymoorchitis in men and pelvic inflammation in women which can cause infertility (62). Newborns exposed to this bacterium during passage through the birth canal of infected mothers can also acquire blindness. Approximately 60 million new cases of gonorrhea disease are presented each year globally.

Furthermore, many strains of *N. gonorrhoeae* have developed resistance to commonly used drugs such as penicillins, tetracyclines and quinolones, increasing the need for new antimicrobial agents to be developed (62). Gaining deeper insight into the molecular mechanisms required for virulence and propagation of this pathogen, including those involved in cell division, such as the Min system, can help identify new targets for future antibiotics development.

Although our studies originate from our interest to understand how pathogenic round cells such as *N. gonorrhoeae* undergo cell division, there is ample evidence that the Min protein mechanism of action is common across bacterial species. While the spherical morphology of coccal cells does not give rise to well-defined cell poles to position the axis of Min protein oscillation, fluorescence microscopy studies in *E. coli* show that Min proteins from both species do oscillate in the same way (63). In fact, it appears that the Min proteins from Ng and Ec are highly interchangeable, since Ng Min proteins can be substituted for Ec Min proteins in *E. coli*, and Min protein oscillation is retained (64,65). For example, Ng-MinD expressed in *E. coli* was able to interact with native Ec-MinE and undergo oscillation (64). Furthermore, overexpression of Ng-MinD in an *E. coli* MinD knockout was able to rescue wild-type morphology. Yeast two hybrid studies have also shown that Ec-MinD interacts with Ng-MinD (66). These results indicate that Min proteins from different species function in the same way, as would be expected based on the high level of sequence homology (*e.g.* 42% sequence identity for MinE). This high level of sequence conservation also implies that the structures of these proteins will be very similar, consistent with the functional equivalence of these proteins. Therefore, the findings obtained for Ng Min proteins in this thesis will be applicable for other Min protein homologues, and particularly those from *E. coli*.

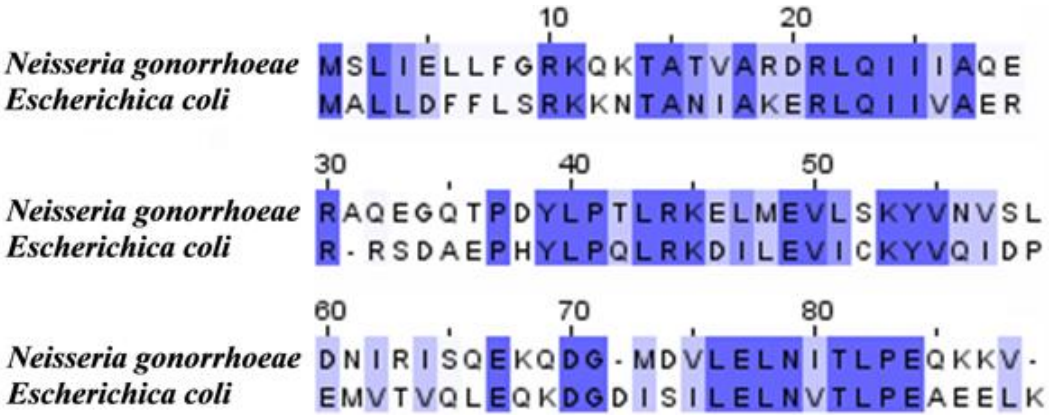

Figure 1.8: Protein Sequence Alignment for MinE from *Neisseria gonorrhoeae* and *Escherichia coli*. COBALT (Constraint-Based Multiple Alignment Tool) (67) was used to align the protein sequences and Jalview (68) was used for visualization of sequence conservation in the two species. Darker blue indicates identical residues and light blue are homologous residues.

1.10: Kinetics of MinE-Stimulated MinD Activity

One of the methods used to study the interaction between MinE and MinD in this thesis is the measurement of MinD ATPase reaction kinetics. Like many regulatory proteins, MinE binds to the MinD enzyme in order to trigger its catalytic activity. The effect of this binding event can be monitored by measuring the kinetics of the reaction catalyzed by the activated enzyme. This can provide information on the affinity of the interaction between the enzyme and its activator, the number of binding sites available, and whether there is any cooperativity to this activation (69). For this type of system, the activity of the enzyme can be measured as a function of activator concentration, and the data fit to the Hill equation:

$$\frac{\theta_{bound}}{\theta_{total}} = \frac{[L]_{total}{}^{h}}{K_{0.5}{}^{h} + [L]_{total}{}^{h}} \qquad \text{(Eq. 1)}$$

where $\theta_{bound}/\theta_{total}$ is the fraction of ligand binding sites that are occupied, [L] is the concentration of ligand, $K_{0.5}$ is the concentration at which there is half-maximal activity, considered to be an apparent dissociation constant, and *h* is the Hill coefficient, a measure of the cooperativity of the system that reflects the minimum number of available ligand binding sites on the receptor (70). When using enzyme activity as an indirect measure of binding, the ratio of the initial rate of reaction (v_o) to the maximal rate (V_{max}) is used to approximate the fraction of occupied ligand binding sites:

$$\frac{v_o}{V_{max}} = \frac{[L]_{total}{}^{h}}{K_{0.5}{}^{h} + [L]_{total}{}^{h}} \qquad \text{(Eq. 2)}$$

In the case of the Min proteins, MinD-catalyzed ATP hydrolysis rates can be measured in the presence of different concentrations of the MinE activator to determine the maximum rate of ATP hydrolysis caused by MinE. The apparent binding affinity and cooperativity can also be measured in these experiments, allowing comparison of these parameters between wild type and various mutants of MinE. Any mutation that decreases the apparent affinity of MinE for MinD in this experiment provides strong evidence for a functional role of the mutated residue in the interaction with MinD.

1.11: CD Spectroscopy to Characterize Structural Changes in MinE

CD spectroscopy is a useful tool for analyzing structural changes of proteins, and was consequently one of the methods employed in this thesis. This type of spectroscopy makes use of the difference in absorption of left- and right-handed circularly polarized light by chiral

molecules. Folded proteins differentially absorb circularly polarized light depending on the structures present in the protein (71,72). Absorption in the ultraviolet range of electromagnetic radiation by the peptide bond is normally used to gain insight into protein secondary structure content, with each secondary structure type absorbing polarized light differently (Fig. 1.9). Specifically, the CD spectrum of an α-helix shows maximum ellipticity at ~190 nm and minima at both 208 nm and 222 nm. β-sheet structures give spectra with a maximum at 196 nm and a minimum at 218 nm while a random coil has a minimum at 195 nm and a maximum at 212 nm (73-75).

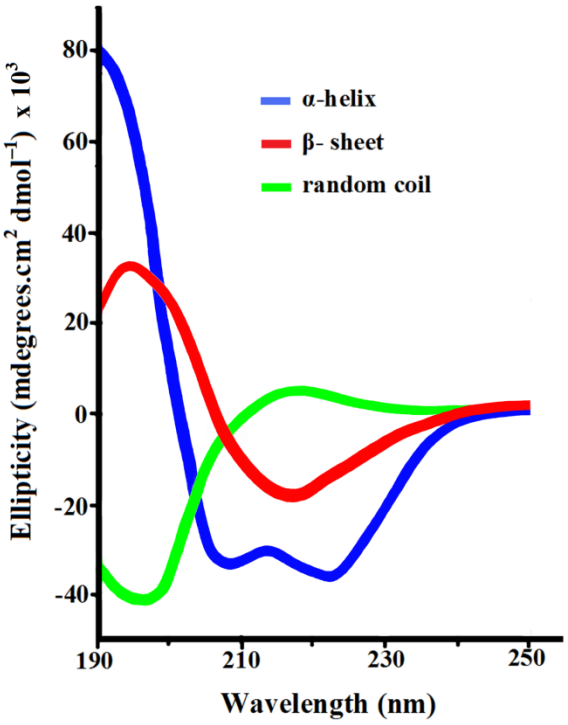

Figure 1.9: Characteristic CD Spectra of Protein Secondary Structure Elements.

It is possible to compare experimental CD spectra with a database of spectra from proteins of known structure to estimate the secondary structure composition of a sample (75).

Servers such as Dichroweb (76,77) provide access to analysis by programs such as CONTINLL and SELCON3 (78) for this purpose. Most of these programs allow specific reference datasets to be chosen which depend on the range of input data and the type of protein being analyzed. Careful selection of the most appropriate reference dataset, usually based on proteins most similar in structure to the protein in question, is important for accurate secondary structure estimation (79). It is also important to note that higher β-sheet contents tends to decrease the accuracy of the prediction, since twisting of the sheets can have a significant effect on the CD spectrum (80). In general, the larger the size of the dataset used, the higher the accuracy of structure prediction, with accuracies typically falling in the range of 71 – 89 % (78).

Aside from secondary structure content estimation, CD spectroscopy is useful for analyzing the effect of different conditions on the total secondary structure content of a protein. In the case of MinE, this approach should be particularly informative for the characterization of any structural changes that might be induced by interactions with lipid vesicles, as will be described in Chapter 4.

1.12: Basic Principles of NMR Spectroscopy

Another powerful technique used for gaining structural information on proteins that was used in this thesis is liquid-phase NMR. This technique makes use of the spin angular momentum inherent in atoms with a spin quantum number greater than zero. Biologically relevant nuclei with non-zero spin angular momentum include ^{1}H, ^{15}N, and ^{13}C, all of which have a nuclear spin quantum number of ½ (81). These nuclei all possess a magnetic moment that, when placed in an external magnetic field, align in either a parallel (the α state) or anti-

parallel (β state) orientation with respect to this field. Since the α state has a slightly lower energy than the β state, there are slightly more nuclei in the parallel orientation, as described by the Boltzmann distribution:

$$\frac{N_\alpha}{N_\beta} = e^{-\left(\frac{\Delta E}{k_B T}\right)} \qquad \text{(Eq. 3)}$$

where N_α is the number of nuclei in the α state, N_β is the number of nuclei in the β state, ΔE is the energy difference between the two states, k_B is the Boltzmann constant and T is the temperature (82). According to this relationship, approximately one in every 10 000 nuclei will be in a lower energy state in a magnetic field strength of 500 MHz (83). The small excess of nuclei in the α state gives rise to a bulk magnetization vector along the direction of the external magnetic field (called the z-axis by convention). It is the bulk magnetization of the sample that enables the NMR signal to be detected, with a larger bulk magnetization vector giving rise to a larger NMR signal. However, since there is normally a very small difference in population between the high and low energy states, higher sample concentrations, usually in the millimolar range for proteins, are required to generate a bulk magnetization vector that is large enough to provide good signal-to-noise ratio in the NMR experiment.

When nuclei in an NMR spectrometer are irradiated with a radiofrequency pulse with an energy matching that of the energy difference between the α and β states, this energy can be absorbed, causing transitions of spins from the lower energy state to the higher energy state (83). The magnitude of the energy difference between these states depends on the strength of the magnetic field of the spectrometer as given in the following equation:

$$\Delta E = h\nu_o \qquad \text{(Eq. 4)}$$

Where *h* is Planck's constant and ν_o is the Larmour frequency or rate of precession of the nucleus. The rate of precession is determined by:

$$\nu_o = \frac{\gamma B_o}{2\pi} \qquad \text{(Eq. 5)}$$

Where γ is the gyromagnetic ratio, an inherent physical property of the nucleus, and B_o is the magnetic field strength of the NMR spectrometer (83). As can be seen, a higher magnetic field strength gives rise to a larger energy difference between the two states. This corresponds to a larger population difference in the parallel and antiparallel orientations, giving a more intense NMR signal.

The frequency at which this absorption of radiation occurs is recorded in the NMR experiment. However, the frequency of absorption depends on the magnetic field strength, and consequently spectrometers with different magnetic field strengths will give rise to different absorbance frequencies for the same samples. To allow data from different NMR spectrometers to be compared in a straightforward manner, it is customary for the observed frequency to be converted into units of parts per million (ppm) chemical shift from a reference compound, (most frequently tetramethylsilane). The conversion is done using the following equation:

$$\delta = \frac{\nu_o - \nu_{ref}}{\nu_{ref}} \times 10^6 \text{ ppm} \qquad \text{(Eq. 6)}$$

where δ is the chemical shift in ppm, ν_o is the frequency of precession of the target nucleus, and ν_{ref} is the absorbance frequency of the reference compound (84).

In addition to the spectrometer field strength, the net magnetic field experienced by each nucleus will also contain contributions from the local chemical environment, largely caused by electron shielding, leading to small differences in absorbance frequencies. Equation 5 can therefore more accurately be written as:

$$v_o = \frac{\gamma B_{net}}{2\pi} = \frac{\gamma B_o(1-\sigma)}{2\pi} \qquad \text{(Eq. 7)}$$

where σ is the shielding factor due to the presence of other atoms in the molecule. The shielding factor is influenced by the number and type of directly bonded atoms, bond order and geometry, as well as non-covalent interactions. Consequently, even when an NMR signal comes from the same nucleus type, there is usually a wide range of potential chemical shifts that can be observed, depending on its local chemical environment (83).

An important factor that influences the quality of the signal obtained is the size of the molecule, or in our case, the protein-detergent/lipid complex. Large molecules will have low tumbling rates due to its slower rotational motion in solution (83), giving rise to rapid loss of coherence of magnetization required to observe the signal. Consequently, large, slowly tumbling complexes tend to have broad peaks in the NMR spectrum, leading to a loss in sensitivity and resolution. When molecular weights exceed approximately 50 kDa, special approaches are required to reduce relaxation rates to allow the observation of signals up to ~100 kDa and higher (85-87). Nonetheless, high-resolution structure determination of these larger complexes is generally not possible by solution NMR. Consequently, optimal samples for structure determination should be relatively small in molecular weight, and remain stably folded at the high concentrations required for solution NMR.

1.13: Screening of Lipid-Mimetic Environments by the ^{15}N HSQC Spectrum

The type of NMR experiment that was performed in this thesis is a 2D correlation experiment called the ^{15}N-HSQC (heteronuclear single quantum coherence) spectrum. This is one of the most commonly used experiments in solution NMR of proteins, since it provides a simplified signature spectrum that reflects the local environment for amide protons (88). In this spectrum the position of a peak is determined by the chemical shift of the amide proton along the x-axis and the chemical shift of the directly bonded ^{15}N nucleus along the y-axis. Consequently, each non-proline amino acid residue in the protein sequence should give rise to a single peak from its backbone amide in this HSQC spectrum. This spectrum also gives some insight into the folded state of the protein, since a spectrum from a stably-folded protein should show a broad range of chemical shifts in the proton dimension (83). In order to acquire the ^{15}N-HSQC, it is useful to generate a sample that has been uniformly labelled with ^{15}N-nitrogen, a requirement that is straightforwardly achieved by bacterial expression of the target protein in a defined medium containing ^{15}N-labelled salts as the sole source of nitrogen.

In order to study the structure of the membrane-bound state of a protein such as MinE, it is necessary to use membrane-mimetic media that can promote the lipid-bound state in solution, while maintaining a complex size that is still compatible with solution NMR (~<100 kDa). In order to identify the most appropriate membrane-mimetic solvent for this purpose, the ^{15}N HSQC can be used to evaluate the structural impact of each system, as well as the effect on the quality of the NMR spectrum.

The most commonly used type of membrane-mimetic system in solution NMR is the detergent micelle. While most detergents tend to remain monomeric when present at low concentrations, above the critical micelle concentration (cmc), the detergent molecules aggregate

into micelles with the polar headgroup on the surface and the hydrophobic portion sequestered away from the aqueous phase in the core of the micelle (89-91). Although the surface of the micelle does possess strong curvature, the small size of these detergent aggregates makes them highly amenable to the study of bound proteins by solution NMR. Table 1.1 shows a list of some of the detergents used for this purpose along with their characteristics.

Another membrane-mimetic environment commonly used in NMR is the small isotropic bicelle (89). These bicelles are formed using a mixture of long and short chain lipids which form disc-shaped bilayers with the edges capped by the short-chain detergent. Some of the most commonly used bicelle formulations use DMPC as the long-chain lipid, and CHAPS or DHPC(C6) as the detergent (89,92). The molar ratio of long chain lipid to short chain bicellar phase detergent, typically referred to as the *q* ratio, is usually around 0.2 – 0.7 for these types of bicelles. A significant advantage of the bicelle medium is that they contain a true lipid bilayer phase which should not exhibit the curvature typical of the surface of a detergent micelle. They are also significantly smaller than liposomes, allowing more native-like interactions involving the membrane surface, while facilitating detection by NMR.

Both bicelles and micelles differ from the lipid membrane in that they are composed of shorter fatty acyl chains, and tend to be more mobile with a higher degree of water penetration than native lipid bilayers (93-96). There is also a significant concentration of monomeric detergent in these solutions, potentially giving rise to undesirable interactions with the protein sample of interest. Meanwhile the headgroup composition is often not like that of a native lipid bilayer, potentially leading to denaturation of associated proteins. Generally, detergents with charged headgroups (e.g. SDS) are more denaturing, though in some cases they can interact more favourably with the protein target of interest (90.97). All these factors indicate that a great deal

of care must be taken when choosing a detergent(s) for use in structural studies of a membrane-associated protein such as MinE. Consequently, it is usually best to screen a wide range of bicelle/micelle solutions to identify the most suitable candidate for solution NMR studies of the protein of interest. This was the approach taken for MinE, as described in Chapter 4.

Table 1.1: Some Commonly Used Detergents/Lipids and Their Characteristics.

Name	Type	cmc (mM)	Aggregation Number
LMPG 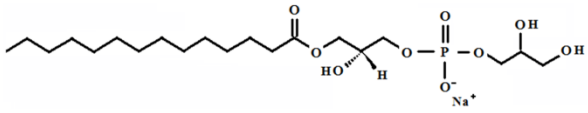	anionic	0.2-0.3	55
SDS 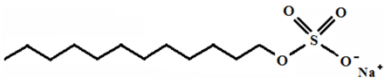	anionic	8.2	62-101
CHAPS 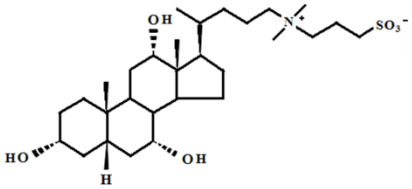	zwitterionic	6-10	4-14
DHPC(C6) 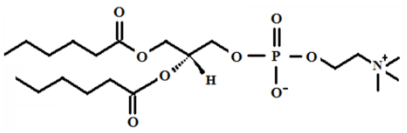	zwitterionic	14	19-25
DMPC 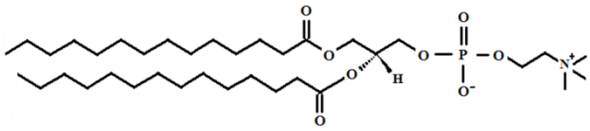	zwitterionic	0.006	N/A
Fos-12 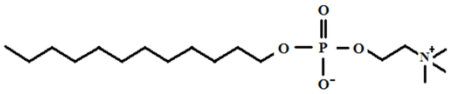	zwitterionic	1.1	N/A
Fos-16 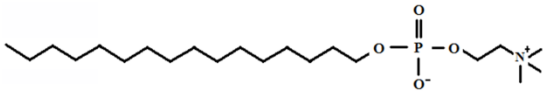	zwitterionic	~0.013	N/A
LMPC 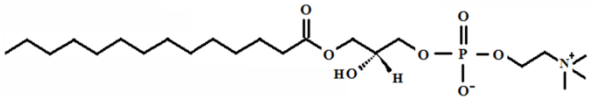	zwitterionic	0.04-0.09	~100

***** Data taken from references (89-91)

Chapter 2: Materials and Methods

2.1: Plasmids and Peptides

All proteins used in this study were from the species *N. gonorrhoeae*. All proteins were expressed from a pet30a-based vector (Novagen) with a kanamycin resistance marker and genes coding for wild type, E46A, or R10A MinE, or wild-type MinD (60). All expressed Min proteins contained a non-native C-terminal LEHHHHHH sequence to allow purification by nickel affinity chromatography. Plasmids were obtained from Christopher Hart and Ali Albadawi (54) in the Goto lab, amplified and their sequences confirmed at the Ontario Genomics Innovation Centre at the Ontario Health Research Institute before being used.

All synthetic peptides were purchased from Genscript USA Inc. at 95% purity. These include MinE(1-22), MinE(1-22) R21A, MinE(1-22) L22A, MinE(1-22) L22D, MinE(1-27), MinE(1-27) I24A, MinE(1-27) I24R, MinE(1-27) I25A, and MinE(1-27) I25R. All peptides were dissolved in ddH_2O and stored at -20^oC. Duplicate samples of each stock solution were sent to the Advanced Protein Technology Centre (Hospital for Sick Children, Toronto) for concentration determination by amino acid analysis.

2.2: Amplification and Isolation of Plasmids

DH5α cells (Invitrogen) freshly transformed with expression plasmids for MinD or wild-type or mutant MinE were used to inoculate, 50 mL of LB media with 50 μg/mL kanamycin (containing 20 g/L of LB broth lennox (Bioshop), and 0.4 mM NaOH). After overnight incubation at 37^oC with shaking at 220 rpm, the bacterial culture was centrifuged at 6,000 rpm,

4°C for 15 min on an Avanti JE centrifuge (Beckman Coulter) with a JA 25.50 fixed angle rotor to harvest the bacterial cells. The Qiagen HiSpeed Plasmid Midi kit (with 2005 edition protocol) was used to isolate DNA which was further purified using Sigma GenElute™ PCR clean-up kit. The purified DNA was stored in 10 mM Tris-HCl, pH 8.5 at -20°C.

2.3: Transformation

Transformation was performed using the $CaCl_2$ method (98). Briefly, 2 µL of plasmid at a concentration of 10 ng/uL (containing MinE WT/mutants or MinD) was added to 20 µL of BL21(DE3) competent cells (Novagen), mixed by gently flicking the tube, and left on ice for 30 min. The tube was then transferred to a water bath at 42°C for 2 min, followed by a 1 min incubation on ice before the addition of 200 µL of LB media. The cells were subsequently incubated at 37°C and 220 rpm for 1 hr. Finally, 200 µL of the culture was plated on a kanamycin resistant LB-agar plate and left at 37°C overnight.

2.4: Bacterial Growth and Overexpression

One colony of the transformed BL21(DE3) cells (Novagen) was transferred to M9 media (48 mM sodium phosphate, 22 mM potassium phosphate, and 8.5 mM NaCl pH 7.4) containing 0.1 mM $MgSO_4$, 10 µM $CaCl_2$, 0.1% (v/v) MEM vitamins (Gibco), 0.1% (w/v) NH_4Cl, 0.3% (w/v) D-glucose, and 50 µg/mL kanamycin which was incubated overnight at 37°C and 220 rpm.

The following morning the 80 mL bacterial culture (with an OD_{600} of 0.5 – 0.7) was used to inoculate 800 mL of M9-kanamycin media in a Fernbach flask and incubated at 37°C,

220 rpm until the OD_{600} was between 0.5 – 0.7. A 1 mL aliquot was removed for SDS-PAGE analysis of the pre-induction culture, and IPTG was added to a final concentration of 0.5 μM to induce expression, and the culture allowed to grow at 16^{o}C with shaking at 220 rpm overnight.

After removal of a 1mL aliquot of the expression culture for SDS-PAGE analysis, the cells were subsequently harvested by spinning at 4,800 g and 4^{o}C for 10 min on an Avanti JE (Beckman-Coulter) centrifuge with a JA 10.50 fixed angle rotor. The pellets were kept at -20^{o}C until required for purification.

The aliquots taken from the bacterial culture for SDS-PAGE analysis were spun at 16,000 g at room temperature for 1 min on an Eppendorf 5415D tabletop centrifuge. The pellets were solubilised with 100 μL of 2X loading buffer (100 mM Tris pH of 6.8, 20% (v/v) glycerol, 4% (w/v) SDS, and 0.02% (w/v) bromophenol blue) and stored at -20^{o}C.

2.5: Purification

Purifications were done as previously described (54,60). Briefly, bacterial pellets containing expressed Min proteins from ~200 mL M9 media were resuspended in 7.5 mL of lysis buffer (50 mM Tris, 250 mM NaCl, and 10 mM imidazole at pH 8.5) and 0.5 mg/mL of benzamidine (Bioshop). The suspension was placed on ice and rocked for 30 min. The cells were then lysed using a Fisher Scientific 500 Sonic Dismembrator for 3 cycles (1 s on and 1 s off) at 45% amplitude and 1 min duration. Lysed cells were spun at 16,000 g, 4^{o}C for 20 min on an Avanti JE centrifuge with a JA 25.50 fixed angle rotor. The supernatant was added to 3 mL of Ni-NTA resin (Novagen) pre-equilibrated with lysis buffer in a 2.7 cm inner diameter column (Kimble). The solution was incubated for 30 min with occasional stirring to ensure all Min

protein bound the resin. The resin was then washed 3 times with 25 mL of lysis buffer. Next, 25 mL of lysis buffer containing 20 mM imidazole was added to the column twice to elute non-specifically bound proteins. The Min protein was then eluted using 3x10 mL aliquots of lysis buffer containing 0.5 M imidazole. EDTA was added to the eluate to a final concentration of 0.5 mM. A 25 µL sample was taken at each step and diluted with 25 µL of 2X loading buffer and stored at -20^{o}C. The resulting ~30 mL of nickel-affinity chromatography purified Min protein was concentrated to a 4 – 6 mL volume with an Amicon Ultra 15 (10 kDa molecular weight cut off (MWCO) for MinE and 30 kDa MWCO for MinD) filter device centrifuged at 3,800 g and 4^{o}C using a Spinchron 15R centrifuge and S4180 hanging bucket rotor.

Prior to the final purification step by size exclusion chromatography, concentrated Min samples were centrifuged at 3,500 g for 2 min at 4^{o}C to remove any aggregates. A Superdex 75 10/300 GL column (General Electric) connected to an AKTA FPLC was equilibrated with size exclusion buffer (50 mM Tris, 100 mM NaCl, 0.2 mM EDTA at pH of 8.5). 2 mL of concentrated Min protein solution was injected at a flow rate of 0.2 mL/min, and the elution carried out at 0.5 mL/min. Absorbance was measured at 280 nm during the elution and 0.7 – 1.0 mL fractions collected from 10 – 15 mL for MinE, and 10 – 14 mL for MinD. All purified samples were stored at 4^{o}C until use. The functional integrity of Min samples was established by performing a control ATPase assay for each sample purified.

2.6: SDS-PAGE

SDS-PAGE was carried out using the Laemmli method (99). Samples that had been prepared in loading buffer were removed from storage at -20^{o}C and left to thaw before being

heated at 100^{o}C for 5-10 minutes. Meanwhile, a precast polyacrylamide gel with a 5% stacking phase and 15% resolving phase (Biorad) was placed in a Mini-PROTEAN Electrophoresis Cell (Biorad) with 500 mL of running buffer (25 mM Tris, 190 mM glycine, and 3.5 mM SDS at pH 6.5-7.0). Each well was washed with running buffer, and 12 µL of each sample was loaded onto the gel. 2 µL of EZ-Run protein markers (Fisher) were added to one well for molecular weight determination. The gel was run at 150 V for 37 minutes. Gels were stained using Coomassie blue (50% methanol, 40% ddH_2O, 10% acetic acid, and 0.1% (w/v) Coomassie brilliant blue) for over an hour. It was destained twice with 50% methanol and 10% acetic acid for approximately 1hr.

2.7: Protein Concentration Determination

Protein concentrations were determined using the BCA (bicinchoninic acid) assay (100,101) using BSA (bovine serum albumin) as a standard (Pierce). 50 µL of each sample was added to 1 mL solutions containing reagent A (200 mM sodium carbonate, 120 mM sodium bicarbonate, 30 mM bicinchoninic acid, 10 mM sodium tartrate, and 0.1 M sodium hydroxide) and reagent B (4% cupric sulphate) in a 50:1 (v:v) ratio. The tubes were incubated at 37^{o}C for 30 min and left to cool to room temperature before absorbances were measured at 562 nm using an Ultraspec 2100 UV/vis spectrometer. Absorbance values for the standard solutions were used to generate the protein standard curve that describes the linear relationship between protein concentration and absorbance, and protein concentrations of protein samples were automatically calculated from this standard.

2.8: ATPase Assay

The MinD ATPase assay was performed as previously described (54). Lipid vesicles for the assays were prepared from DOPG (1,2-dioleoyl-*sn*-glycero-3-[phosphor-*rac*-(1-glycerol)]), DOPC (1,2-dioleoyl-*sn*-glycero-3-phosphocholine) and *E.coli* lipid extracts dissolved in chloroform in borosilicate glass test tubes (Avanti Polar Lipids). The chloroform was evaporated by blowing a stream of argon gas on the solution for ~30 min. The tube was kept in the fume hood overnight to allow any residual chloroform to evaporate. The next day, reaction buffer (25 mM Tris, 50 mM NaCl pH 7.5) was used to dilute the lipids to a concentration of 10 mg/mL. Lipid suspensions were stored at -20^{o}C.

Just prior to use in the ATPase assay, lipid suspensions were thawed and extruded with Hamilton syringes in an Avanti Mini-Extruder. DOPG and DOPC phospholipids were extruded using 0.1 µm polycarbonate filters. *E. coli* lipids were extruded first using 1.0 µm polycarbonate filters and then 0.1 µm filters. The *E.coli* lipids were extruded at ~50^{o}C due to its higher phase transition temperature. The lipids were then stored at 4^{o}C for no longer than three days prior to use.

For the malachite green reagent, 10 mL of 4.2% (w/v) ammonium molybdate and 4 M HCl was added to 30 mL of 0.045% (w/v) malachite green (102-104). The solution was placed in a rocker for 1 hr and then filtered using a 0.22 µm MF-Millipore membrane. The solution was stored at 4^{o}C when not in use. Just before use, tween was added to a final concentration of 0.15% (v/v) in the malachite green reagent being used. The solution was wrapped in foil and left at room temperature for at least 30 min before use.

To set up the ATPase assay, microfuge tubes containing 65mM Tris-HCl, 50mM KCl, 80mM NaCl, 5mM $MgCl_2$, 1mM ATP, 2.7 µM MinD, 500 µg/mL lipids and MinE (at various concentrations) at pH 8.2 were prepared. The ATP was added to each tube at the end to start the reaction. 40 µL aliquots were taken at 5, 15, 28, and 41 min. The tubes were heated to 100^{o}C for 50 s to stop the reaction before being centrifuged at 16,000g for 4.5 min. 15 µL samples from each tube were added to 70 µL of malachite green reagent in a polystyrene 96-well microplate (Fisher) and incubated for 15 min. Absorbances were measured at 620 nm on a Molecular Devices SpectraMax Plus 96 well plate reader.

All experiments were performed with a minimum of three trials. Each trial consisted of a new batch of purified Min proteins. The peptides were prepared individually in each trial by dilution from stock solutions. The parameters obtained using the Hill equation for each trial was used to calculate average values with standard deviations.

2.9: Generation of the Phosphate Standard Curve

In order to convert absorbance values from the malachite green reaction into concentrations of phosphate, a standard curve was generated using a range of phosphate concentrations. The absorbance of phosphate standards subjected to the malachite green assay in the same reaction conditions as used for the MinD assay was plotted as a function of phosphate concentration (Fig. 2.1). The slope obtained from this curve was highly reproducible using different preparations of malachite green reagent and standard phosphate solution. Consequently, the slope obtained (0.35 ± 0.03 AU/nmol P_i) from three independent trials was then used to

convert absorbance values into concentrations of phosphate for all subsequent ATPase assay experiments.

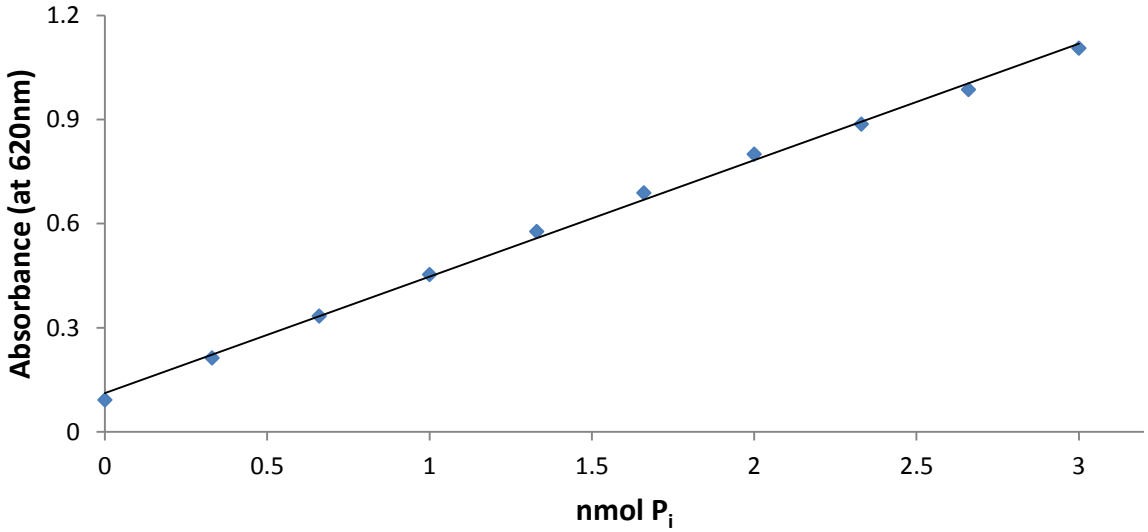

Figure 2.1: Representative Plot of Absorbance vs. Concentration of Inorganic Phosphate. 15 μL of phosphate solution was added to 70 μL of malachite green reagent. The solution was allowed to incubate at room temperature for 15 min before the absorbance was measured. The slope of the line obtained from three trials is 0.35 $\pm$ 0.03 AU/nmol P_i with an R^2 value of at least 99.7% for each.

2.10: Circular Dichroism Spectroscopy

Wild type (WT), R10A, and E46A MinE were stored at 4^{o}C after purification. Prior to CD spectroscopy, MinE samples were subjected to buffer exchange by five rounds of concentration and dilution into 10 mM Tris, 0.1 mM EDTA, pH 8.5 (CD buffer) with an Amicon Ultra 15 (10kDa MWCO) filter device centrifuged at 3,800g and 4^{o}C. MinE was then centrifuged in an eppendorf tube at 16 000g for 2 min to get rid of aggregates before being stored at 4^{o}C. Lipid suspensions were also extruded in the same way as mentioned previously for the ATPase assays, and stored at 4^{o}C until the next day.

The following morning, MinE samples were centrifuged again to remove any aggregates, and another BCA assay was performed for accurate protein concentration determination. Then solutions were made containing: 1) CD buffer (blank run) 2) CD buffer + 0.5 mg/mL lipid (as blank) 3) MinE (WT or mutant) in CD buffer and 4) MinE (WT or mutant) + 0.5 mg/mL lipid. The MinE concentration was calculated to be approximately 15 µM. At least three trials were performed for each experiment using different MinE purifications.

The solutions were then placed in a quartz cell (Hellma Canada Ltd.) with a 1.00 mm path length. CD spectra were recorded on a JASCO J-810 or J-815 spectrometer over the range 200-250 nm at 22^{o}C, with a 0.5 nm pitch at 0.2 nm/min, using a response time of 8 s, bandwidth of 1 nm, and 8 accumulations. The quartz cell was washed with ethanol and ddH_2O and dried with argon gas before each new sample was loaded.

The CD spectrometer measures the observed ellipticity. This is then converted to mean residue ellipticity θ_{MRE} by the following equation:

$$\theta_{MRE} = \frac{\theta}{N \times C \times l}$$

where θ is the ellipticity in millidegrees, l is the pathlength in centimetres, C is the concentration of protein in dmol/cm^3, and N is the number of residues in the protein (75).

2.11: NMR Spectroscopy

^{15}N-labeled MinE E46A was prepared using the same methods as used for all other Min proteins except that $^{15}NH_4Cl$ was used as the sole nitrogen source in the expression medium.

After the last purification step, ^{15}N-MinE E46A in size exclusion buffer was added to an Amicon Ultra 15 (10 kDa MWCO) filter device with 10 mL of NMR buffer (10 mM Tris, 0.2 mM EDTA, pH of 8.0 or 7.5 as specified for each experiment), and centrifuged at 3,800 g and 4^{o}C for 8 min. Another 10 mL aliquot of NMR buffer was added and the solution mixed by pipetting up and down before being centrifuged again. This process was done approximately five times to ensure ^{15}N-MinE E46A was transferred to NMR buffer. Finally, the protein solution was centrifuged at 16 000g for 2 min to remove aggregates. Another BCA assay was performed as described previously and the ^{15}N-MinE E46A was diluted with NMR buffer to the desired concentration for NMR.

Lipids were extruded as described earlier. Bicelles were made by making stock solutions of each detergent/lipid (ie. CHAPS, DMPC, DHPC C6 or C7) and then adding the desired amount of each to a microcentrifuge tube. The bicelle solution was vortexed and then underwent five cycles of heating at 40^{o}C for 30 min and cooling at 4^{o}C for 30 min (105). The bicelle solution was either used immediately or kept at 4^{o}C for use the following day.

^{15}N-HSQC spectra were recorded on a Varian Inova 500 MHz spectrometer using a gradient enhanced coherence selection sequence (106) with a spectral width of 1270 Hz and 64 increments. Typically about 256 transients were acquired for each experiment. The spectra were processed using NMRPipe (107) and analysed with NMRView (108).

Results presented in Chapter 3 were published in:

Ghasriani H., Ducat T., Hart C.T., Hafizi F., Chang N., Al-Baldawi A., Ayed S.H., Lundstrom P., Dillon J.R., and Goto N.K. (2010). Appropiation of the MinD Protein-Interaction Motif by the Dimeric Interface of the Bacterial Cell Division Regulator MinE. *Proceedings of the National Academy of Sciences*. 107, 18416-18421.

Chapter 3: Identification of MinE Residues Necessary for Anti-MinCD Activity

3.1: Protein Purification

In order to test the activity of MinE-stimulated MinD ATPase activity, it was necessary to express and purify both proteins. For this purpose, BL21(DE3) cells were transformed with a plasmid containing the genes for either MinE or MinD, and induced with IPTG. As shown by SDS-PAGE gel analysis of whole cell lysates before and after induction of expression (Fig. 3.1), very little Min protein was present before induction, but very strong band intensities at the expected molecular weights (11 kDa for MinE, 32 kDa for MinD) were visible after expression.

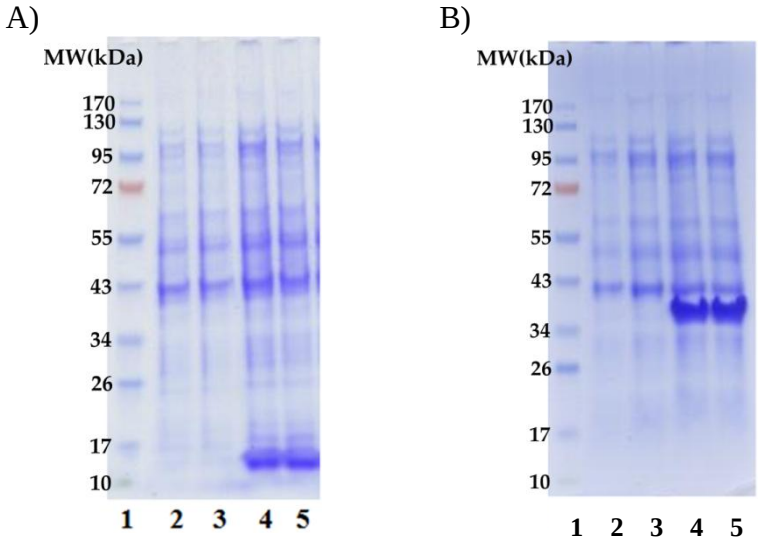

Figure 3.1: Coomassie-Stained SDS-PAGE Gels of MinE and MinD Expression. Whole cell lysates from BL21(DE3) cells transformed with the expression plasmid for A) MinE, and B) MinD from *N. gonorrhoeae* before (lanes 2 and 3) and after (4 and 5) induction with IPTG.

Min proteins were purified using nickel affinity chromatography as previously described (54,60). As shown in Figure 3.2, both purifications allowed >90% pure Min protein to be isolated.

A)

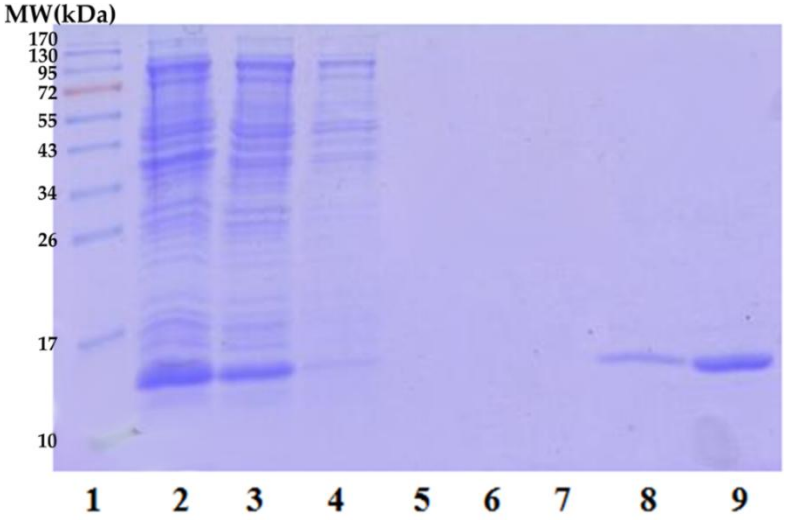

B)

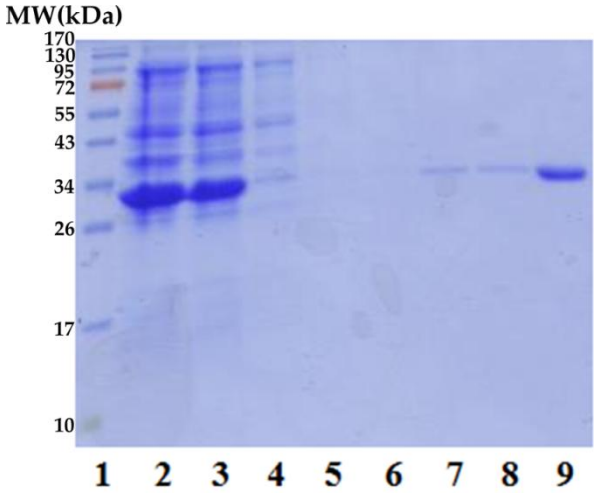

Figure 3.2: SDS-PAGE Analysis of Fractions from Min Protein Purification by Nickel Affinity Chromatography. The purification is shown for A) MinE and B) MinD. For both gels lane 2 contains lysed bacterial cells after sonication, 3 shows the supernatant after centrifugation, 4 - 6 show the flow-through fractions from the nickel affinity column, and 7, 8 contain fractions from the column wash steps. Lane 9 contains purified MinE in A) and MinD in B) that was eluted with a high concentration of imidazole.

An additional purification step was subsequently performed on both Min proteins using size exclusion chromatography (Fig. 3.3 and 3.4). For both MinE and MinD, the majority of the protein eluted as a single peak at the expected elution time for a dimeric species. A smaller peak was often observed at the column void volume, likely corresponding to nucleic acid contaminants as had been previously established (109). SDS-PAGE analysis of both purifications demonstrate the high purity of the final protein samples (>95%).

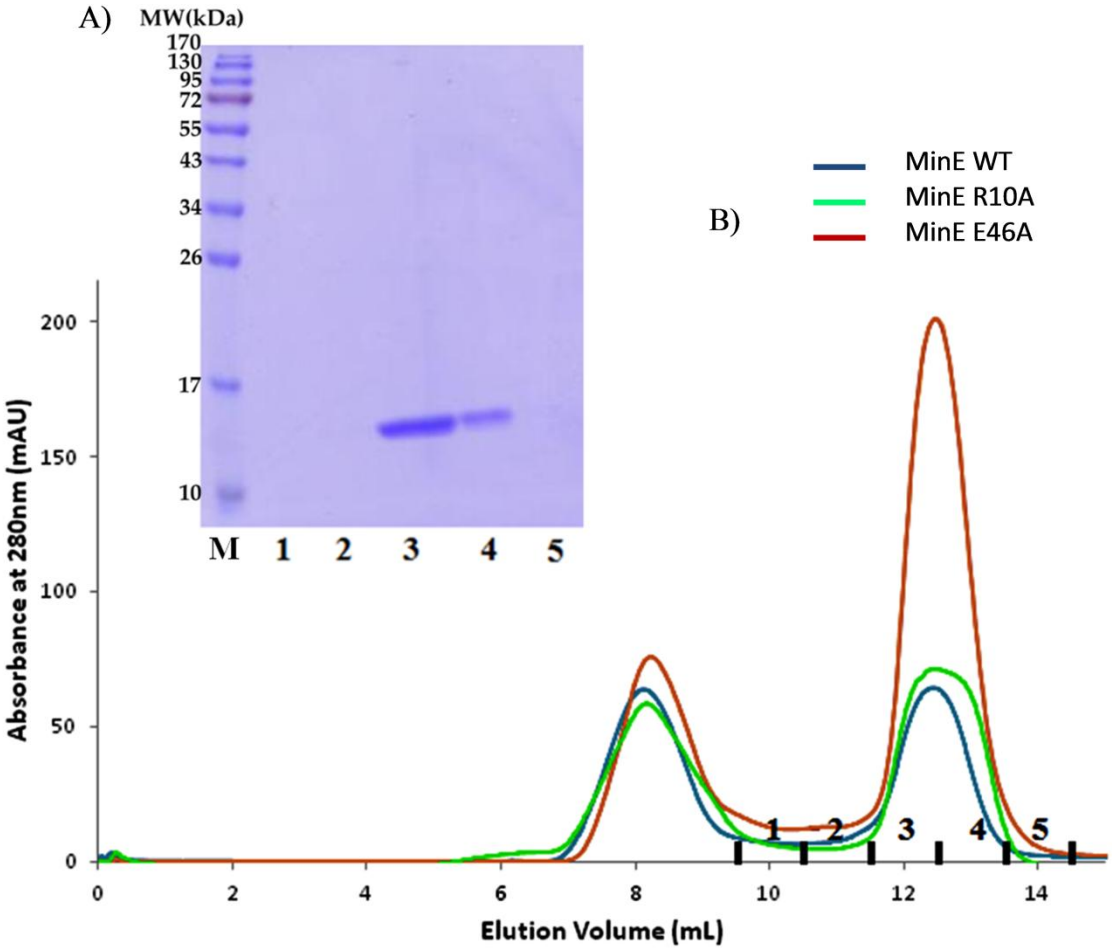

Figure 3.3: Size Exclusion Chromatography Elution Profile and SDS-PAGE of MinE Wild-Type and Mutant Samples. A) Lane M contains the protein molecular weight standards. Lanes 1-5 contain elution fractions of MinE indicated on the profile in B. Protein from elution fractions 3 and 4 were retained for experiments described in subsequent parts of the thesis. B) SEC elution profiles for WT (blue), E46A (red) and R10A (green) MinE. The higher intensities obtained for E46A reflects its higher solubility relative to WT and R10A MinE. Elution fractions collected are shown on the profile along the x-axis.

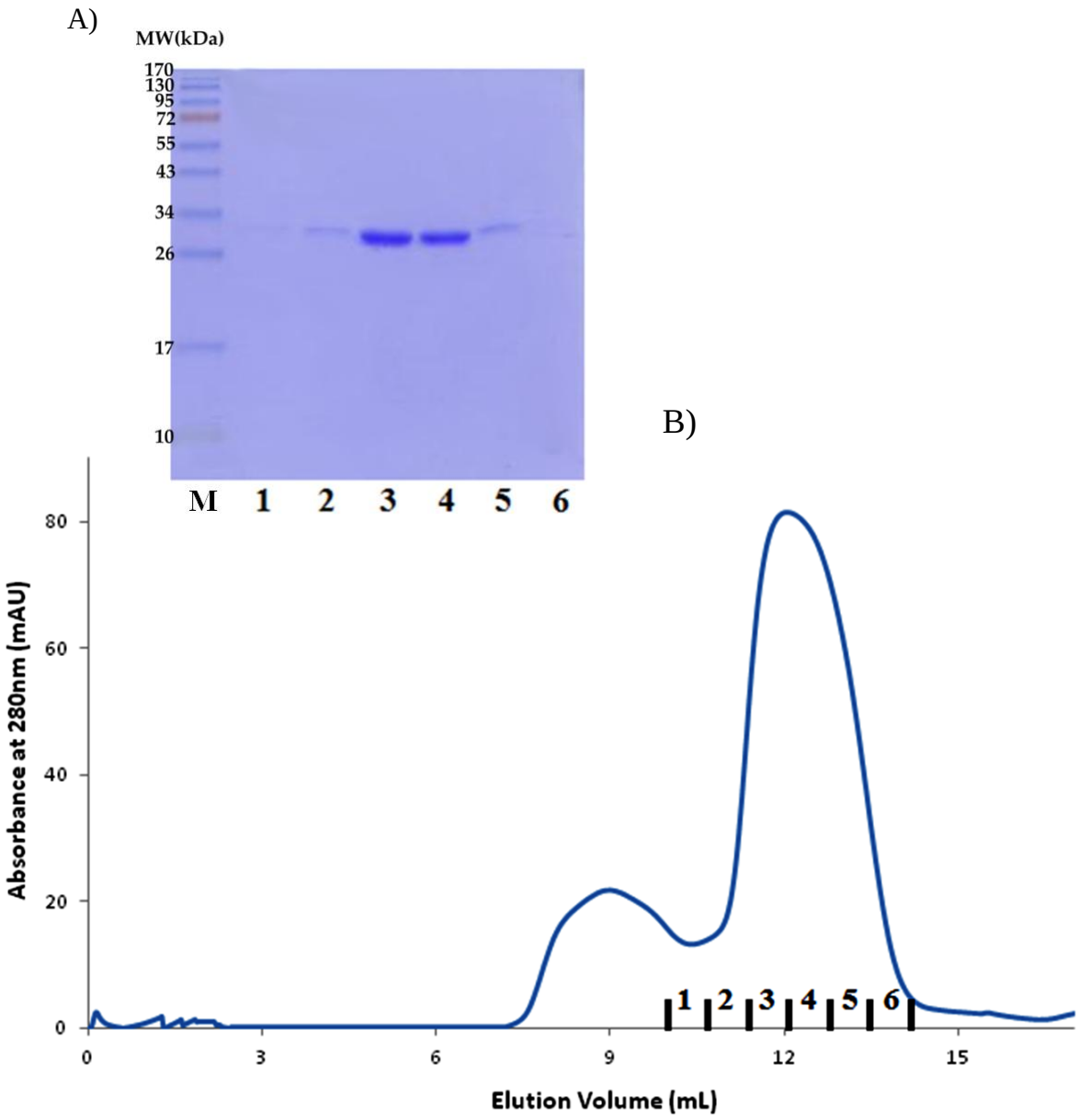

Figure 3.4: Size Exclusion Chromatography Elution Profile and SDS-PAGE of MinD. A) Lane M contains the molecular weight standards. Lanes 1-6 contain elution fractions shown on the elution profile. Protein from elution fractions 3-5 were retained for experiments described in subsequent parts of the thesis. B) SEC elution profile of MinD with elution fractions collected shown on the profile along the x-axis.

3.2: The Control Assay

Each time MinE and MinD proteins were purified, a control MinD ATPase assay was performed to confirm that both proteins had been isolated in an active form. Both positive and negative controls were run in the assay, an example of which is shown in Figure 3.5. The positive control contained all the necessary requirements for MinD ATPase stimulation. In the negative controls, at least one of the required components was omitted.

In these assays the concentration of free phosphate in the solution was monitored at various times during the reaction by a colorimetric assay using ammonium molybdate with malachite green (103,104). Using this assay, the amount of phosphate released can be monitored at 620 nm and converted into phosphate concentrations by comparison with a standard curve. A linear increase in phosphate concentrations over time was generally observed, the slope of which provided a measure of the initial rate of ATP hydrolysis.

Figure 3.5 shows the calculated reaction rates from one of these control assays. The basal activity for MinD in the absence of MinE was ~2 nmol P_i/min/mgMinD. In the presence of MinE, this was increased to ~37 nmol P_i/min/mgMinD, approximately a 15-fold difference as expected from previous observations (29,31). All the other solutions had small background signal indicating that there was no other contribution to ATP hydrolysis rates in these solutions.

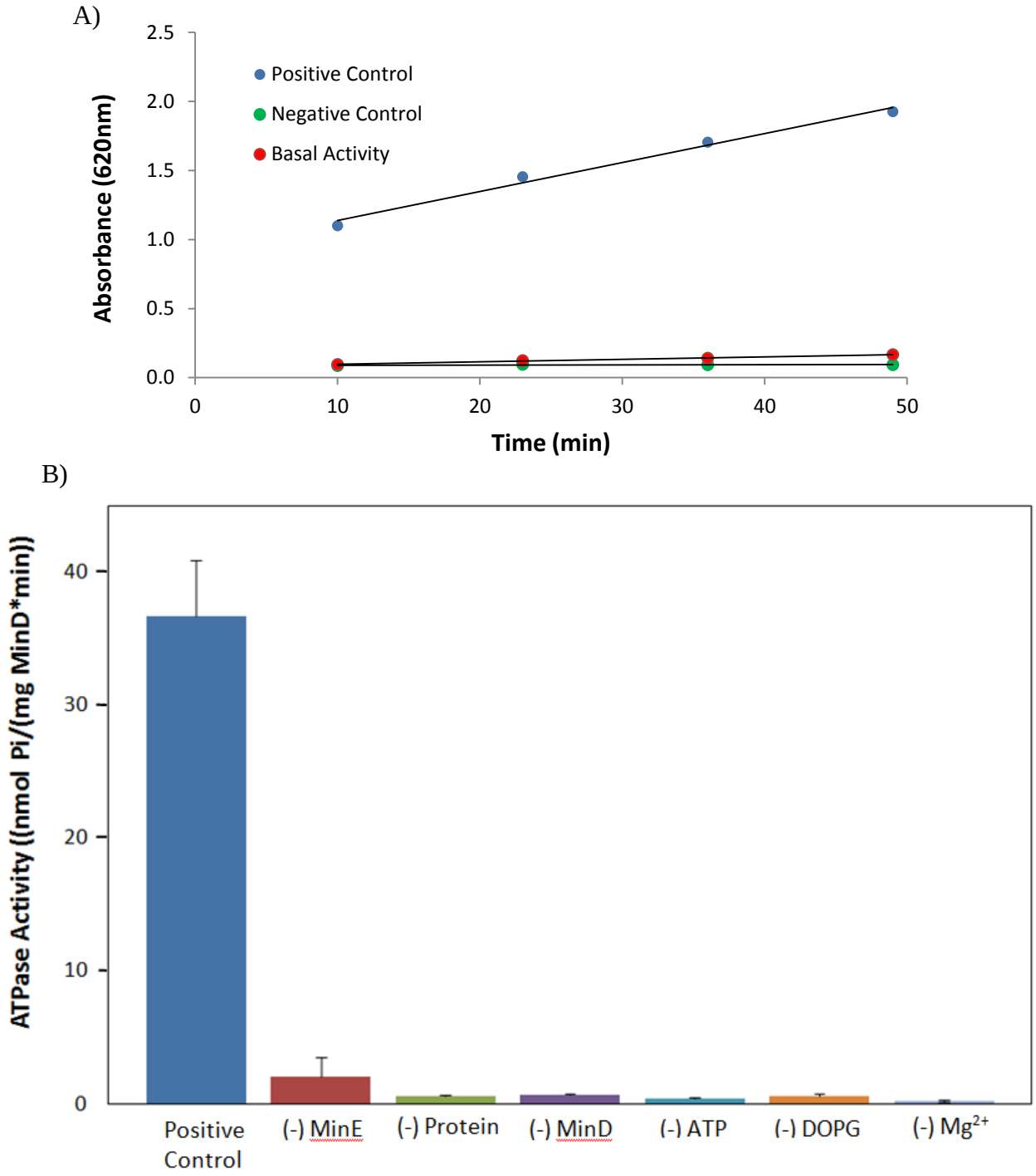

Figure 3.5: MinE Stimulation of MinD ATPase Activity in the Control Assay. A) Basal activity represents MinD-catalyzed ATP hydrolysis in the absence of MinE. Also shown is a representative sample of a negative control from a reaction missing one of the key reaction components required for ATP hydrolysis (e.g. phospholipid vesicles, ATP, Mg^{2+} or MinD (31)). B) Initial rates of ATP hydrolysis by MinD determined from the slopes of absorbance versus time plots such as those shown in A obtained with the malachite green asssay. MinE was used at 3 µM and MinD at 2.7 µM. (-) means the component was missing in the reaction.

3.3: Hill Analysis of MinE-Stimulated MinD ATPase Activity

In order to obtain a measure of the apparent affinity of MinE to bind to MinD, ATP hydrolysis rates were measured over a range of MinE concentrations using cellular concentrations of MinD (31). Assuming that ATP hydrolysis is related to the amount of MinE bound to MinD, the rate of ATP hydrolysis as a function of MinE concentration can be fit to the Hill equation. This allows the maximum specific MinD ATPase activity (V_{max}), as well as the concentration of MinE at which there is half-maximal specific MinD ATPase activity ($K_{0.5}$), to be determined. The cooperativity of the interaction is also provided by the hill coefficient (h). $K_{0.5}$ is of particular interest since it can provide information on the apparent affinity of MinE for MinD, allowing comparison with MinE mutants to identify residues that are important for stimulation of MinD ATPase activity.

An example of the rate profiles for this type of assay is shown in Figure 3.6 for a range of MinE concentrations. As the concentration of MinE increases, the rate of phosphate release also increases, as shown by the increase in slope.

These rates can be plotted as a function of MinE concentration and fit to the hill equation, as shown in Figure 3.6, to yield an apparent affinity of 0.11 $\pm$ 0.02 μM for the MinE interaction with MinD. The graph shows a sigmoidal shape, indicative of a significant amount of cooperativity. This cooperativity was reflected in the hill coefficient of 2.9 $\pm$ 0.3. This value implies that a minimum of ~3 sites in the MinD complex are cooperatively linked, such that MinE binding at one site increases the affinity for MinE binding at two or more other sites. This was somewhat surprising since a dimeric state of membrane-bound MinD would predict that the cooperativity of MinE binding should not exceed two, since a dimer does not have more than

two MinE binding sites that are physically associated with each other. However, it has been shown that MinD forms an ordered polymeric structure on lipid membranes, suggesting that functional coupling involves multiple MinD proteins (33).

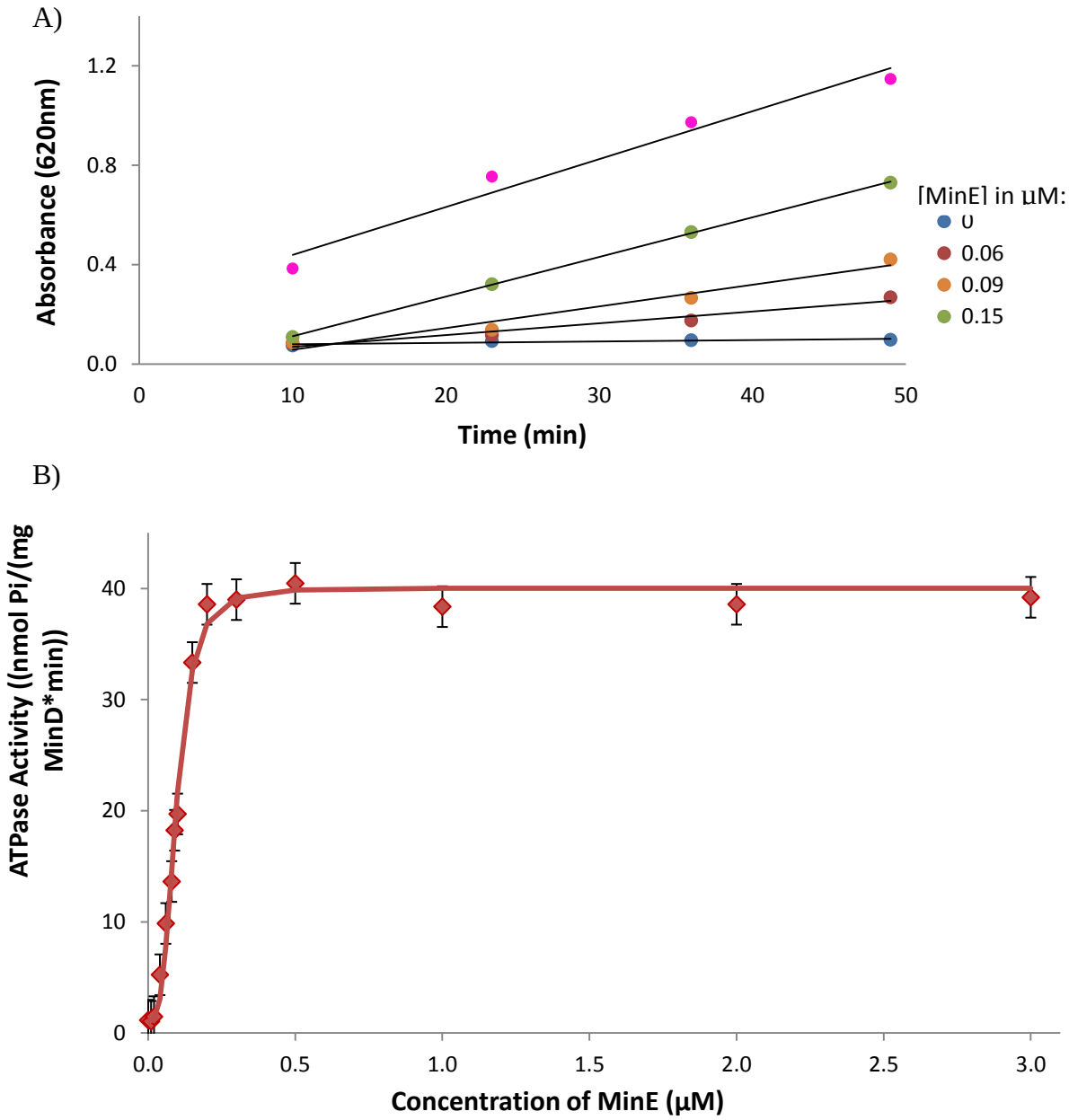

Figure 3.6: Kinetic Profile for ATP Hydrolysis by MinD at a Range of MinE Concentrations. A) Representative MinD reaction rate profiles at different concentrations of MinE. B) Measured rates obtained from profiles shown in A) (diamonds) were fit to the hill equation (solid line) to yield values for V_{max}, $K_{0.5}$ and h of 37.5 $\pm$ 1.5 nmol Pi/min/mgMinD, 0.11 $\pm$ 0.02 µM, and 2.9 $\pm$ 0.3 respectively.

3.4: Evaluation of the Role of MinE Leu22 in MinD Binding

Previous experiments have shown that mutation of L22 disrupts the MinE-MinD interaction and displacement of MinC from the MinCD complex (52). However, as mentioned earlier, it is not known if L22 directly interacts with MinD, or if the conformational change due to mutation of this residue inactivates MinE. To address the role of Leu22 in MinD binding we decided to utilize a truncated version of MinE that only contains the first 22 residues from the anti-MinCD domain. It has been shown that this peptide is capable of disrupting the MinCD complex in *E. coli* (18), while solution NMR experiments have demonstrated that this peptide is largely unstructured (55). Therefore mutants of MinE(1-22) will only show reduced binding affinity for MinD if the mutated residues are directly involved in an interaction with MinD, since it is unlikely that the unstructured conformation of this peptide will be altered by these mutations.

A comparison of MinD ATPase stimulation by full-length MinE with that of the MinE(1-22) peptide is shown in Figure 3.7. Although the maximum ATPase activity is similar in the two profiles, the apparent affinity of the MinE(1-22) peptide, as measured by the concentration required to attain half-maximal activity $K_{0.5}$ is significantly lower than that of the full-length protein (kinetic parameters summarized in Table 3.1). This is not unexpected, since the peptide is likely missing structural elements required for a high affinity interaction. However, the profile for the mutant MinE(1-22) L22D peptide (Fig. 3.8) showed a drastic difference, with virtually no ability to activate MinD activity, even when added to concentrations as high as 50 μM.

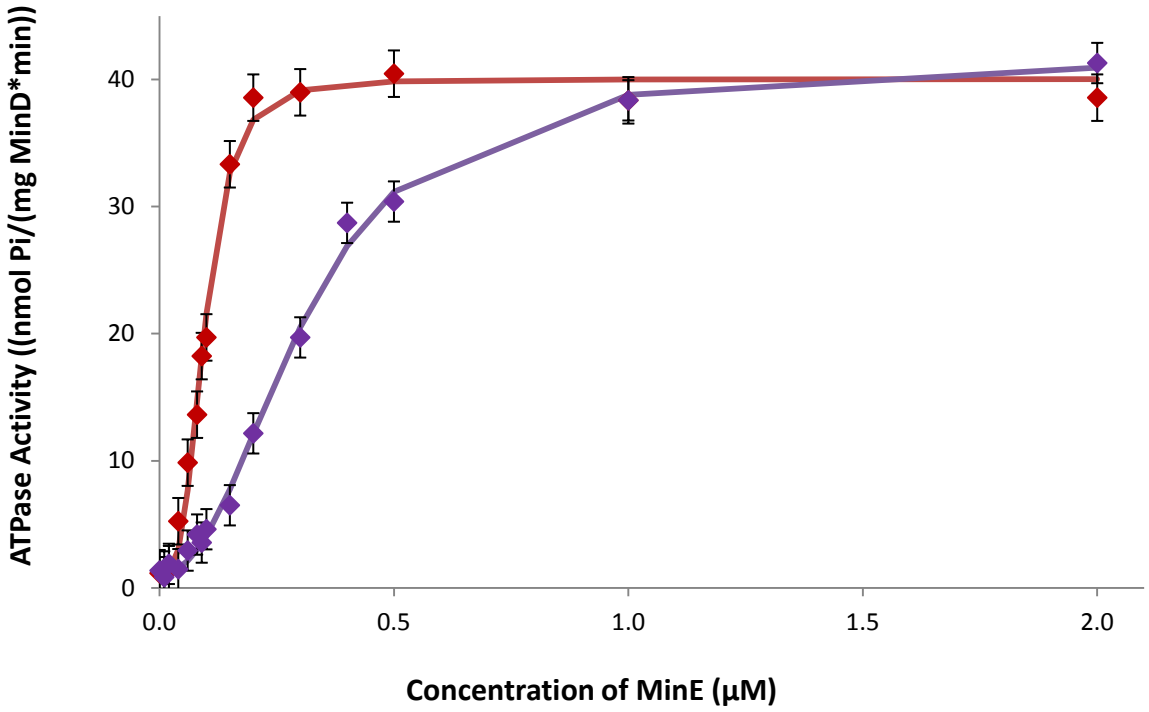

Figure 3.7: MinE(1-22) Shows Lower Affinity for MinD than Wildtype MinE. The data for full-length MinE is the same as that shown in Fig. 3.6 (red) together with data obtained using the N-terminal peptide MinE(1-22) in purple. The values obtained for the peptide for V_{max}, $K_{0.5}$ and h were 39.2 $\pm$ 2.3 nmol Pi/min/mgMinD, 0.5 $\pm$ 0.4 μM, and 2.2 $\pm$ 0.1 respectively.

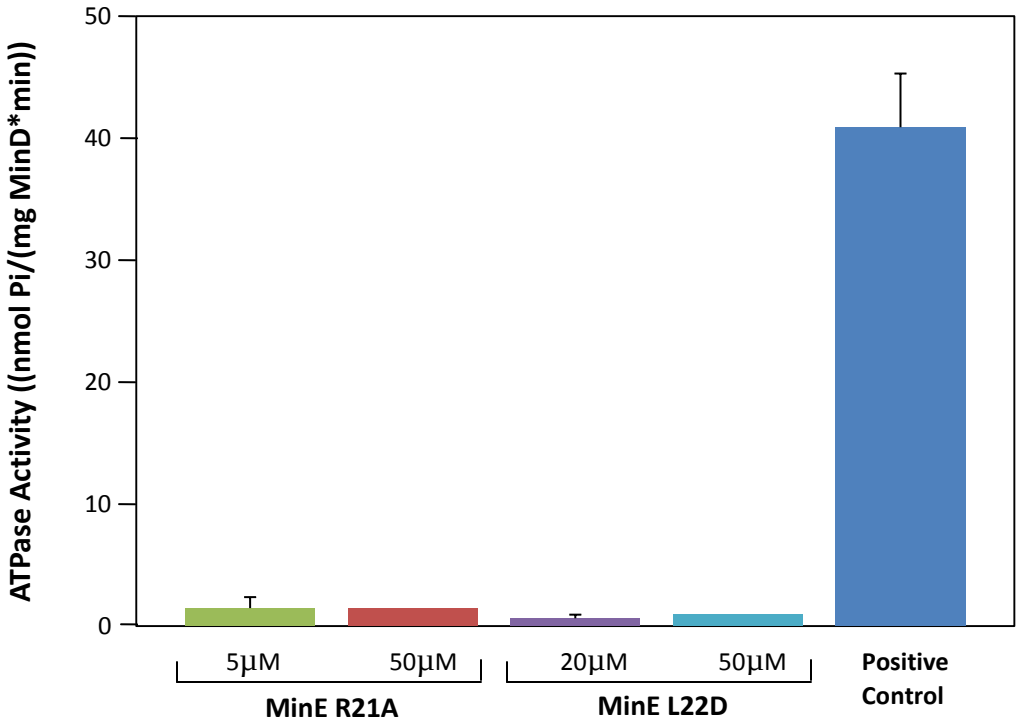

Figure 3.8: The MinE(1-22) L22D and MinE(1-22) R21A Mutant Peptides are Inactive. MinE(1-22) was used at 3µM as the positive control. All other reactions used mutant 1-22 peptides as indicated. These were inactive even at concentrations of 50µM.

Since the mutation of Leu22 to a negatively charged amino acid may have interfered with interactions involving MinD with adjacent residues, the less disruptive mutation of Leu22 to alanine was also tested. As shown in Figure 3.9, the effect of this mutation was less severe, with stimulation of MinD to maximal levels being possible at very high concentrations of MinE(1-22) L22A. The apparent affinity was 5 $\pm$ 3 µM, about ten times lower than that for MinE(1-22). The results indicate that not only is L22 important for stimulating ATPase activity of MinD, but it appears to be directly involved in MinD binding.

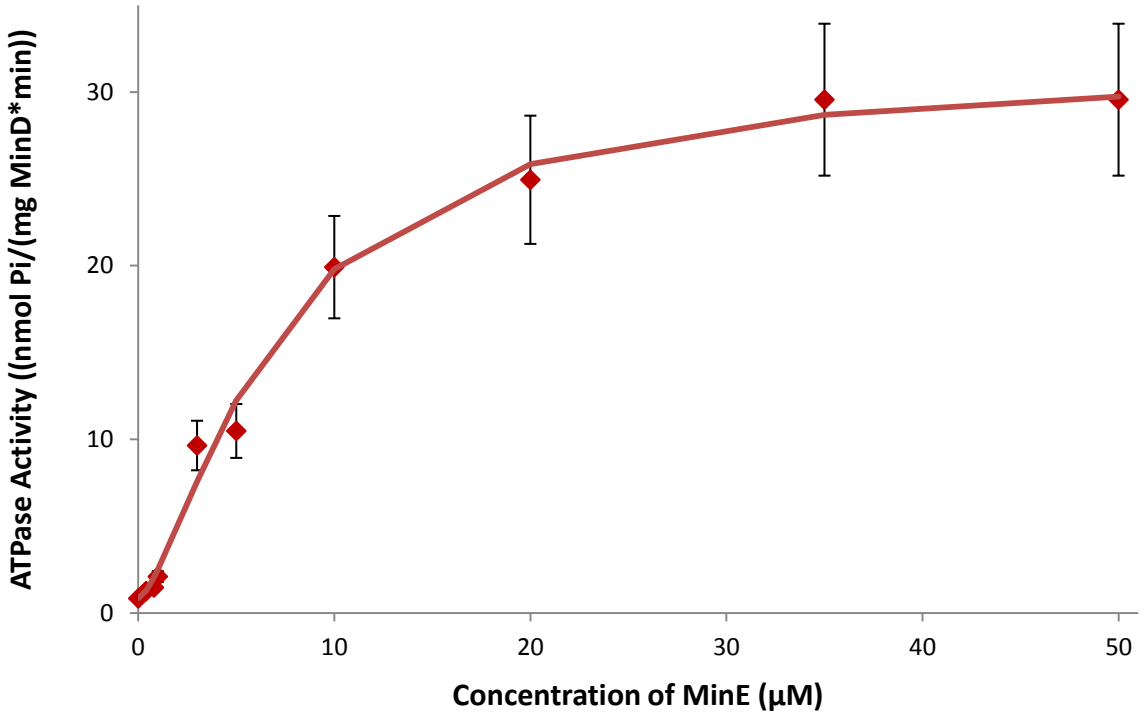

Figure 3.9: MinE(1-22) L22A Peptide Shows Lower Affinity for MinD than Full-length Wildtype MinE. The values obtained for V_{max}, $K_{0.5}$ and h were 35.4 $\pm$ 4.9 nmol Pi/min/mgMinD, 5 $\pm$ 3 μM, and 1.4 $\pm$ 0.1 respectively. The apparent affinity is approximately 10-times lower than MinE(1-22) (summarized in Table 3.1).

Another residue that was tested in this assay was R21, which had previously been shown to have reduced activity when mutated in the full-length protein (54). As this residue is also located in the β1-strand and not in a flexible loop region, the mutation may have introduced structural changes as well. However, when the mutation R21A was introduced into the unstructured MinE(1-22) peptide, no stimulation of MinD ATPase activity was observed, even when very high concentrations were used (shown in Fig. 3.8). Therefore this residue is also likely to be directly involved in interactions with MinD.

3.5: MinE(1-27) Behaves Like Full-length MinE

The results obtained so far show that two residues in structured regions of MinE, namely R21 and L22 appear to be involved in direct interactions with MinD. The ability of residues that are part of the dimeric MinE interface in the full-length protein to directly interact with MinD raises the possibility that other residue(s) outside of this region are also capable of participating in this interaction with MinD. Some evidence for this possibility is provided by the lower affinity of MinE(1-22) for MinD relative to that of the full length protein. Moreover, it has been shown that mutations at Ile25, but not Ile24, compromise binding of MinE(1-33) to MinD in a yeast 3-hybrid study (52). To test the importance of residues beyond the 22 residue N-terminal region of MinE to bind to MinD, a longer peptide (MinE(1-27)) was tested for its ability to stimulate MinD ATPase activity.

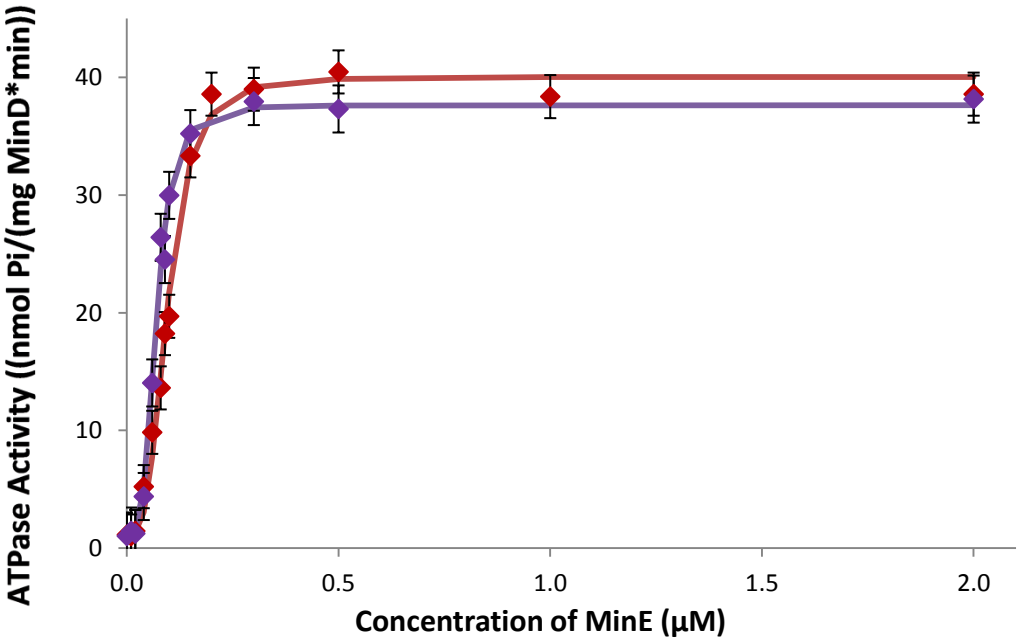

Figure 3.10: WT-like Ability of MinE(1-27) to Stimulate MinD Activity. MinE(1-27) data is shown in purple, and full-length MinE data (from Figure 3.6) in red. The values obtained for the peptide for V_{max}, $K_{0.5}$ and h were 36.2 $\pm$ 1.1 nmol Pi/min/mgMinD, 0.08 $\pm$ 0.02 µM, and 3.4 $\pm$ 0.7 respectively.

The results shown in Figure 3.10 reveal a rate profile for MinE(1-27) that is highly similar to that of the full-length MinE protein, with comparable V_{max}, $K_{0.5}$ and h values (summarized in Table 3.1). This indicates that one or more amino acids between residues 23-27 are also important for interactions with MinD. To test the specificity of this enhanced affinity, the activity of MinE(1-27) I25A and MinE(1-27) I24A were also tested in the MinD stimulation assay (Fig.3.11). As outlined in Table 3.1, a small reduction in apparent MinD binding activity was observed with the I25A peptide. However, if the more drastic mutation of Ile to Arg was introduced at these sites, a significant decrease in apparent affinity was observed, but only for the peptide containing this mutation at Ile25.

Table 3.1: Summary of Kinetic Parameters for MinE-Stimulated ATP Hydrolysis by MinD.

	$K_{0.5}$ (uM)	V_{max} (nmol P_i/min/mg MinD)	Hill Coefficient
WT	0.11 ± 0.02	37.5 ± 1.5	2.9 ± 0.3
1-22	0.5 ± 0.4	39.2 ± 2.3	2.2 ± 0.1
1-22 (R21A)	NA*	NA*	NA*
1-22 (L22D)	NA*	NA*	NA*
1-22 (L22A)	5 ± 3	35.4 ± 4.9	1.4 ± 0.1
1-27	0.08 ± 0.02	36.2 ± 1.1	3.4 ± 0.7
1-27 (I24A)	0.08 ± 0.04	37.5 ± 1.3	3.2 ± 0.5
1-27 (I25A)	0.12 ± 0.05	43.1 ± 6.1	2.6 ± 0.1
1-27 (I24R)	0.05 ± 0.01	39.9 ± 4.2	2.2 ± 0.7
1-27 (I25R)	3.8 ± 0.7	42.5 ± 1.6	1.5 ± 0.1

* – not active

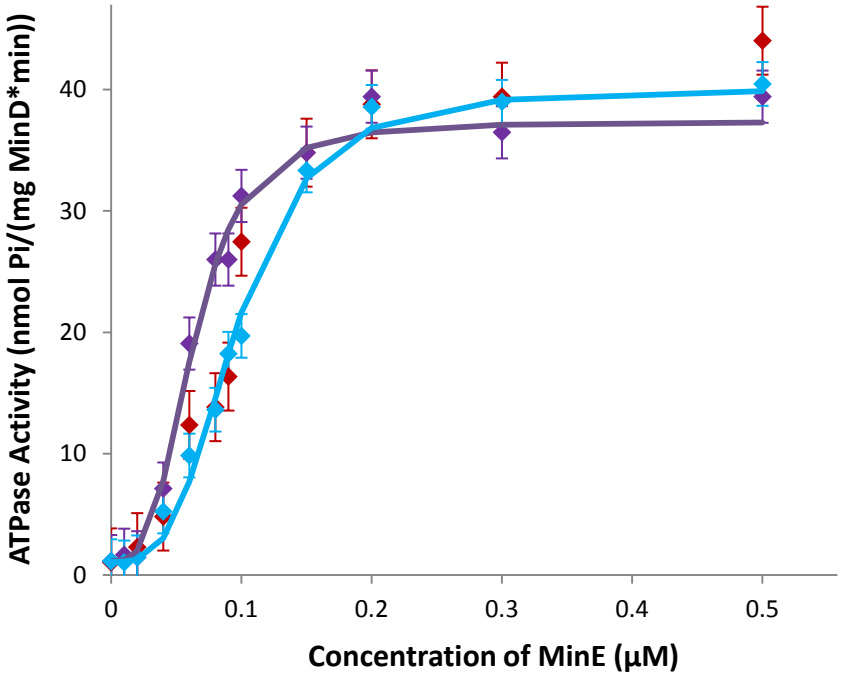

Figure 3.11: Stimulation of MinD ATPase Activity by MinE(1-27) I24A and MinE(1-27) I25A. MinE(1-27) I24A is shown in purple. MinE(1-27) I25A in red and WT in blue.

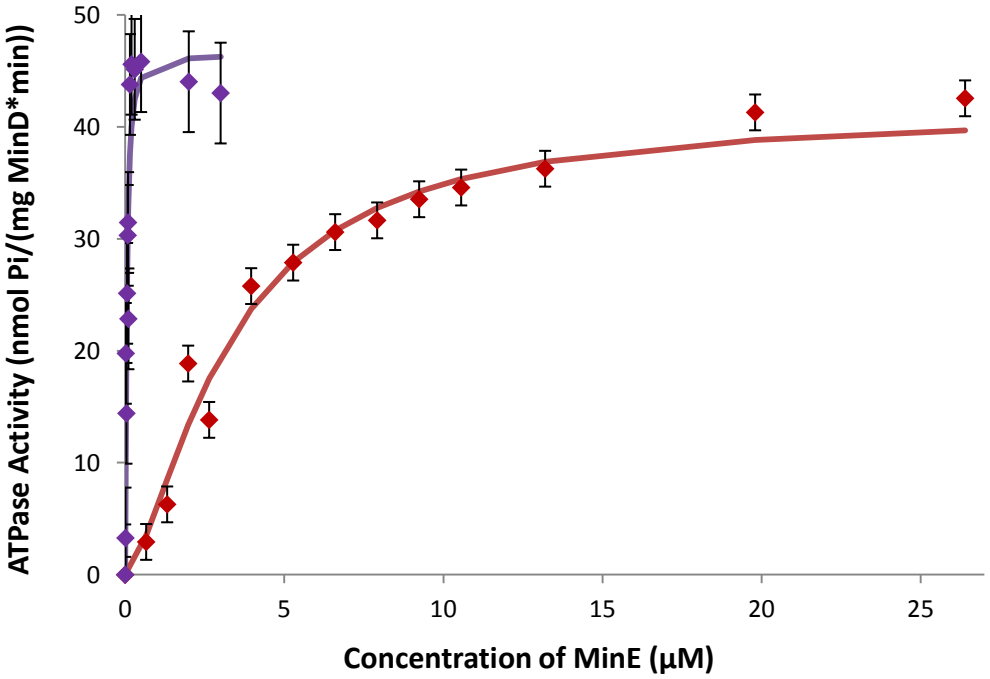

Figure 3.12: Residue 25 is Important for MinD ATPase Activity Stimulation. MinE(1-27) I24R is shown in purple and has a profile that is very similar to that of WT MinE(1-27). MinE(1-27) I25R is shown in red and has much lower apparent affinity for MinD.

As shown in Figure 3.12, MinE(1-27) I24R showed a kinetic profile that was virtually indistinguishable from that of the wild type peptide. In contrast, MinE(1-27) I25R showed much lower apparent affinity for MinD, suggesting that I25 also directly interacts with MinD.

3.6: Results Summary

In summary, the MinD ATPase assay has enabled us to identify residues in MinE that are directly involved in the interactions with MinD that stimulate its activity. Utilizing truncated versions of MinE that only contain the first 22 or 27 residues from the anti-MinCD domain, we were able to examine the function of the mutants without considering the effect of structure change. Novel findings arising from these experiments are:

- MinE(1-22) has lower affinity for MinD than full-length MinE but can stimulate MinD ATPase activity to the same maximal levels induced by full-length MinE levels.
- Residues important for stimulation of MinD ATPase activity on MinE are located within the first 27 residues.
- Residues Arg21 and Leu22 are directly involved in MinD interactions.
- I25 is also important for MinD interaction, but I24 is not.

The results that are indicated here show that residues which are not exposed in MinE appear to be directly involved in MinD-binding. In particular, L22 and I25 are buried inside the hydrophobic dimeric interface of MinE but are still important for stimulation of MinD ATPase activity. Thus, a conformational change in MinE is likely to take place before interactions with MinD can occur to expose these residues for interaction.

Chapter 4: Investigation of the Interaction Between MinE and Lipids

4.1: Lipid Vesicles Cause Conformational Changes in MinE

The results obtained with MinD activation by MinE peptides provide strong evidence that residues which are buried in the MinE dimer interface in the NMR structure directly interact with MinD. In addition, other data provided by solution NMR, analytical ultracentrifugation (54) and cross-linking (110) strongly indicate that the dimer does not dissociate when interacting with MinD. This suggests that there must be a dramatic conformational change of the MinE dimer that would allow these critical MinD binding residues to become accessible for these interactions. A mechanism for this transformation has been proposed based on the recent evidence that MinE may directly interact with anionic lipids (61). The lipid-protein interaction may provide the driving force for this conformational change of MinE.

To investigate the potential for interactions with lipid to induce a change in MinE structure, circular dichroism (CD) spectra were acquired in the presence and absence of lipid vesicles. Figure 4.1 shows that the CD spectrum of MinE in the presence of DOPG vesicles is significantly different from the spectrum acquired in the absence of lipids. The magnitude of the ellipticity as well as shape of the spectrum is significantly different from that acquired in the absence of lipids, with a new minimum at approximately 208 nm. These changes provide strong evidence that MinE undergoes a significant change in structure when bound to lipid vesicles comprised of DOPG, potentially reflecting an increase in α-helical structure.

Similarly, a structural change was also observed in CD spectra acquired for MinE in the presence of *E.coli* lipids. The spectrum for MinE with *E.coli* lipids showed some similarity to that with DOPG lipids, with a new minimum at ~210 nm, and larger ellipiticity overall relative to the lipid-free spectrum. However, the magnitude of the change was smaller than that seen for DOPG, potentially reflecting a larger proportion of MinE bound to DOPG than was bound to the *E.coli* lipid vesicles. Alternatively the differences in the spectra may arise from structural differences between the two vesicle-bound states.

Vesicles made from the zwitterionic lipid DOPC were also tested for the ability to bind MinE. As shown in Figure 4.1, the spectrum of MinE showed no difference in the presence and absence of DOPC vesicles. This demonstrates that MinE structure is influenced by anionic, but not zwitterionic lipids, potentially reflecting the absence of an interaction with the neutral lipid.

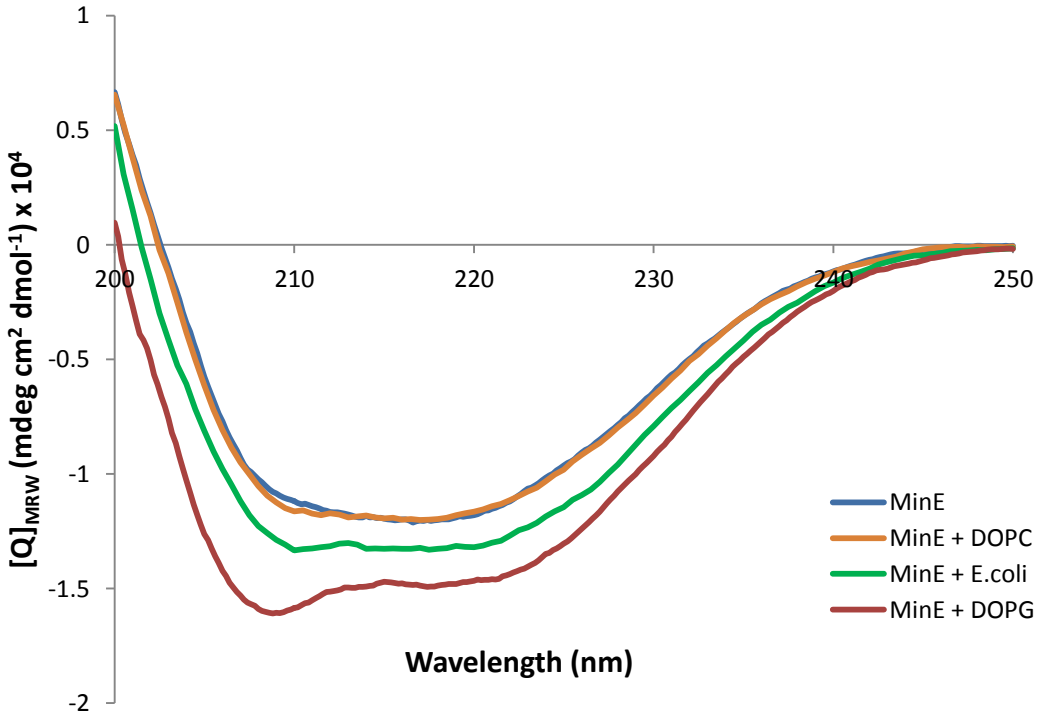

Figure 4.1: Change in MinE Secondary Structure Content Induced by Lipid Vesicles Containing Anionic Lipids. Solutions contained ~15 µM MinE in 10 mM Tris with/without 0.5 mg/mL lipids vesicles at pH 8.0.

4.2: The Role of Arg10 in MinE-Lipid Interactions

Previous studies have shown that the positively charged residues R10, K11, and K12 in *E.coli* MinE may be important for interactions with lipids (61) corresponding to R10, K11 and Q12 in *N.gonorrhoeae* MinE. R10 is the most highly conserved of these three residues, and is located in a flexible solvent-exposed loop between α1 and β1. To investigate the importance of this residue on the MinE-lipid interaction, the mutant R10A was studied by CD (Figure 4.2). As expected, the CD spectrum of R10A MinE was virtually superimposable with that of the wild-type protein, establishing that there was minimal structural perturbation introduced by this mutation.

The structure of R10A MinE was also examined in the presence of lipid vesicles as had been done for wild-type MinE. As expected, there was a smaller impact on the secondary structure of R10A MinE using *E.coli* lipids, as the spectrum looked almost the same as when there were no lipids present. Surprisingly, the mutant reproducibly showed a significantly larger change in secondary structure in the presence of DOPG, even though previous studies suggest that the loss of a positively charged residue at R10 should reduce the affinity of MinE for lipids. However, in those studies, a negatively charged residue was substituted for this arginine residue, which would have been inhibitory for any interaction involving negatively charged lipids. Our results suggest that the R10A mutant may instead have an increased affinity for lipid vesicles. Given the unique nature of the membrane-binding properties of this mutant, we decided to test its ability to stimulate MinD ATPase activity to gain insight into the role of this interaction on the Min protein cycle.

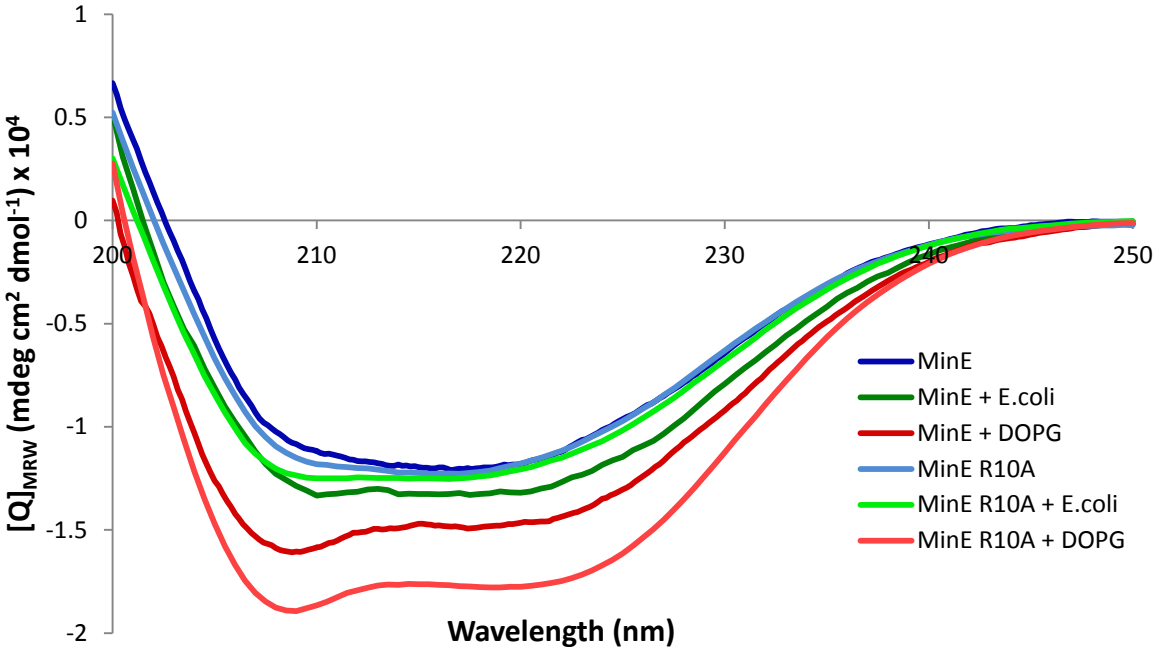

Figure 4.2: Changes in MinE R10A Secondary Structure Induced by Lipids is Different from that of Wildtype MinE. Solutions contained ~15 µM MinE in 10 mM Tris pH 8.0 with/without 0.5 mg/mL lipid vesicles made from DOPG or *E.coli* lipid extracts.

To determine if the observed differences in MinE lipid-binding properties will affect its ability to stimulate MinD ATPase activity, kinetic profiles were evaluated as a function of R10A and WT MinE concentrations. As shown in Figure 4.3, a graph of the initial reaction rate versus the concentration of MinE gives rise to very similar profiles for WT and R10A MinE when using *E. coli* lipid extracts as the bilayer medium. As summarized in Table 4.1, there is no significant difference in the hill equation parameters obtained for the two proteins. This suggests that the small difference in structure for wild-type and R10A MinE in the presence of *E.coli* lipids does not have an effect on MinD ATPase stimulation activity.

Table 4.1: Summary of Hill Equation Parameters for MinE Stimulated MinD-ATP Hydrolysis.

	$K_{0.5}$ (μM)	V_{max} (nmol P_i/min/mg MinD)	Hill Coefficient
MinE WT (DOPG)	0.11 ± 0.02	37.5 ± 1.5	2.9 ± 0.3
MinE WT (*E.coli*)	0.07 ± 0.01	31.2 ± 1.4	2.7 ± 0.4
MinE R10A (DOPG)	0.18 ± 0.03	49.2 ± 11.6*	1.9 ± 0.1
MinE R10A (*E.coli*)	0.09 ± 0.02	31.8 ± 1.7	2.8 ± 0.5
MinE E46A (DOPG)	0.08 ± 0.02	39.0 ± 0.5	2.6 ± 0.7

* - T-test analysis showed that this high V_{max} was statistically insignificant relative to wild-type.

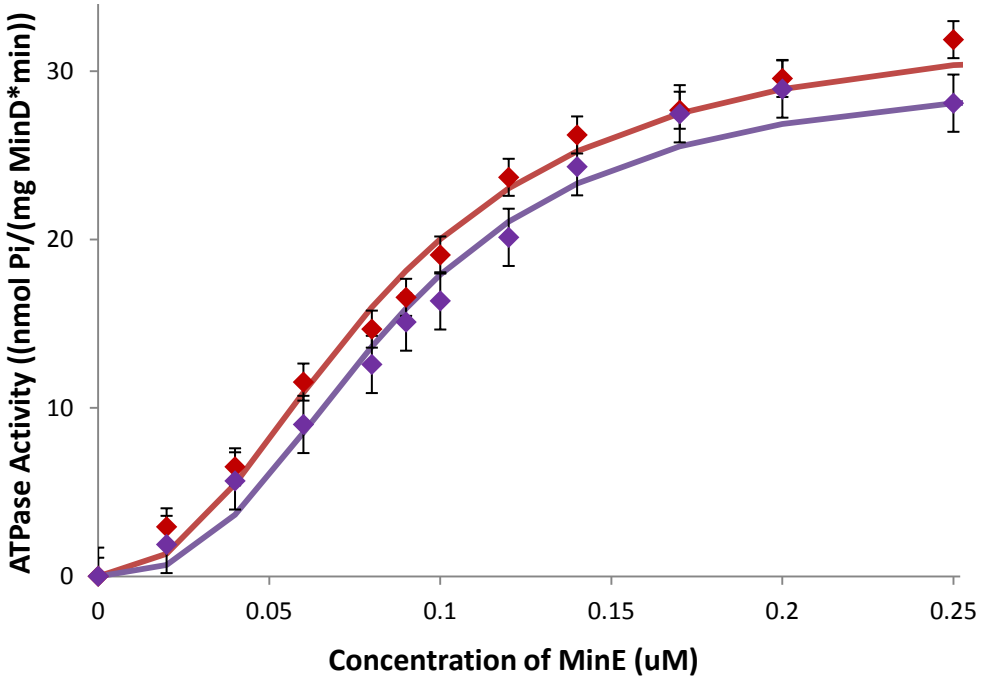

Figure 4.3: R10A has Similar Ability to Stimulate MinD Compared to Wildtype MinE in the Presence of *E. coli* Lipids. Reactions contained 2.7 μM MinD, 65 mM Tris-HCl, 50 mM KCl, 80 mM NaCl, 5 mM $MgCl_2$, 1 mM ATP, and 500 μg/mL *E.coli* lipids at pH 8.2. Lines represent the graph of the hill equation that provides the best fit to the experimental data for MinE (red) and R10A (purple) with parameters summarized in Table 4.1.

In contrast with the results obtained with *E. coli* lipids, ATPase assays using lipid vesicles comprised of DOPG showed a difference in MinD-stimulating activity between wild-type and R10A MinE. Specifically, a higher concentration of R10A MinE was required to attain half-maximal activity, with a $K_{0.5}$ value of 0.18 ± 0.03 μM (compared to 0.11 ± 0.02 μM for wild-type), suggesting a reduced affinity for MinD. In addition, the maximum ATPase activity (V_{max}) appeared to be higher for the mutant (Table 4.1). However, the large error in this value makes this difference insignificant as analyzed using a student's t-test.

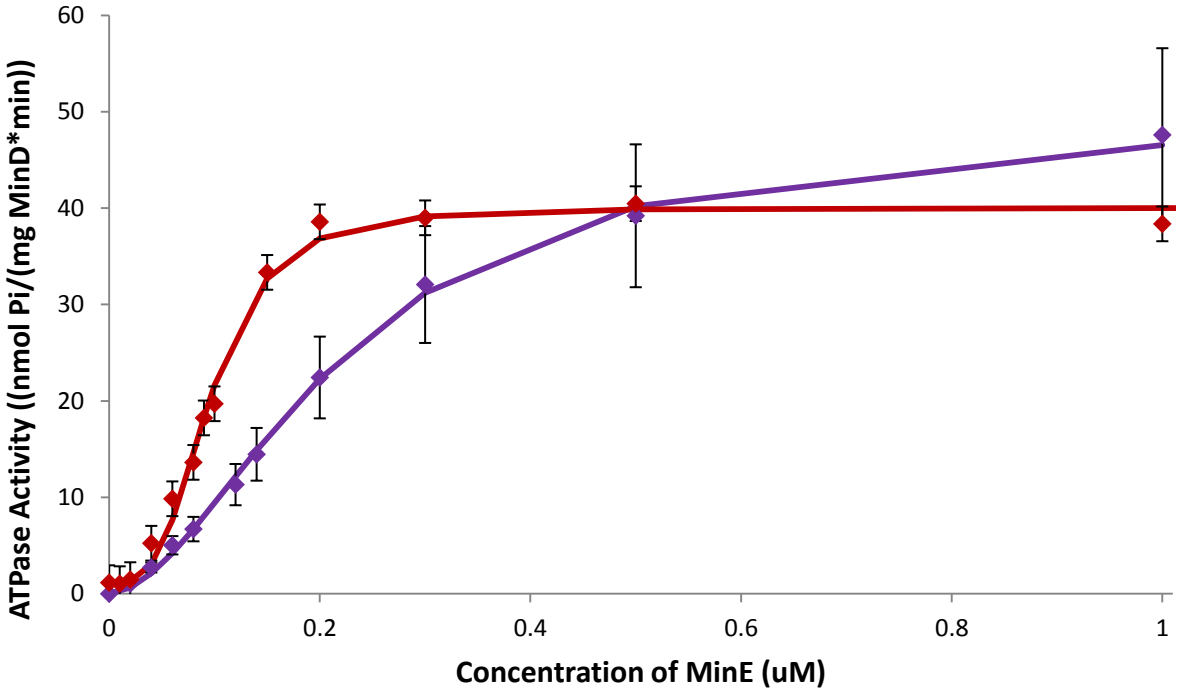

Figure 4.4: MinD-Stimulation Activity for R10A and Wild-type MinE with DOPG Vesicles. Reactions contained the same components as that shown in Figure 4.3 except the lipid vesicles were composed of DOPG. Data with wild-type MinE is shown in red and R10A in purple.

Thus far, the results indicate that a change in the interaction between MinE and the membrane can affect the affinity of MinE with MinD. Our results also confirm that R10 plays a

role in MinE-membrane interactions, although the difference in secondary structure content between the membrane-bound R10A and WT MinE suggest that this mutant might actually have a higher affinity for the membrane.

Overall, our results confirm that there is a direct interaction between MinE and the lipid membrane, and that this interaction gives rise to a structural transition. In order to gain a higher-resolution picture of this new structure I have worked towards the development of a membrane-bound MinE sample for analysis by solution NMR spectroscopy.

4.3: Evaluation of MinE E46A Membrane-Binding Properties

Previous NMR structures had been done with the MinE mutant E46A, which displayed structural properties that were the same as the WT protein, but had the more favourable solubility characteristics required for solution NMR. While it would be convenient to continue using this mutant for our studies, its membrane-binding properties had not been evaluated and therefore required confirmation of WT-like behaviour.

As shown in Figure 4.5, CD spectra of E46A MinE confirm that it has the same secondary structure as wild-type MinE, as had previously been demonstrated (60). Furthermore, the structural changes imparted by the addition of either *E.coli* or DOPG lipid vesicles that were observed for E46A MinE were identical to those obtained with the WT protein. Similarly, the ATPase assays also showed similar kinetic parameters for stimulation of MinD activity by E46A and WT MinE (Fig. 4.6 and Table 4.1). These results all confirm that the E46A mutant is a suitable substitute to use in NMR experiments of the lipid-bound state of MinE.

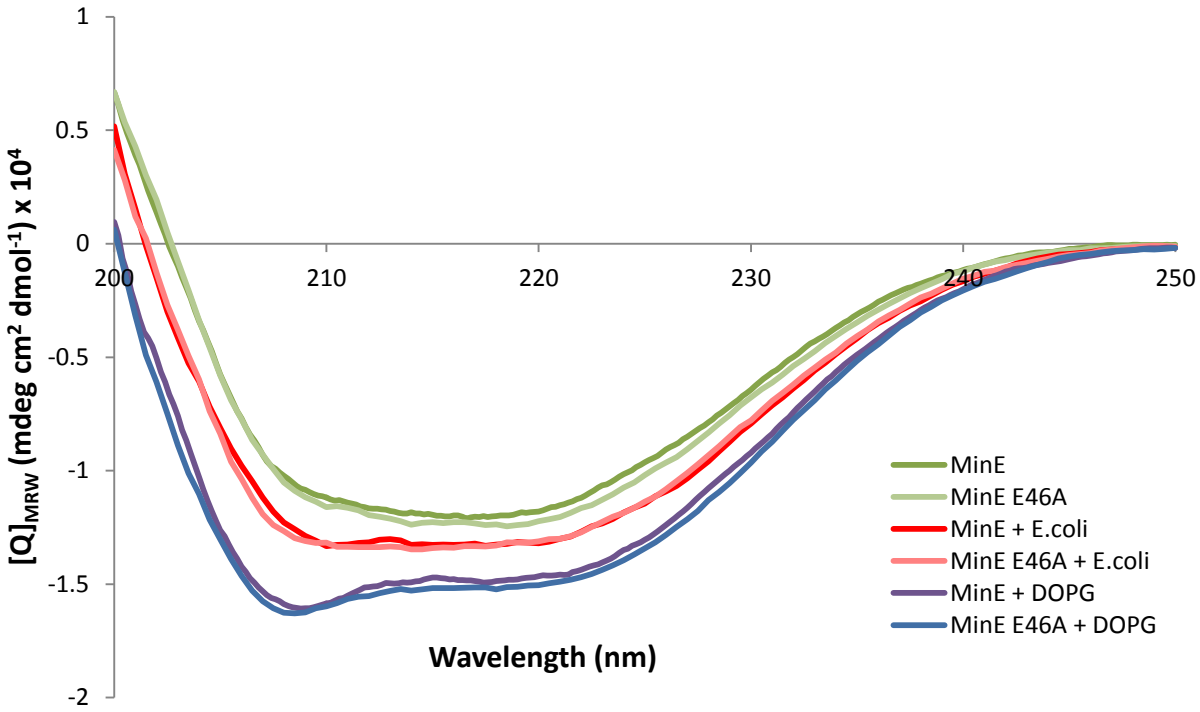

Figure 4.5: MinE E46A has a Similar Secondary Structure as Wildtype MinE in the Presence and Absence of Lipids. Solutions contained ~15 µM MinE in 10 mM Tris with/without 0.5 mg/mL lipids at pH 8.0.

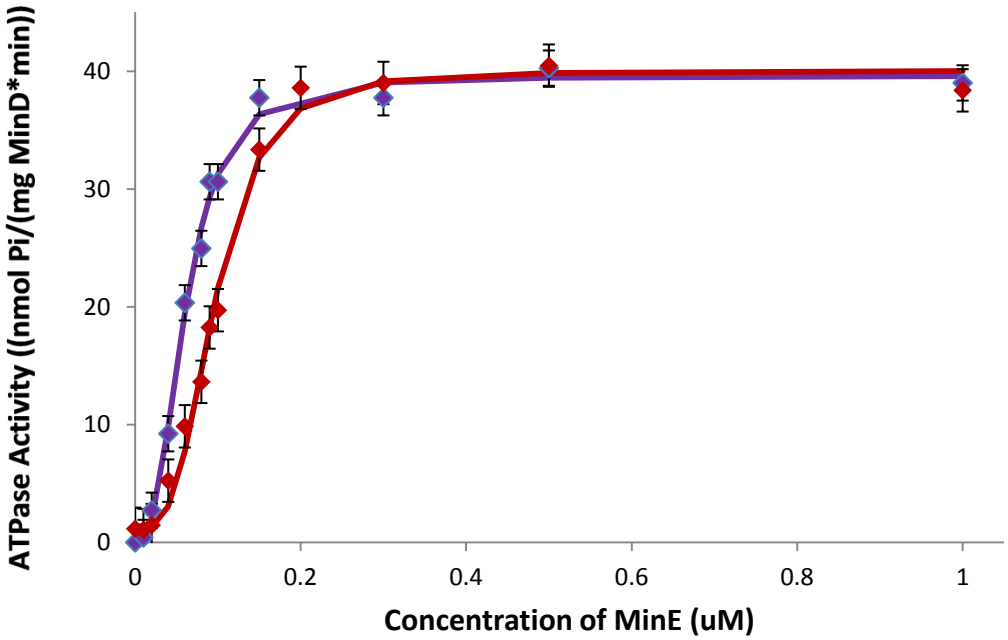

Figure 4.6: E46A MinE (purple) has a Similar Ability to Stimulate MinD ATPase Activity as Wild-type (red) MinE. Reactions conditions were the same as those used for previous assays with DOPG vesicles.

4.4: Solution NMR Investigation of the Membrane-Bound Form of MinE

4.4.1: Lipid Vesicles

We first evaluated the spectral quality of MinE in the presence of lipid vesicles using ^{1}H-^{15}N HSQC spectra. Although a lower pH is more ideal for this type of experiment since it reduces the rate of amide proton exchange with solvent water, we initially used a pH of 8.0 to minimize the tendency for aggregation.

The HSQC spectrum of MinE E46A was essentially the same as previously demonstrated (111), except some of the peaks from surface-exposed residues were not visible due to the rapid exchange between solvent and amide protons. As expected for a stably folded protein, the peaks in the spectrum were spread over a broad range of proton chemical shifts. Figure 4.7 shows the spectra of MinE E46A pH of 7.5 and 8.0 that were used as the reference spectra for all subsequent screening experiments of detergent/lipid conditions.

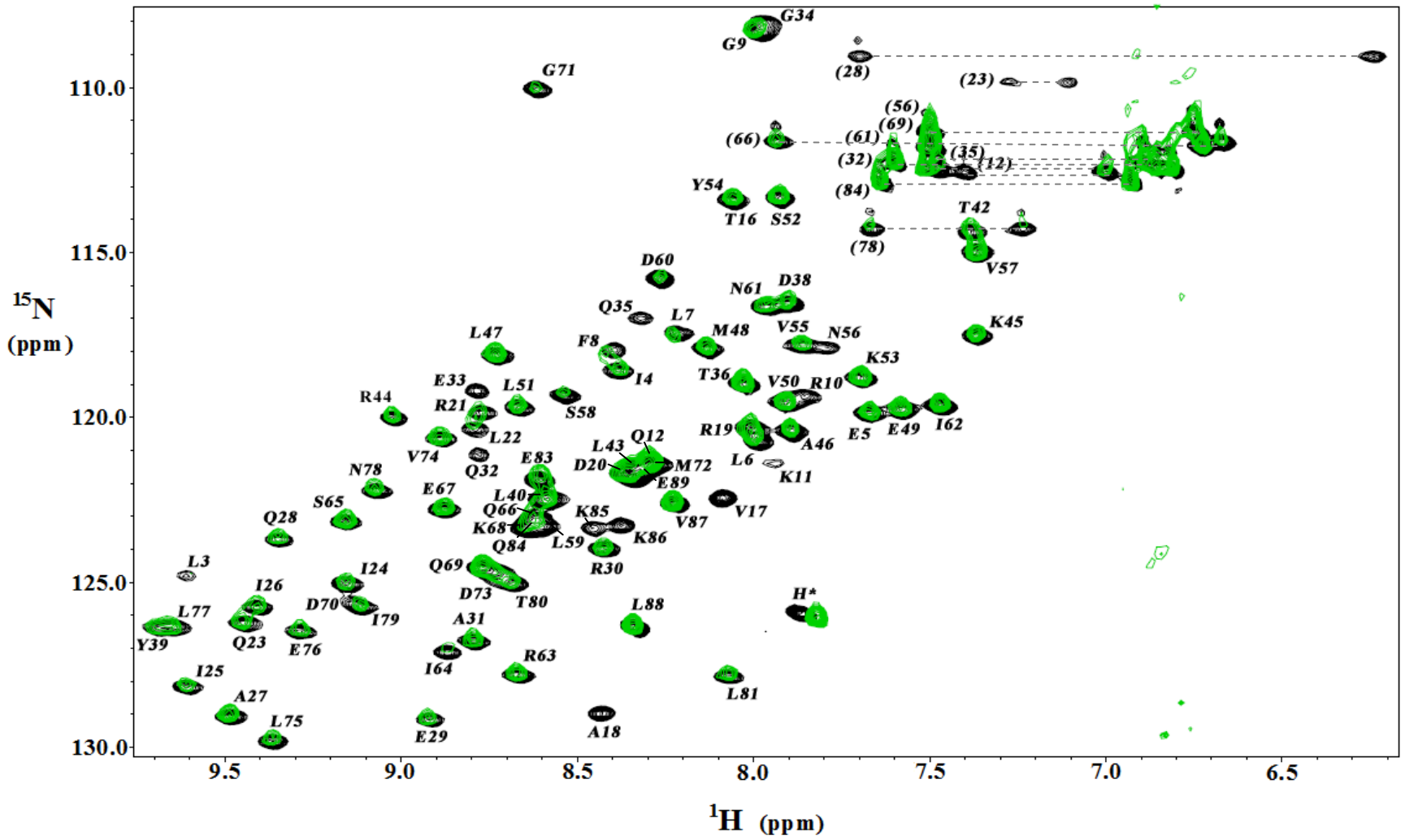

Figure 4.7: HSQC Spectra of MinE E46A. Spectra are shown for 0.2 mM E46A at pH 8.0 (green) and 0.45 mM E46A pH 7.5 (black) in the presence of 10 mM Tris and 100 µM EDTA. Peaks from the histidine tag are labeled with an *asterisk* and Gln/Asn side chain peaks are connected with *lines*. Note that the E46A reference spectra will be drawn in green in all subsequent figures.

An HSQC spectrum of 0.2 mM E46A in the presence of 8.2 mg/mL small unilamellar vesicles comprised of DOPG (a lipid to protein ratio higher than what was used in CD to ensure acquisition of the lipid-bound state) was acquired and superimposed with the spectrum of E46A in the absence of lipids (Fig. 4.8). However, only a very small subset of the expected peaks from backbone resonances were observed (~6 out of 84), and these were generally broad in appearance with low signal to noise ratio. The loss of most of the peaks was likely due to the strong association of E46A with the DOPG vesicles, leading to the formation of macromolecular complexes that are too large to be seen by solution NMR.

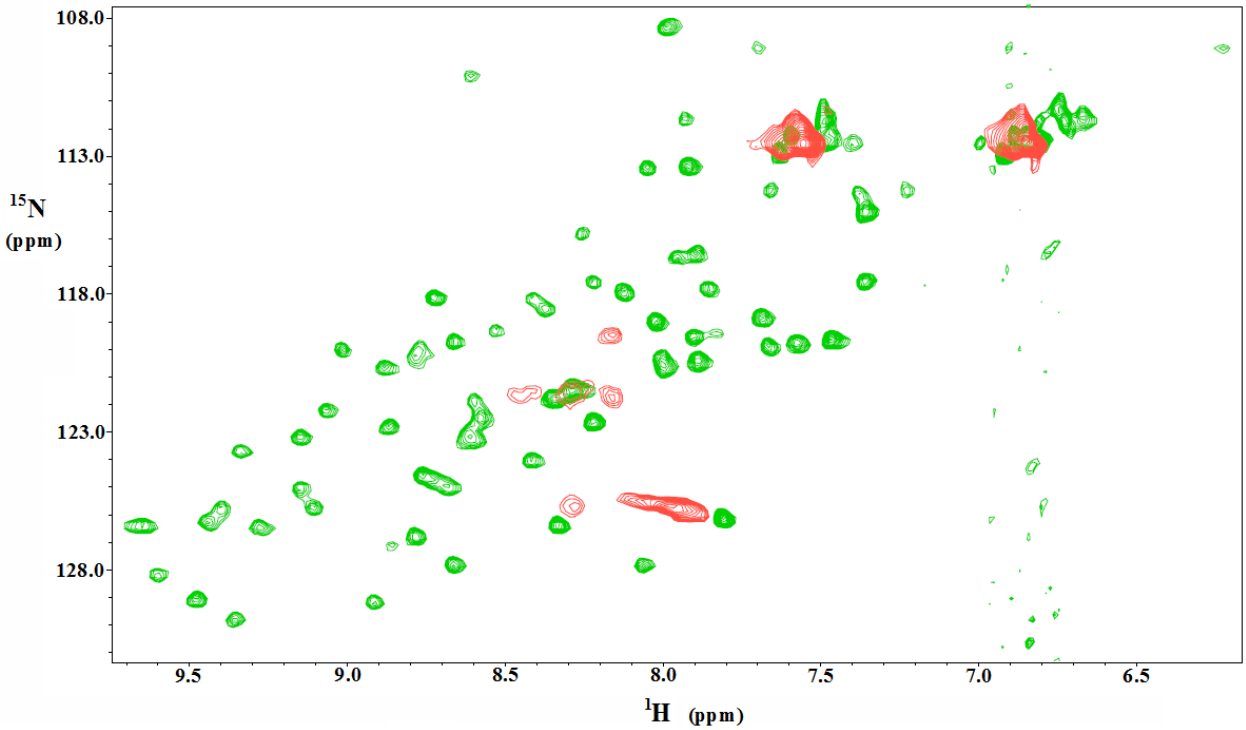

Figure 4.8: HSQC Spectrum of E46A MinE with DOPG (red) Superimposed on the E46A Reference Spectrum (green). Both samples contain 0.2 mM E46A MinE in 10 mM Tris, and 100 µM EDTA, pH 8.0, with the sample for the red spectrum also including 8.2 mg/mL DOPG.

Since MinE E46A shows smaller changes in secondary structure with *E. coli* lipids, it may have a lower affinity for this membrane, potentially giving rise to more rapid binding dynamics that would favour detection of signals from affected residues. As shown in Figure 4.9, more peaks were present in this spectrum than with DOPG. However, the poor signal to noise in the spectrum hindered quantitative comparison of relative peak intensities between the two samples to be carried out accurately, preventing the identification of residues with differential peak broadening from this spectrum.

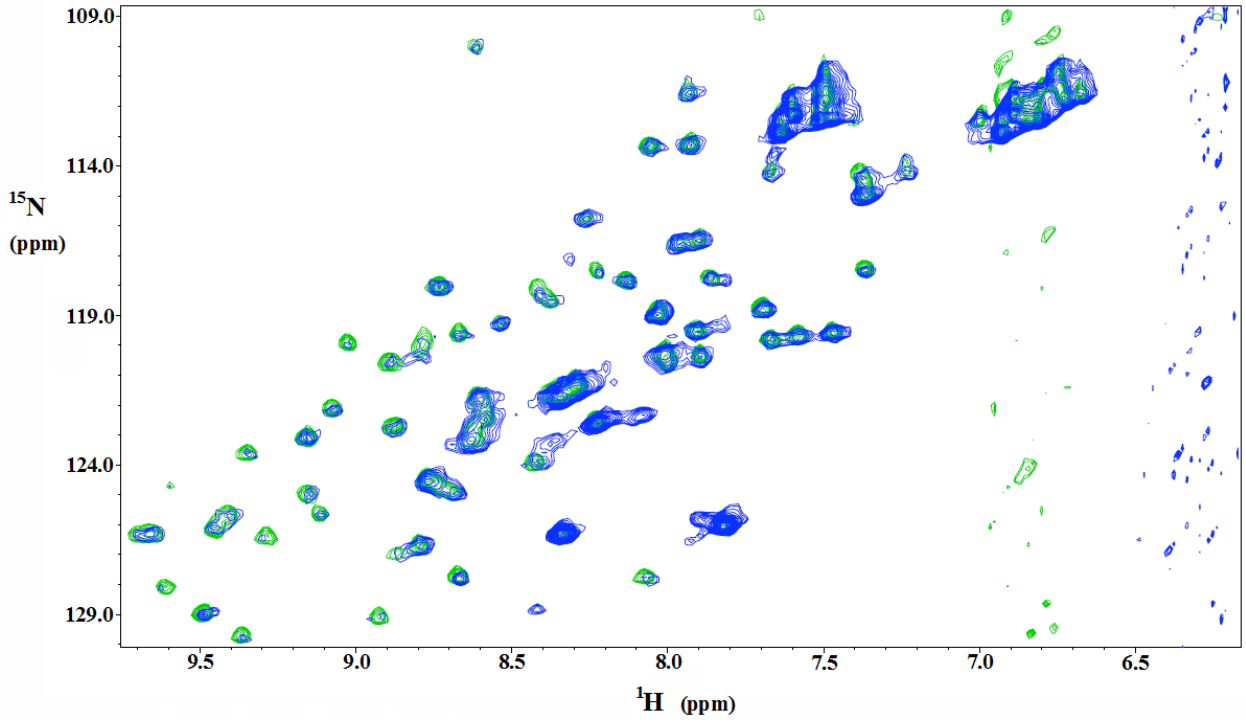

Figure 4.9: HSQC Spectrum of MinE E46A (green) with *E. coli* Lipids (blue). The spectrum in blue was acquired with 0.5 mM E46A in the presence of 7.0 mg/mL *E.coli* lipids.

In order to improve the signal to noise of the spectrum in the presence of lipids and determine if there was a variable change in signal intensity for different residues in MinE, the

previous experiment was repeated using a lower concentration of *E.coli* lipids (0.06% w/v). The pH of the solution was also decreased to 7.5 to improve spectral quality by inhibiting exchange between amide and solvent water protons. As shown in the Appendix (Fig. A2), the spectrum acquired in the presence of this lower concentration of *E.coli* lipids was highly similar to MinE E46A. Most importantly, peak intensity ratios between spectra with and without *E. coli* lipids were uniform for all residues in MinE. This suggests that the only part of MinE that can be seen in the spectrum is the fraction that is not bound to the lipid vesicle, and that no localized change in chemical shifts or peak intensities can be used to help characterize the lipid-bound state of E46A MinE.

4.4.2: Bicelles

As described in Section 1.13, small isotropic bicelles are commonly used as a membrane mimetic medium for solution NMR studies of membrane-associated proteins. Since MinE appears to associate strongly with the membrane, the bilayer encapsulated by the bicellar complex may be small enough to allow the spectrum of the lipid-bound state of MinE to be observed. The first bicelle that was tested was comprised of DMPC/CHAPS (with q = 0.3), a formulation that has been commonly used for solution NMR of membrane proteins (89,92). As shown in Figure 4.10, the NMR spectrum of 0.45 mM E46A in 100 mM DMPC/CHAPS bicelles showed strong signal to noise, with some differences in chemical shifts occurring for a subset of these residues. When mapped onto the structure of MinE E46A (Fig. 4.10), these shift changes localized to two regions; 1) the N-terminal α1-helix, with proximal residues on the β-sheets showing smaller shifts and; 2) along the length of the α2 helix.

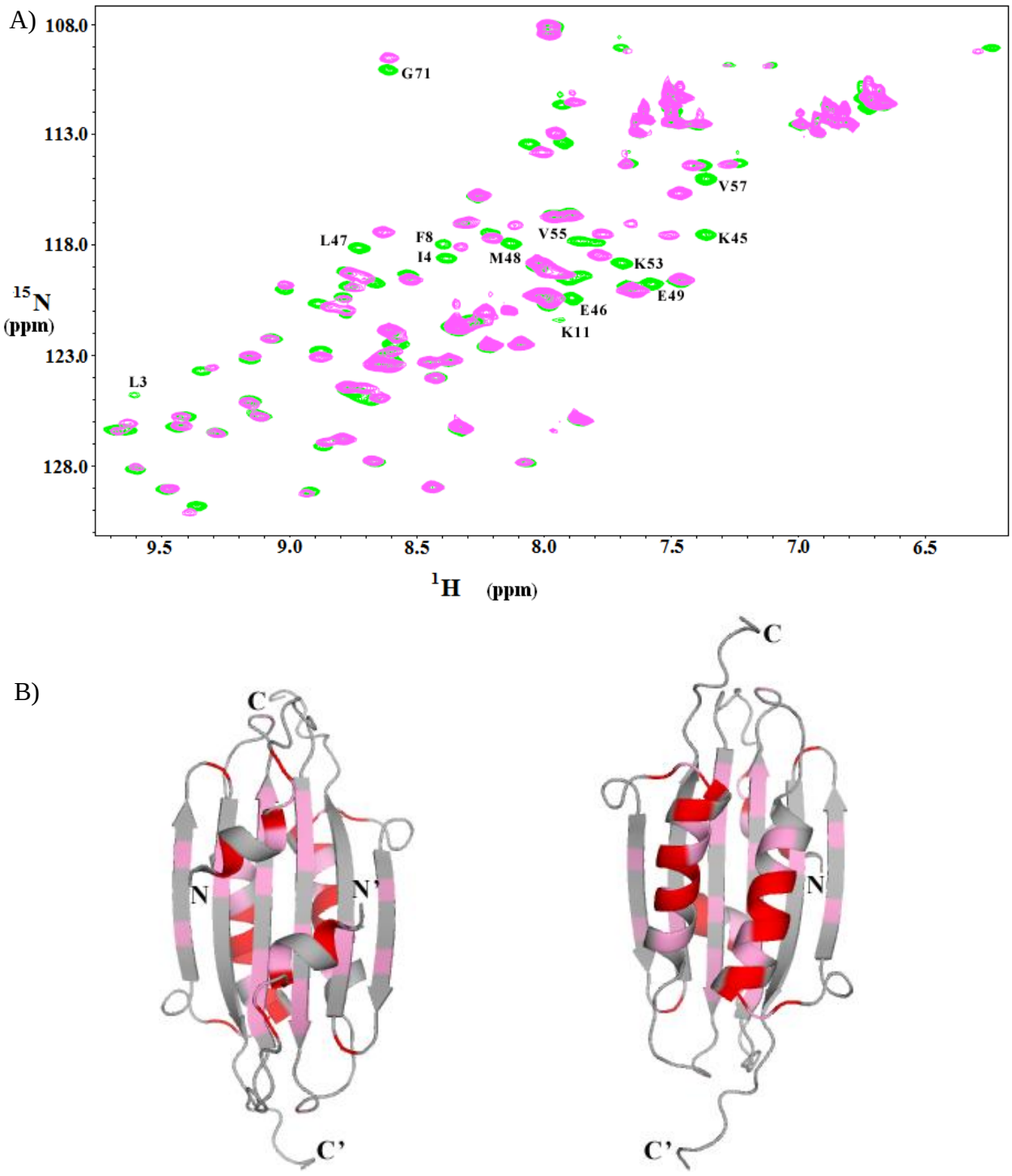

Figure 4.10: MinE E46A Interaction with Bicelles. A) HSQC spectrum of E46A at pH 7.5 in the absence (green) and presence of 100 mM CHAPS/DMPC bicelles with a molar ratio of 0.3:1 (pink). Peaks completely shifted from their positions in the reference spectrum are labeled. B) Chemical shift changes are mapped onto the structure of MinE E46A. Peaks that are displaced to a distinct position in the spectrum are shown in red, while those peaks that showed smaller shifts (*i.e.* could still be correlated with the peak in the reference spectrum) are shown in pink.

Although these results suggested that E46A MinE could be binding to bicelles, a significant amount of monomeric CHAPS also exists in equilibrium with the bicelle-bound state, raising the possibility that the observed changes were the result of an interaction with these detergent monomers. To test this idea, an HSQC spectrum of E46A MinE was acquired in the presence of 3 mM CHAPS, the approximate concentration of monomeric detergent expected to be in the bicelle solution (89-91). This spectrum showed chemical shift changes in the same subset of residues that showed changes in the presence of bicelles (Fig. 4.11), although the magnitude of these shifts was not as large with the detergent alone. This suggested that the spectrum of MinE E46A in the presence of the CHAPS/DMPC bicelles did not purely reflect the spectrum of the bicelle-bound state.

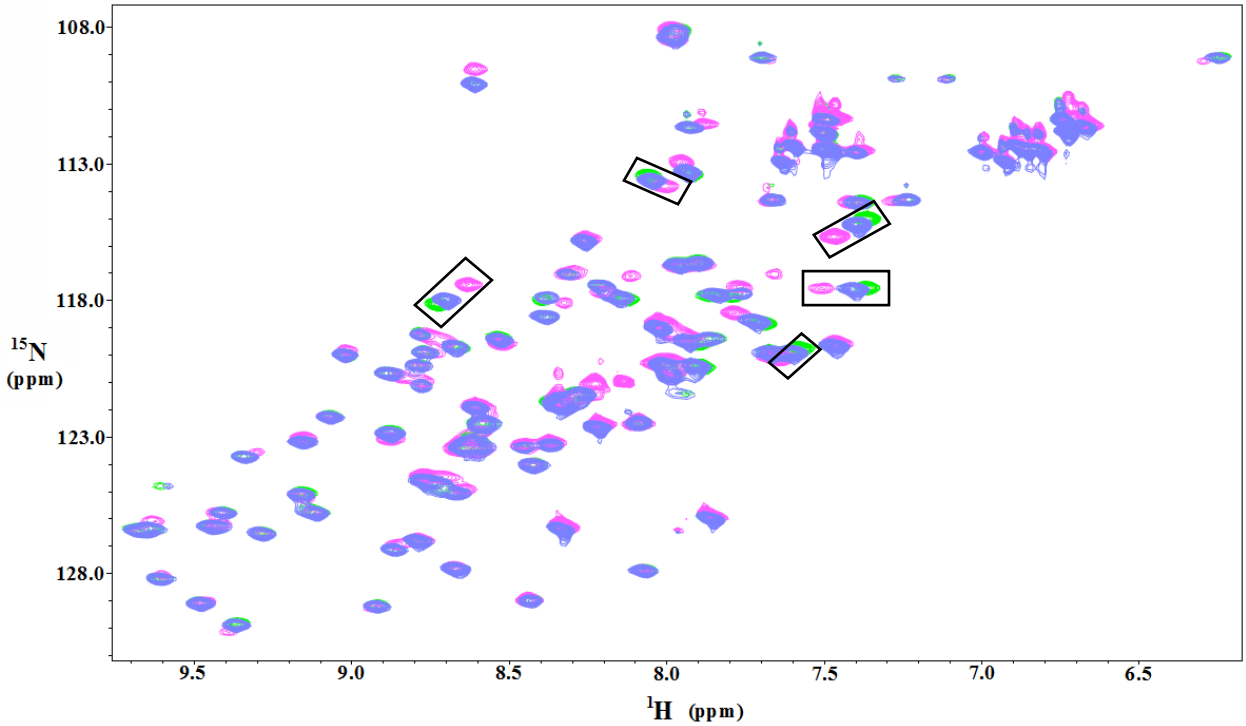

Figure 4.11: Comparison of the MinE E46A Interaction with CHAPS/DMPC Bicelles versus CHAPS Alone. HSQC spectrum of E46A at pH 7.5 with bicelles from Fig. 4.10 (pink), and with sub-micellar CHAPS (3 mM, purple) superimposed on the spectrum of detergent/lipid-free E46A (green). Some of the peaks that show intermediate chemical shift changes with the CHAPS solution are highlighted with boxes.

Since interactions with free CHAPS seemed to be making contributions to the observed NMR spectrum, we decided to use the short-chain lipid dihexanoyl-phosphatidylcholine (DHPC(C6)) in place of CHAPS for the bicelles. The difference in the chemical structure of DHPC(C6) relative to the planar CHAPS molecule may reduce the tendency for the monomeric form to bind to hydrophobic patches on MinE, potentially allowing the bicelle-bound state to be observed. As shown in Figure 4.12, the spectrum obtained for E46A in the presence of DMPC/DHPC(C6) bicelles only showed sharp peaks for residues from the C-terminus (residues 87 – 89, plus the single peak from the C-terminal H-tag peak, along with very broad peaks from residues 84, 85 and 86 (Fig. A3)). This suggested that MinE did bind the bicelles, however, only the most mobile portion that is not associated with the bicelle is visible in the spectrum. Moreover, there was a significant amount of precipitation that occurred as soon as the bicelles were added to the E46A solution, reducing the amount of sample available for this interaction. Virtually identical results were also obtained when the slightly longer-chain dihepatanoyl-phophatidylcholine (DHPC(C7)) was used in place of DHPC(C6) (Fig. A3). These results suggest that while MinE might bind these bicelles without interfering effects from interactions with monomeric detergent, the bicelle-bound complex does not have favourable NMR spectral properties.

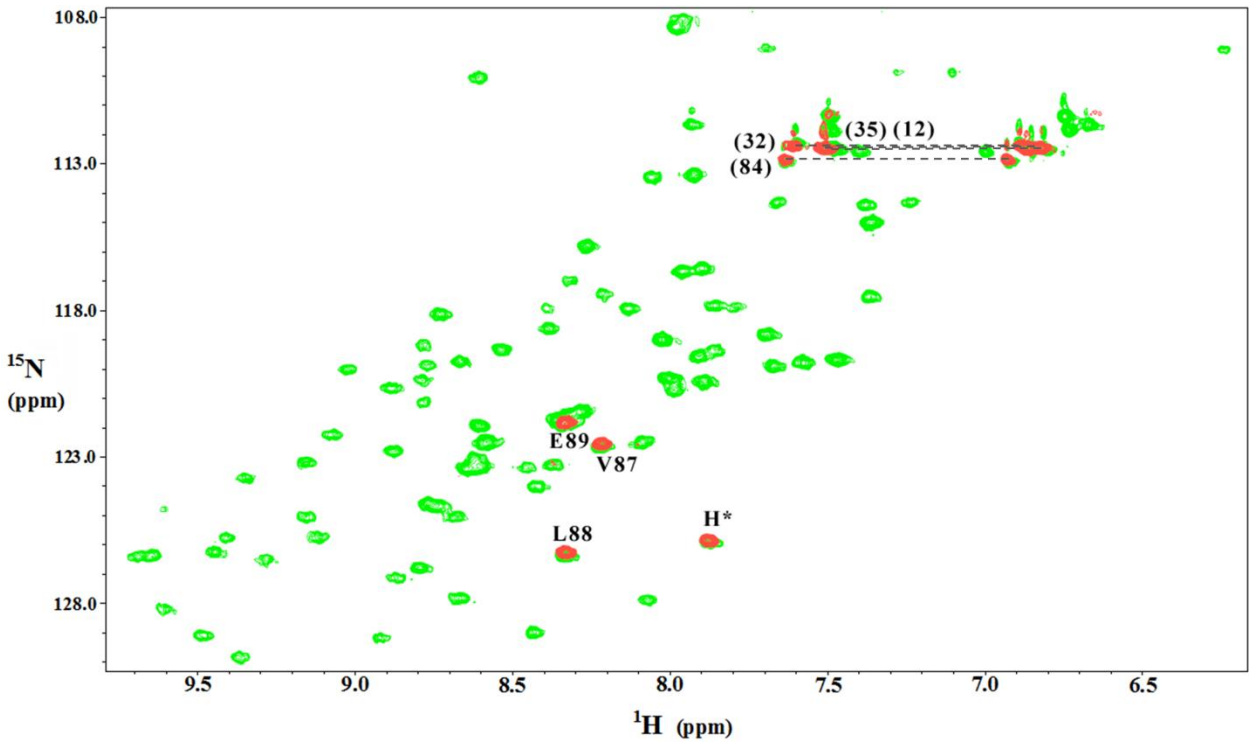

Figure 4.12: HSQC Spectrum of E46A MinE in DHPC(C6)/DMPC Bicelles. E46A at pH 7.5 with 0.30 mM E46A and 100 mM DHPC(C6)/DMPC bicelles at a q ratio of 0.3:1 is shown in red, superimposed on the reference spectrum in green. The peak from the histidine tag is labeled with an *asterisk* and Gln side chain peaks are connected with *lines*.

4.4.3: Detergents

The absence of peaks in the bicelle-bound MinE spectrum may be due to the size of the bicelle-protein complex. If this complex is very large (e.g. > 100 kDa) then it would not be possible to observe protein signals using the ^{15}N HSQC experiment. For this reason, we decided to explore the possibility that a smaller membrane-mimetic system, namely the detergent micelle, might create a membrane-bound structure of MinE that would be more amenable to analysis by solution NMR.

The first detergent tested for its compatibility with E46A MinE was dodecylphospho-choline (Fos-12), a zwitterionic amphiphile widely used in solution NMR of membrane-binding

proteins (90). However, when the HSQC spectrum of E46A was acquired with submicellar concentrations of Fos-12 (1 mM), signal intensities significantly decreased relative to the reference spectrum. Moreover, significant precipitation of MinE was observed upon addition of low concentrations of Fos-12 (Fig. 4.13), suggesting that this loss of signal was due to the reduction in concentration of soluble E46A. In addition, a few peaks also showed small chemical shift differences for residues around the ends of α2, with residues 39, 49, 54, and 57 showing the largest perturbations (Fig. 4.13). These results indicate that monomeric Fos-12 tends to interact with MinE, and may potentially lead to partial unfolding, reducing its solubility. This effect became more severe at higher Fos-12 concentrations, with micellar concentrations of Fos-12 essentially eliminating all but a handful of the most intense peaks (Fig. A4).

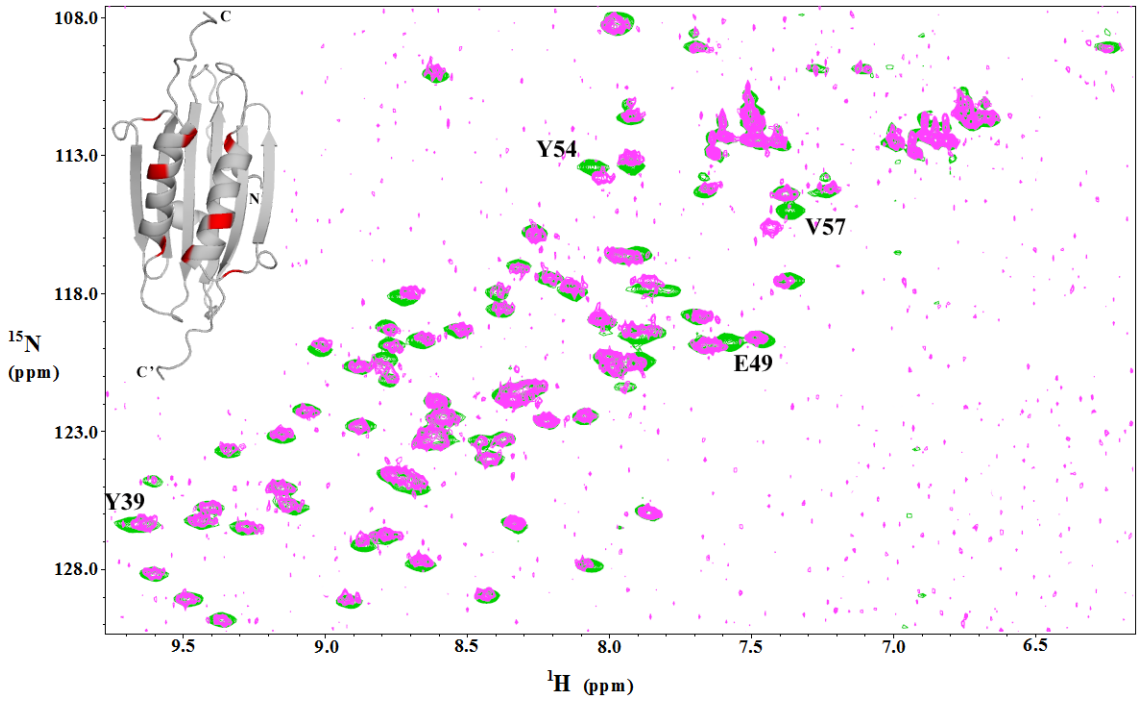

Figure 4.13: HSQC Spectrum of MinE E46A with a Sub-Micellar Concentration of Fos-12. The spectrum from 0.25 mM E46A at pH 7.5 in 1 mM Fos-12 (pink) is superimposed onto the reference spectrum (green). Assignments for peaks showing the largest perturbations are labeled in the spectrum, and highlighted in red in the MinE structure shown (inset).

We also evaluated the ability of the anionic detergent SDS to support the membrane-bound conformation of E46A MinE. Although SDS is often used as a denaturant, it has also been commonly used for examining membrane-protein interactions (112). However, similar to results obtained with Fos-12, submicellar concentrations of SDS (0.1 mM) led to a loss of signal intensity in many of the peaks in the spectrum, with the same subset of peaks showing small chemical shift changes as was seen with Fos-12 (data not shown).

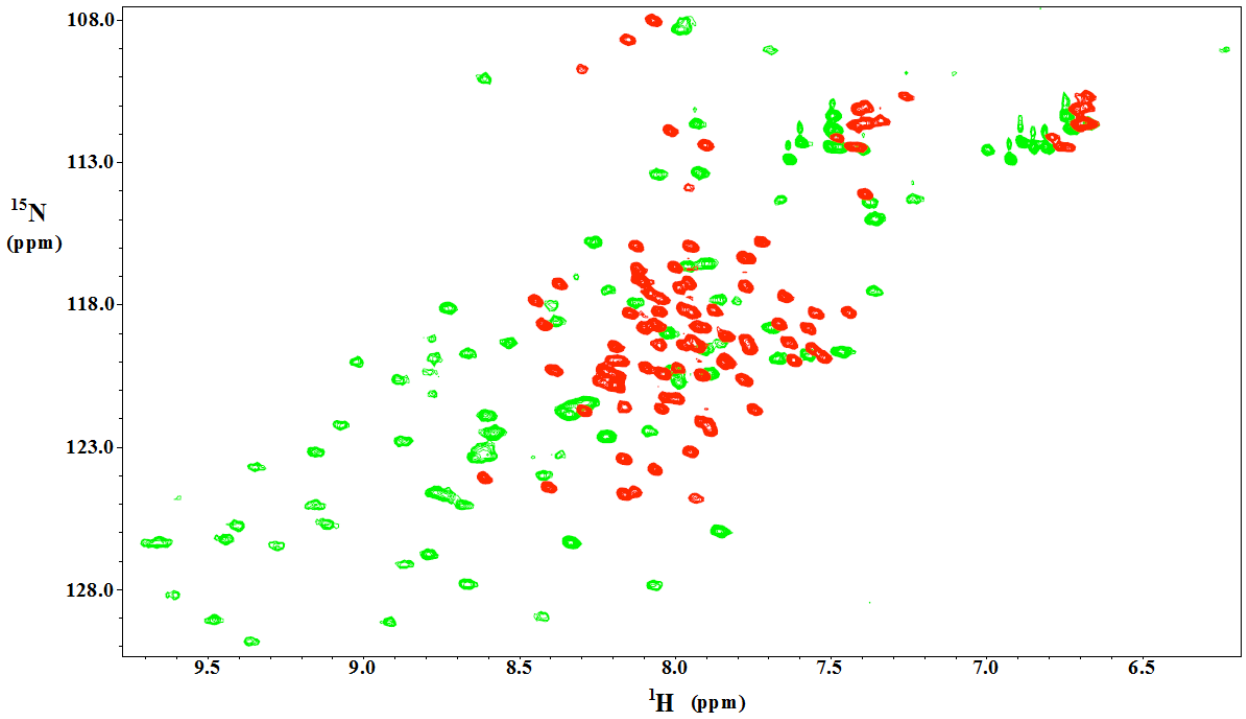

Figure 4.14: HSQC Spectrum of MinE E46A with SDS Micelles. 0.26 mM E46A at pH 7.5 in the same buffer with 40 mM SDS (red) is superimposed on the reference spectrum (green).

In contrast with the Fos-12 results, when the concentration of SDS was raised above its critical micelle concentration of 8.2 mM (89) peak intensities were restored, however, the appearance of the spectrum was completely different from the reference spectrum (Fig. 4.14).

Only approximately half the number of peaks were detected, and the range of chemical shifts in the proton dimension was significantly smaller. The appearance of the spectrum suggested that MinE was largely unfolded under these conditions, indicating that SDS was also not a suitable medium for solution NMR studies with MinE.

Since most of the results up to this point indicate that interactions with monomeric detergent could be interfering with our attempts to reconstitute the membrane-bound state of MinE, we decided to test other detergents with lower critical micelle concentrations. For example, hexadecylphosphocholine (Fos-16) has a cmc of 0.013 mM (91), along with a longer alkyl chain that may be too large for non-specific interactions with hydrophobic patches on MinE. Nonetheless, addition of 25 mM Fos-16 gave rise to significant precipitation of the sample, and most peaks in the corresponding spectrum were not visible, similar to what was seen with Fos-12 (Fig. A4).

Since dodecylphosphocholine detergents showed interactions with MinE that appeared to trigger aggregation, we decided to examine more physiologically relevant lysolipids to see if this problem could be avoided. However, in the case of lysomyristoyl phosphatidylcholine (LMPC) very similar results were obtained compared to those obtained with Fos-12, with sub-micellar concentrations uniformly decreasing signal intensities due to precipitation of MinE, although no change in chemical shifts were observed. At micellar concentrations signal intensity was lost for all backbone resonances, except for the last ~3 residues at the C-terminus, along with the His-tag peak. Although some of the missing peak intensities could be restored by recording these spectra at higher temperatures (Fig. 4.15B), many peaks were still missing and the quality of the spectrum was very low.

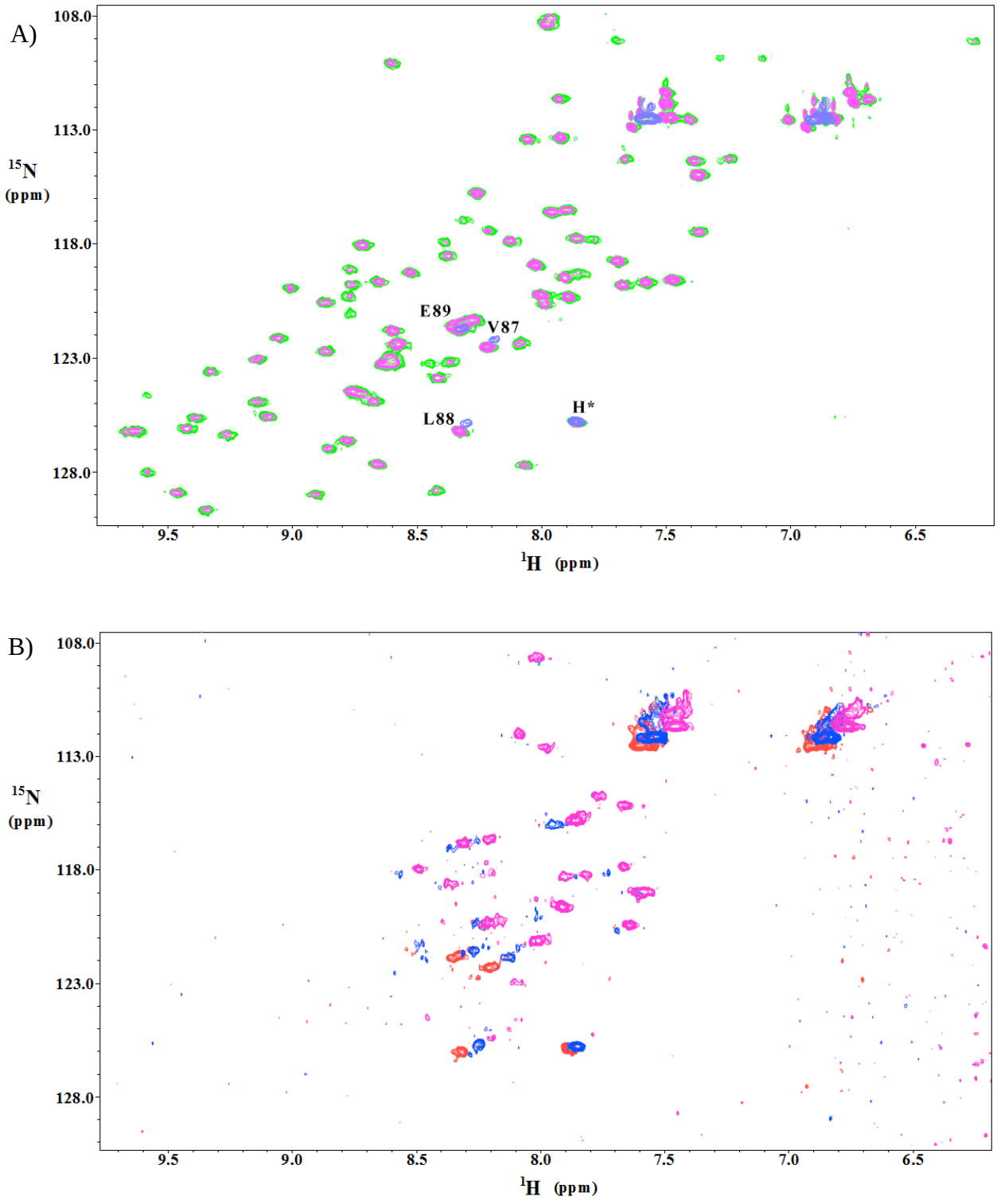

Figure 4.15: HSQC Spectra of MinE E46A in LMPC. A) E46A at pH 7.5 is shown in the absence of detergent (green), in 0.01 mM LMPC (pink), and 40 mM LMPC (blue). B) Spectra were acquired for the solution containing 40 mM LMPC at 25°C (red), 35°C (blue), and 50°C (pink). Note that temperature–dependent chemical shifts are expected (with a range of -16 to +4 ppb/°C for $^{1}H^{N}$ (113).

The anionic lysolipid LMPG was also tested in a similar set of experiments (Fig. 4.16), and showed a significant reduction in the number and intensity of peaks as well, similar to the results obtained with SDS. Like the SDS spectrum, there was a narrow range of proton chemical shifts, suggesting that this system was denaturing. To reduce the denaturing tendencies of this system, an equimolar amount of LMPC was subsequently added. Some chemical shift changes were observed in the new spectrum (Fig. 4.16), but the general quality of the spectrum remained poor, even when elevated temperatures were used (data not shown).

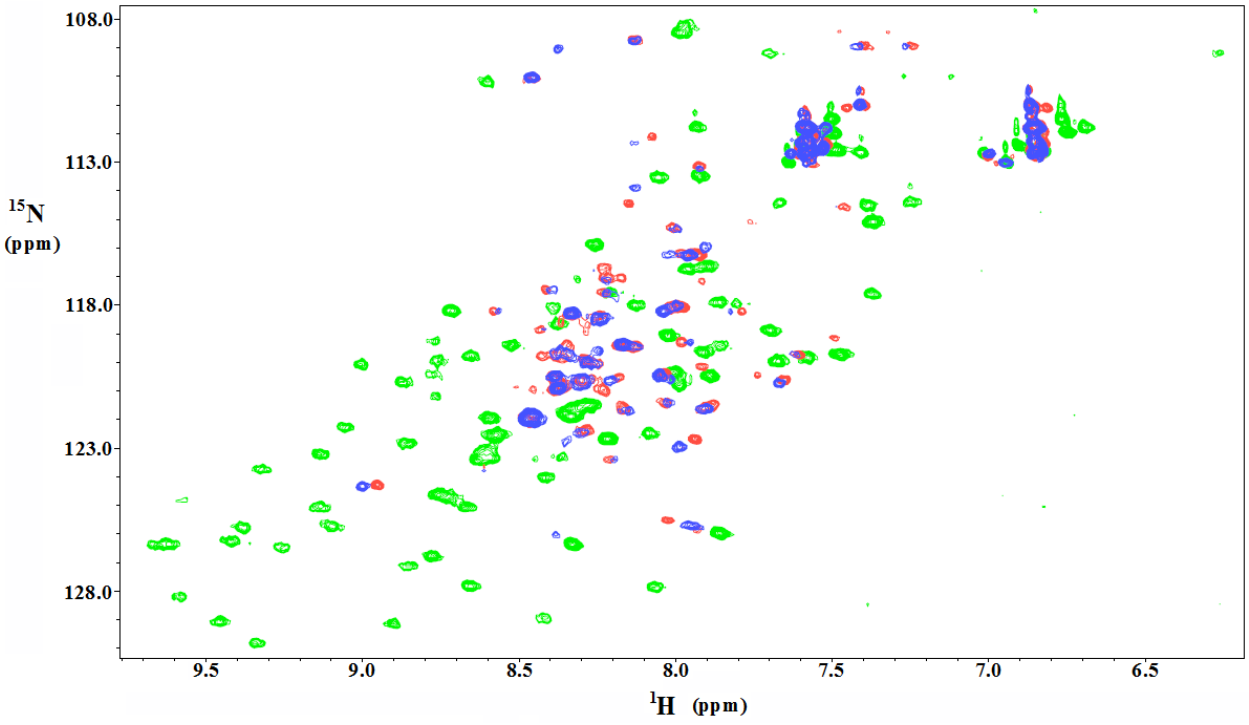

Figure 4.16: HSQC Spectrum of E46A MinE with LMPC/LMPG Micelles. The spectrum of 0.2 mM E46A in 30 mM LMPG without (red) and with 30 mM LMPC (blue) are overlaid with the reference spectrum (green).

Table 4.2: Summary of NMR Experiments Performed Using MinE E46A.

pH		No.	Lipid/Bicelle /Detergent Type	Protein Conc. (mM)	Lipid/Bicelle/ Detergent Conc.	Quality of ^{1}H-^{15}N HSQC Spectrum	Thesis Section	Temp. (^{o}C)
8.0	None	1	None	0.20	NA	Some peaks missing due to solvent exchange	4.7	25.0
	Lipid	2	DOPG	0.20	8.2 mg/mL	Many peaks missing, some shifts & peak broadening	4.8	
		3	E.coli	0.50	7.0 mg/mL	Peak broadening, low signal to noise	4.9	
7.5	None	4	None	0.45	NA	Good, more peaks visible than in (1)	4.7	
	Lipid	5	E.coli	0.45	0.06% (w/v)	Similar to (5)	A2	
	Bicelles	6	CHAPS/DMPC	0.45	100 mM (q = 0.3)	Shift in some peaks	4.10	
		7	DHPC(C7)/DMPC	0.30	80 mM (q = 0.3)	Very few peaks visible	A3	
		8	DHPC(C6)/DMPC	0.30	100 mM (q = 0.3)	Very few peaks visible	4.12, A3	
	Detergents	9	CHAPS	0.43	3 mM	Shift in some peaks	4.11	
		10	Fos-12	0.25	1 mM	Slight peak shifts, poor signal to noise	4.13	
		11	Fos-12	0.25	10 mM	Very few peaks visible	A4	
		12	Fos-16	0.25	25 mM	Very few peaks visible	A4	
		13	SDS	0.26	0.1 mM	Slight peak shifts, poor signal to noise	NS*	
		14	SDS	0.26	40 mM	Some peaks missing, lots of peak shifts	4.14	
		15	LMPC	0.31	0.01 mM	Poor signal to noise	4.15A	
		16	LMPC	0.31	40 mM	Very few peaks visible	4.15A	
		17	LMPC	0.26	40 mM	Very few peaks visible	4.15B	
		18	LMPC	0.26	40 mM	Very few peaks visible	4.15B	35.0
		19	LMPC	0.26	40 mM	Very few peaks visible	4.15B	50.0
		20	LMPG	0.23	30 mM	Some peaks missing, lots of peak shifts	4.16	25.0
		21	LMPC/LMPG	0.23	30 mM (LMPC) 30 mM (LMPG)	Some peaks missing, lots of peak shifts	4.16	
		22	LMPC/LMPG	0.23	30 mM (LMPC) 30 mM (LMPG)	Some peaks missing, lots of peak shifts	NS*	35.0

NS* - Not Shown

4.5: Results Summary

In summary, structural changes in MinE in different lipid environments have been observed using CD. Our results indicate that MinE interactions with membranes that contain anionic lipids lead to conformational changes in MinE. ATPase activities on wild-type MinE showed higher ATPase stimulation (V_{max}) in the presence of DOPG vesicles than *E. coli* lipids. Moreover, the mutant R10A which showed larger structural perturbations in DOPG than wild-type MinE showed lower affinity for MinD. Furthermore, CD and ATPase experiments have also shown that the lipid-binding behaviour of E46A MinE is virtually identical to that of wild-type MinE and was therefore used for solution NMR experiments in place of wild-type.

We subsequently tested a wide range of membrane-mimetic media to identify a system capable of reconstituting the membrane-bound form of E46A MinE suitable for study by solution NMR. As outlined in Table 4.1, conditions that gave rise to micelle, bicelle or vesicle-bound MinE did not give rise to NMR spectra of sufficient quality for further structural characterization. In other cases, interactions with monomeric detergent led to sample aggregation or did not provide an accurate reflection of the membrane-MinE interaction. These results strongly suggest that high-resolution structural studies of the membrane-bound state remain a significant challenge.

Chapter 5: Discussion

5.1: Location of MinD-Binding Residues on MinE

Results obtained from this thesis using anti-MinCD peptides for the stimulation of MinD-catalyzed ATP hydrolysis provide strong evidence that residues buried inside the dimeric interface of MinE directly participate in MinD interactions. For example, R21, L22 and I25 are required for maximal activation of MinD, even in the context of the largely unstructured peptide MinE(1-22), yet are either partially or completely buried in the full-length dimer structure. This raises an interesting question regarding how MinD might gain access to these residues.

One of the most straightforward scenarios in which MinD-binding residues in MinE could become more accessible for this interaction is through dissociation of the MinE dimer. However, several lines of evidence argue against this possibility. Firstly, analytical ultracentrifugation experiments showed only one peak for the dimeric form at the lowest possible concentrations that could be used for this experiment (~3 μM), indicating that the affinity of the self-interaction is very high (54). Backbone amide solvent exchange experiments also showed that the regions of the protein that are most highly protected from this exchange reaction localize to the central part of the dimer interface (54). Since hydrogen bonding interactions inhibit this exchange, this indicates that the most stable hydrogen bonds are actually those that form between subunits across the dimer interface. In addition, MinE cross-linking experiments currently being performed in the Goto lab indicate that a MinE protein that is locked in the dimeric state by an intermolecular disulfide bond still retains full activity (110). Taken together, these data all strongly suggest that it is the dimeric state of MinE that interacts with MinD, and therefore

another mechanism must be responsible for providing access to these residues for binding by MinD.

New insight into the structural features of this interaction has more recently been provided by a crystal structure of MinD bound to MinE (114) that was released after the completion of my experiments delineating the MinD-binding domain of MinE (54). The MinD used to produce this complex was the same as that used to determine the structure of the dimer (45), with the inactivating D40A mutation along with a C-terminal truncation. In addition, the MinE also contained a mutation of an anti-MinCD residue that had been found to be buried in the hydrophobic core of the dimer interface in the previously determined MinE structures (54,59), namely I24N. This mutation was designed to cause a disruption in the interactions of the β1 strands at the dimeric interface. In addition, this MinE construct was also truncated at the N-terminus by 11 residues (MinE*) (114), an unexpected modification due to proteolysis during purification. This turned out to be a fortuitous truncation, since the solubility of the complex was greatly improved compared to full-length MinE.

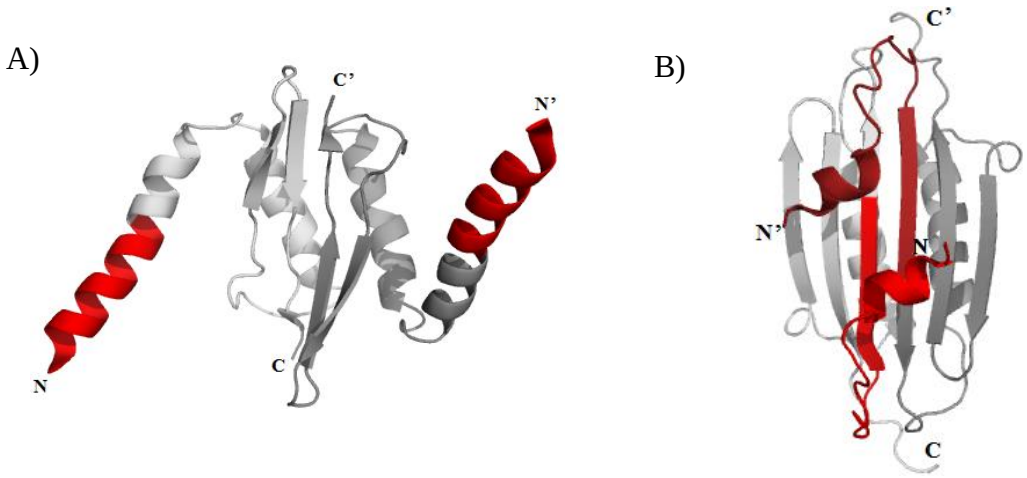

Figure 5.1: Structure of MinE as was Found in the Complex with MinD. A) Residues 13-25 from the anti-MinCD domain are highlighted in red in the open state. The structure is obtained from PDB ID: 3R9J B) Structure of the full-length Ng-MinE protein determined in the absence of MinD, with residues 1-25 highlighted in red (PDB ID: 2KXO).

As shown in Figure 5.1, the structure of MinE* I24N bound to MinD was significantly different from the structure of the full-length protein in the absence of MinD. In fact, the main body of the structure had a very similar fold to that of the trypsin resistant TSD domain (residues 30 – 88), with a four β-stranded dimer formed by inter-molecular hydrogen bonding involving residues that had been found in β3 in the full-length structure. Residues required for MinD binding that had been found at the dimer interface in the structure of full-length MinE were no longer part of this interface, instead projecting out from the main body of the structure to form an α-helix that interacts with MinD.

Although the resolution of the complex determined with I24N MinE* was low (4.3Å), atomic details of the MinE-MinD interface could be resolved in a crystal structure determined for a complex of MinD with a MinE peptide containing residues 12-31 (at 2.6Å) (114). This structure showed that MinE residue K19 forms hydrogen bonds with MinD residue D198 and that MinE R21 forms a network of hydrogen bonds involving the E53 side chain, along with backbone carbonyl groups from L48, S221, and N222. Likewise, A18, L22 and I25 all localize to one side of the MinE helix and engage in van der Waals interactions with MinD. These findings are in complete agreement with the results obtained from the in vitro ATPase assays presented in this thesis. In addition, residue T14 on MinE which had not been analyzed in our work was also found to participate in the interaction, forming hydrogen bonds with N222 on MinD.

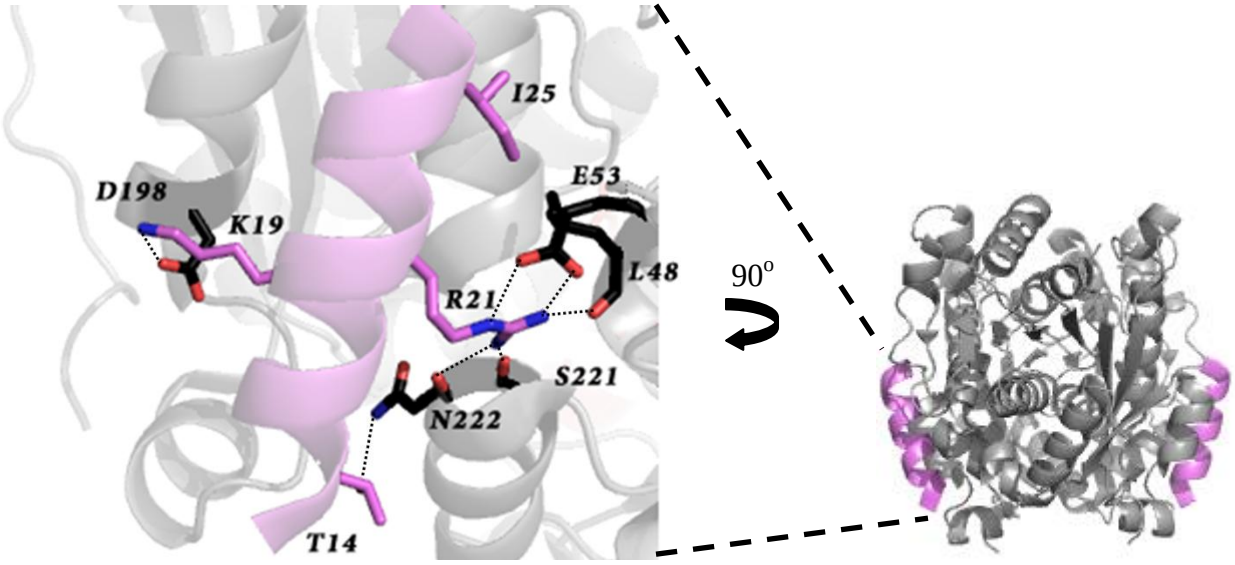

Figure 5.2: High Resolution Structure of MinE Interaction with MinD. The x-ray structure of MinE(12-31) (violet) bound to two sites on the MinD dimer (grey) (PDB ID: 3R9I). Hydrogen bonds formed between MinE and MinD are indicated.

The most unusual aspect of the MinE-MinD interaction is the large conformational change in MinE required for the interaction to occur. This transformation would require that many intra- and inter-molecular hydrogen bonds and Van der Waals interactions between the β-strands be disrupted in order to release β1 from the dimer interface and allow a new dimeric interface to be formed between the β3 strands. Approximately 20 hydrogen bonds in the dimer would have to be disrupted in the β-strands alone to convert MinE from the closed to the open form. In the case of MinE* I24N, the incorporation of β1 into the dimer interface would have been disfavored by the introduction of a polar side chain at a site that is normally buried in the hydrophobic core of the dimer, thereby favoring the four-stranded structure. Although this mutation was required to allow the structure of the MinE-MinD complex to be determined, it nonetheless retains the ability to bind MinD. Evidence for this was provided in a bacterial 2-hybrid experiment that showed I24N MinE could interact with MinD (114). In addition, this

mutant could also restore cell viability in *minB* knockout mutants that overexpressed MinC and MinD. These data suggest that the conformation of I24N MinE* that was observed in the crystal structure represents a functional state for MinE.

Although a large number of interactions must be disrupted in order for this significant conformational transition to occur in the WT MinE protein, it was proposed that the interaction with membrane-bound MinD, termed the ‘sensing step', would be sufficient to promote the structural change in MinE (114). However, this model does not seem consistent with data presented in the same paper showing that mutations in the N-terminal amphipathic helix designed to disrupt membrane binding (e.g. L3E and F7E) were not able to inhibit MinCD activity. In contrast, experiments using the L3E/I24N and F7E/I24N double mutants showed that the mutation at Ile24 rescued MinE anti-MinCD activity. This suggests that the ‘sensing step’ that triggers the conformational change in MinE requires more than just an interaction with membrane-bound MinD, but may involve interactions between MinE and the membrane itself. The CD data presented in my thesis supports this idea, since direct interactions with the membrane trigger a conformational change in MinE, with both the shape and intensity of the MinE spectrum being altered by the addition of liposomes to the sample. Moreover, previously published NMR relaxation data suggests that the N-terminal amphipathic helix dissociates from the main body of the MinE structure (54), a motion that would facilitate interactions between the N-terminal amphipathic helix and the membrane. Interactions with the lipid membrane could shift this conformational equilibrium to favor a larger population for the dissociated state.

It is surprising to find that membrane binding can be so crucial for MinE function when MinE has only recently been suggested to act as a membrane-binding protein itself. In fact, fluorescence microscopy has shown that it has cytoplasmic distribution when expressed in *E. coli*

in the absence of MinD (51). The idea that the N-terminal amphipathic helix of MinE has flexibility to coexist in two different conformations, one interacting with the main structure and the other interacting with the membrane, along with the small change in CD spectra in the presence of *E.coli* lipids suggest that the MinE-membrane interaction may be relatively weak in vivo. However, since MinE mutants that cannot bind the membrane do not have anti-MinCD activity (114), both MinE-lipid and MinE-MinD interactions may be important for causing MinE to convert from the closed to the open state. In this scenario, interactions with solvent-exposed residues in MinE (e.g. T14, A18, K19) by MinD may shift the equilibrium between membrane-bound and free MinE, allowing the the N-terminal amphipathic helix and β1-strand to dissociate from the main body of the MinE dimer. This type of conformational change triggered through simultaneous interactions with protein and lipid appears to be unique to the Min protein system.

5.2: MinE Residues Important for Membrane Binding

In the paper describing the structure of the MinE-MinD complex, there was strong evidence provided suggesting that the N-terminal amphipathic helix is responsible for the membrane-binding properties of MinE mutants. Some mutants of MinE that disrupt the interaction between the amphipathic helix and the main part of MinE (I25R), or the six-stranded structure obtained in the absence of MinD (I24N), appear to localize to the membrane. However, polar mutations made on the hydrophobic side of the amphipathic helix were enough to prevent these interactions from occurring, indicating that this N-terminal helix was functioning as a membrane-targeting sequence (MTS). Subsequent results published after I completed my CD studies showed that MinE(1-12) adopts some helical structure that is stabilized in the presence of

liposomes (115), providing additional evidence that the N-terminal helix binds the membrane. The same research group also performed tryptophan fluorescence assays on MinE(1-31) with one residue in the N-terminal helix being mutated to Trp at a time. The results indicated that residues from the hydrophobic face of the N-terminal amphipathic helix, namely A2, L3, and F6, were the most important for membrane interaction, as they showed the largest blue shifts in Trp fluorescence (115). These results all suggest that the N-terminal amphipathic helix is a membrane targeting sequence which can bind to the membrane. Nonetheless, it is important to note that results obtained for isolated fragments of MinE may not necessarily be the same as might be obtained in the context of the full-length protein, highlighting the importance of performing further studies with full-length MinE.

In addition to the N-terminal amphipathic helix, residues just C-terminal to this structural element have previously been implicated in MinE-membrane interaction, as was described in Chapter 1. Specifically, a triple mutant involving residues R10/K11/K12 had previously been shown to disrupt MinE interactions with *E.coli* lipid membranes (61). However, it is important to keep in mind that mutating three residues at once may have multiple effects on the function and structure of any protein. This was one of the reasons we focused on a single point mutant for my thesis, acquiring CD and functional data on a mutant of the most highly conserved basic residue in this cluster, namely R10A. As described in Chapter 4, this mutant showed smaller conformational changes in *E.coli* lipids than wild-type MinE, yet a greater change in the spectrum with DOPG liposomes. Moreover, differential effects were observed in the assay of MinD activation, with R10A showing wild-type like activity with *E. coli* lipid liposomes, but a reduced capability to activate MinD with DOPG, requiring approximately 2 fold larger amounts to reach half-maximal levels of activity compared to that of wild type. This indicates that

residues C-terminal to the proposed N-terminal membrane targeting sequence may also play a role in the membrane-binding interaction, and that these effects may depend on the physical properties of the membrane involved in the interaction.

A potential explanation for the differences that were observed with the R10A mutant in the two different lipid systems tested may be the differences in binding affinities for the different lipid types. Specifically, the larger signal in the CD spectrum for R10A in the presence of DOPG vesicles may reflect a larger population being bound to the liposomes. However, even if this mutation does cause more lipid-bound MinE to be available for MinD activation on DOPG vesicles, the requirement for higher concentrations of this mutant to activate MinD suggest that this interaction with the membrane is inhibitory in the case of DOPG. Another possibility is that the larger conformational change observed for R10A with DOPG reflects a different conformation for this mutant that is less favorable for MinD interactions compared to the wild-type protein. In fact, when the model of the N-terminal amphipathic helix is extended to include additional residues on the C-terminal side, Arg10 falls on the hydrophobic side. Thus, its mutation to an alanine could cause deeper insertion of the amphipathic helix into the fatty-acyl portion of the lipid membrane. In order to distinguish between these possibilities it should be possible to perform future experiments that measure the affinity of MinE for vesicle binding, potentially through isothermal titration calorimetry (116). The effect of the R10A mutation on lipid binding may also be probed using tryptophan fluorescence assays (115) with the tryptophan probe being introduced by mutation of a residue in the N-terminal helix. Differences in the magnitude of the blue shift obtained for WT versus R10A MinE could help determine if the amphipathic helix inserts to a different extent for the R10A mutant. Results from these

experiments should help determine the interplay between membrane binding, the MinE ‘sensing step’ and MinD activation.

5.3: Importance of the Dimeric State for MinE

Although the crystal structure of the complex between MinE and MinD suggests that only one anti-MinCD domain from a MinE dimer can bind to a MinD dimer at a time, a dimeric state nonetheless persists for MinE, both in the MinD-bound and free state. This raises questions regarding the purpose of maintaining a dimeric state for MinE. For the free form of MinE, it is likely that the dimer is required to hide the anti-MinCD domain from MinD to prevent promiscuous interactions with cytoplasmic MinD dimers or with the membrane, allowing free diffusion through the cytoplasm in regions of low MinD density.

Important insight into another potential role for the dimeric state of cytoplasmic MinE has also been provided by experiments with MinE(21-88), a fragment that is missing MinD- and membrane-binding residues from its N-terminus. These experiments showed that this truncated mutant was able to form heterodimers with the full-length protein in vivo, but that these heterodimers had no anti-MinCD activity (54,56). Moreover, when the mutation I25R was introduced into this truncation of MinE, the same inhibition of anti-MinCD activity of the wild-type protein was observed. Yet I25 normally interacts with the MTS, essentially anchoring it to the main body of MinE, so mutation of this residue should enhance the ability of the MTS to bind the membrane. When considered with the results from this thesis, as well as from other studies showing the importance of MinE-membrane interactions (61,114,115) it is possible that a dimer containing only one N-terminal helix for interaction with the membrane is not sufficient to allow the six-stranded dimer to convert to the four-stranded form. This would suggest that the

dimer provides two amphipathic helices to interact with the membrane with both being required to provide the energy necessary for the conformational transition in MinE.

Based on the observation that one MinE dimer can only bind at one of the two MinE-binding sites present in the MinD dimer, the Lutkenhaus group proposed a model for MinE activity, memorably named the 'Tarzan of the jungle' model (114), that suggested a functional role for the dimeric state of MinD-bound MinE. According to this idea, just as Tarzan moves from one vine to the next using one arm at a time, so was MinE proposed to move from one MinD to the next, using one 'arm' (*i.e.* anti-MinCD domain) at a time; the dimeric state essentially ensures that Tarzan (aka MinE) has two 'arms'. Although the crystal structure showed a single MinE dimer bridging two MinD dimers arranged at a 90^{o} orientation relative to each other, the Tarzan model proposes that the orientation of the anti-MinCD domain helices are not fixed in this position, as they are connected to the main body of the MinE dimer by a loop that could be flexible. This would allow both N-terminal helices to bind to the membrane simultaneously while maintaining a dimeric four-stranded TSD structure. During stimulation of ATP hydrolysis and dissociation of MinD from the membrane, membrane-bound MinE would have its free anti-MinCD domain available to bind to another MinD dimer. If it does not encounter another MinD dimer in close proximity, then it could dissociate from the membrane and convert back to the six-stranded cytoplasmic form. Thus, MinE would remain associated with the membrane in a region with a high density of MinD, whereas in a region of low membrane-bound MinD density, MinE would 'fall off the vine', in other words, dissociate from the membrane and revert back to the six-stranded conformation.

Although the Tarzan model is consistent with much of the available data, it is not yet known if the membrane-bound state of MinE can dissociate from the membrane. Our attempts to

find conditions that would allow the observation of NMR spectra for the membrane-bound state of MinE showed that the system was likely in slow exchange between bound and free states (i.e. the lifetime of membrane bound MinE was seconds or longer). In order for the six-stranded conformation to be recovered, the extensive hydrogen-bonding and van der Waals interactions holding the four-stranded dimer together would have to be disrupted to allow the six-stranded configuration to form. This likely poses a significant activation barrier to the process, which could require additional interactions to promote the transition. One possibility is that interactions with MinD could provide the energy required to stimulate this transition as it catalyzes ATP hydrolysis and dissociates from the membrane. Consequently, while the Tarzan model provides an interesting basis for future investigations of the Min cycle, the role of interactions between MinE and the membrane and/or MinD for triggering conformational transitions in MinE will require further study to establish its validity.

One way to gain insight into the conformational change that occurs with MinE in the presence of lipids could involve cysteine mutants of MinE designed to form intermolecular disulfide bonds between the β1 strands to lock the structure into the six-stranded conformation. Examination of the Ng MinE structure suggests that the MinE mutant I25C may form intermolecular cross-links when oxidized. CD spectroscopy of this mutant in the presence and absence of different types of lipids could be used to probe for lipid interactions. The amount of conformational change that occurs using this mutant can be compared with wild-type MinE in order to gain insight into whether the membrane-bound MinE structure is composed of the six-stranded or four stranded conformation, and help to unravel the role of the membrane in the conformational transition.

5.4: The E-Ring and Functions of the TSD

Another aspect of MinE function that may be affected by the two structural states is E-ring formation. It is not yet known if this subcellular structure involves additional interactions between dimers of MinE, dimers of MinE and MinD and/or the lipid bilayer. However, an interesting potential mechanism for E-ring formation was introduced by the crystal structure of Hp MinE (59). Within the crystal, MinE dimers were found to form contacts with other dimers such that the oligomer formed a polymeric spiral structure (Fig. 5.3). The dimeric state captured in these structures was the six-stranded state, however, higher order oligomers were also observed, with van der Waals and hydrogen bond interactions between adjacent β2 strands of two MinE dimers in an antiparallel configuration. The interactions at this interface were not as extensive as those in the dimeric interface, which is consistent with the requirement for MinE to reversibly assemble and disassemble the polymeric structure (59). However, the interactions at β2 should also be possible in the four-stranded structure, and may even bring the α2 helices in closer proximity for additional interactions.

An important caveat to the oligomeric structure observed for the Hp-MinE structure is that the higher-order interactions may actually arise from crystallization artifacts that do not necessarily reflect a physiologically relevant interaction. Nonetheless, this model for polymerization is consistent with some of the experimental data on E-ring formation. For example, overexpression of the isolated TSD gives rise to minicell formation in wild-type *E. coli* (51) suggesting that this part of the protein must be more than a simple carrier for the anti-MinCD domain. This is particularly interesting given that the TSD does not form heterodimers with full-length cytoplasmic MinE in vivo (114), suggesting that the disruptive effect more likely

occurs through interactions with the four-stranded MinE structure, potentially through interactions with β2. However, this oligomerization model does not explain why some TSD mutants, such as V49A in Ec-MinE, are no longer able to localize properly, disrupting symmetric cell division when expressed in wild-type *E. coli* (56,58). These mutations are not found in β2, but rather in α2 at the dimeric interface, and do not appear to disrupt the structural integrity of the dimer (58). Moreover, residues that comprise β2 are generally not well conserved across species. A mutation made to one of the most conserved residues in β2 of Ec-MinE (*i.e.* E66A) did not disrupt Min protein function in wild-type *E. coli* (58). These results all indicate that the mechanism of E-ring formation and the role of the TSD in forming this superstructure are still not understood, and therefore remains an interesting topic for future investigation.

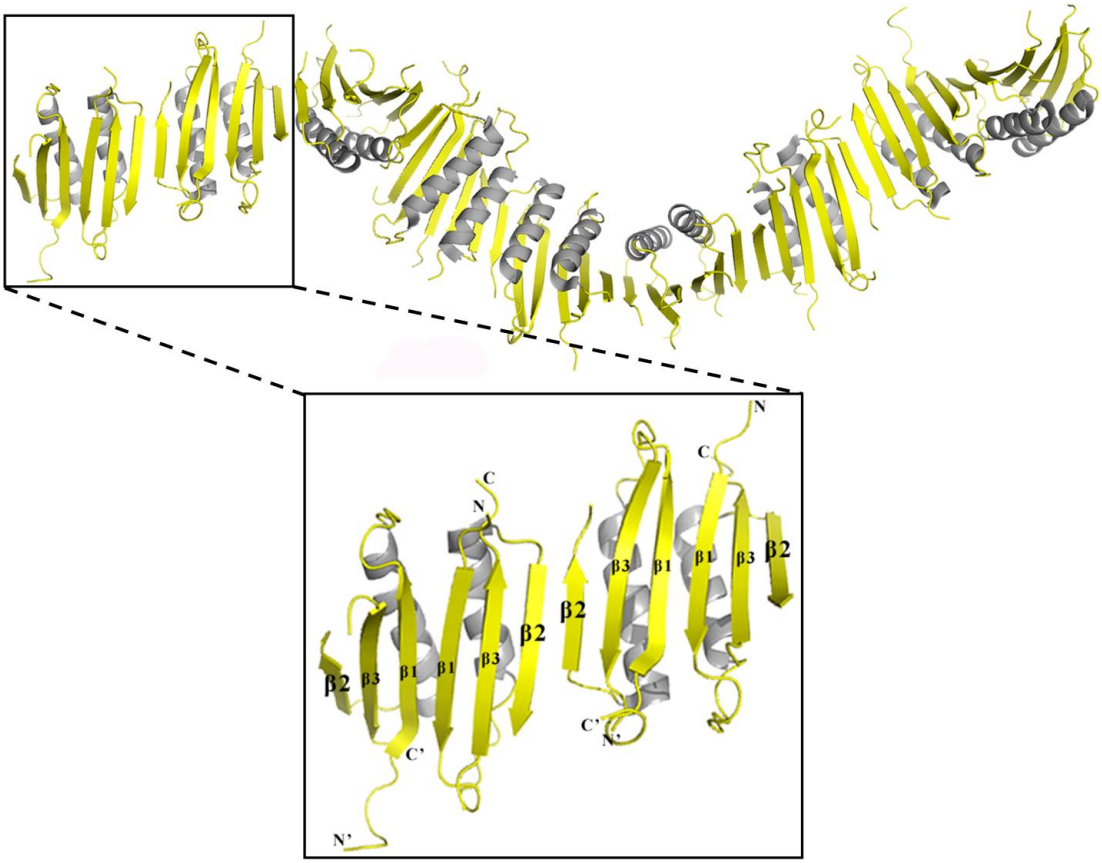

Figure 5.3: The Polymeric Structure of MinE from *Helicobacter Pylori*. The width and length of a single turn was approximately 5.5 and 12.5 nm (59).

5.5: The Effect of Lipid Microdomains on Min Oscillation

The potential for MinE to form a polymeric superstructure may also have an impact on the lipid membrane that could then further influence the Min cycle. In fact, it has been shown that MinD binding to the membrane affects its viscosity and order (117), and that the fluidity of the lipid membrane also alters the strength of the MinD-membrane interaction (118). While it is not known if a similar relationship occurs for MinE and the membrane other similarities have been shown with electron microscopy, with both MinE or MinD inducing lipid tubule structures when bound to liposomes in vitro (53,61). This similarity raises the possibility that interactions between MinE and the membrane could also cause a change in some aspect of the physical properties of the lipid bilayer which in turn could influence some part of the Min cycle.

It should also be noted that biological cell membranes are not made up of a homogenous composition of lipids, but rather tend to contain microdomains enriched in different lipid types (119). In particular, the *Escherichia coli* cell membrane contains three main types of lipids: PE (~55%), PG (~15%), and CL (~10%), all of which have a tendency to segregate into these microdomains (119). MinD has been shown to have higher affinity for negatively charged lipids (118), and similarly, our CD spectra suggest that MinE also prefers binding to anionic lipids. These lipid binding preferences raises questions regarding the potential effect of lipid microdomains on the dynamic organization of Min proteins in vivo.

Another physical property of the lipid bilayer that influences microdomain formation and may affect the localization of Min proteins is membrane curvature. For example, when membrane curvature is manipulated by confining *E. coli* spheroplasts in microchambers of defined dimensions, anionic lipid CL was found to localize to regions of negative membrane

curvature such as that which would be found at the cell poles (120). Since MinD has a preference to bind CL membranes, this may promote the localization of MinD at the cell pole, potentially leading to the nucleation of an initiation center for polymer formation. In addition these regions may have a greater tendency to retain Min proteins at the poles at the end of a depolymerization phase. Initiation of a new polymer at this site may be inhibited by these persistently-bound Min proteins, allowing cytoplasmic MinE and MinD to diffuse through the cytoplasm to form a new subcellular structure at the opposite pole. Thus, the CL-enriched domains at the cell poles could serve two functions: 1) to facilitate formation of the initiation centre at the cell pole, and; 2) to retain some Min proteins at the membrane at the end of a depolymerization phase to delay onset of another initiation centre. Consequently, it would be interesting to see if MinE also has a preference for CL-enriched domains, or if there is a different anionic lipid type that is favored by this protein.

Additional evidence for a role of membrane composition in Min protein localization was provided by experiments using GFP-MinD in wildtype *E.coli* cells containing a PE knockout. In these cells, MinD did not localize at the cell poles or show any oscillation (118). Instead it formed dynamic focal clusters throughout the cell which would appear and disappear at given intervals. Our CD spectra indicate that there is conformational change in MinE when it interacts with anionic but not zwitterionic liposomes. Thus, it is possible that a PE knockout also perturbs the localization of MinE although this possibility has yet to be investigated. Nonetheless, these studies clearly indicate the importance of lipid membrane composition and suggest that microdomains may play a role in the localization of Min proteins, potentially directing the formation of dynamic Min subcellular structures seen in vivo.

Given the ability of MinE to bind to the membrane, it will be interesting to determine how the different lipid compositions of membranes in different organisms might affect oscillation of Min proteins. For instance, the cell membrane in *N. gonorrhoeae* contains only trace amounts of CL but also contains shorter fatty acyl chains compared to the *E. coli* membrane, a trait that would be expected to increase its fluidity (121). In addition, different cell morphologies will have different amounts of membrane curvature, affecting lipid microdomain formation. In the future, it will be important to gain insight into these issues in order to propose a more detailed and realistic model of how the Min system operates in vivo.

5.6: Closing Statements

In summary, the data in this thesis supports the model forwarded by Lutkenhaus, et al. (114) as well as our own lab (122) suggesting that MinE undergoes a dramatic conformational change in order to bind MinD. This conversion will involve a significant energy barrier in order to break the numerous hydrogen bonds at the dimeric interface to allow the anti-MinCD domain to interact with MinD. Although MinD binding may provide some of the energy necessary for conversion of MinE from the closed to the open state, data presented in this thesis indicate that direct interactions with lipids should also aid in this conversion, with anionic lipids being particularly effective for this purpose.

Models of the Min system that have been published recently do explain some behaviours observed in MinE interaction with MinD and lipids, yet still fall short in explaining others as discussed above. There is still much to learn about the interactions involving MinE and MinD especially in terms of their interactions with the cell membrane. Yet, my screen of various

membrane-mimetic environments shows that it will be challenging to obtain the membrane-bound state for MinE under conditions compatible with solution NMR. Therefore, it may be necessary to instead look at the structure of N-terminal peptides from MinE since the TSD may be playing a role in aggregation. Future studies that can unravel the contributions of the interactions between MinE and the membrane or MinD will be instrumental for understanding the molecular details of the dynamic Min protein pattern formation that gives rise to an important control mechanism in bacterial cell division. Ultimately, our understanding of these events can provide a basis for future development of antimicrobial compounds that target this fascinating group of proteins.

References

1. Nasmyth K. (1996). Viewpoint: Putting the Cell Cycle in Order. *Science.* 274, 1643-1645.
2. Lutkenhaus J., Addinall S.G. (1997). Bacterial Cell Division and the Z Ring. *Annual Review of Biochemistry*. 66, 93-116.
3. Vicente M., Rico A.I., Martinez-Arteaga R., et al. (2006). Septum Enlightenment: Assembly of Bacterial Division Proteins. *Journal of Bacteriology*. 188, 19-27.
4. Bi E., and Lutkenhaus J. (1993). Cell Division Inhibitors SulA and MinCD Prevent Formation of the FtsZ Ring. *Journal of Bacteriology*. 175, 1118-1125.
5. Sun Q., Yu X.C., and Margolin W. (1998) Assembly of the FtsZ ring at the Central Division Site in the Absence of the Chromosome. *Molecular Microbiology*. 29, 491-503.
6. Barak Imrich, and Wilkinson A.J. (2007) Division Site Recognition in *Escherichia coli* and Bacillus Subtilis. *FEMS Microbiological Review*. 31, 311-326.
7. Fu Xiaoli, Shih Yu-Ling, and Rothfield L.I. (2001). The MinE Ring Required for Proper Placement of the Division Site is a Mobile Structure that Changes its Cellular Location During the *Escherichia Coli* Division Cycle. *Proceedings of the National Academy of Sciences*. 98(3), 980 – 985.
8. De Boer P.A., Crossley R.E., and Rothfield L.I. (1989). A Division Inhibitor and a Topological Specificity Factor Coded for by the Minicell Locus Determine Proper Placement of the Division Septum in *E. coli*. *Cell*. 56, 641-649.
9. Bernhardt T.G., and De Boer P.A.J. (2005). SlmA, a Nucleoid-Associated, FtsZ Binding Protein Required for Blocking Septal Ring Assembly over Chromosomes in *E.coli*. Molecular Cell. 18, 555-564.
10. Tonthat N.K., Arold S.T., Pickering B.F., et al. (2011). Molecular Mechanism by which the Nucleoid Occlusion Factor, SlmA, Keeps Cytokinesis in Check. The EMBO Journal. 30, 154-164.
11. Cho H., McManus H.R., Dove S.L., et al. (2011). Nucleoid Occlusion Factor SlmA is a DNA-Activated FtsZ Polymerization Antagonist. *Proceedings of the National Academy of Sciences*. 108, 3773-3778.
12. Wu L.J., and Errington J. (2011). Nucleoid Occlusion and Bacterial Cell Division. *Nature Reviews Microbiology*. 10, 8-12.
13. De Boer P.A., Crossley R.E., and Rothfield L.I. (1988). Isolation and Properties of minB, a Complex Genetic Locus Involved in Correct Placement of the Division Site in *Escherichia Coli*. *Journal of Bacteriology*. 170, 2106-2112.
14. De Boer P.A., Crossley R.E., and Rothfield L.I. (1992). Roles of MinC and MinD in the Site-Specific Septation Block Mediated by the MinCDE System of *Escherichia Coli*. *Journal of Bacteriology*. 174, 63-70.

15. Hu Z., and Lutkenhaus J. (1999). Topological Regulation of Cell Division in *Escherichia Coli* Involves Rapid Pole-to-Pole Oscillation of the Division Inhibitor MinC Under the Control of MinD and MinE. *Molecular Microbiology*. 34, 82-90.
16. Hale C.A., Meinhardt H., and De Boer P.A.J. (2001). Dynamic Localization Cycle of the Cell Division Regulator MinE in *Escherichia Coli*. *The EMBO Journal*. 20, 1563-1572.
17. Huang J., Cao C., and Lutkenhaus J. (1996). Interaction Between FtsZ and Inhibitors of Cell Division. *Journal of Bacteriology*. 178, 5080-5085.
18. Zhao C.R., De Boer P.A.J., and Rothfield L.I. (1995). Proper Placement of the *Escherichia Coli* Division Site Requires Two Functions that are Associated with Different Domains of the MinE Protein. *Proceedings of the National Academy of Sciences*. 92, 4313-4317.
19. Raskin D.M., and De Boer P.A.J. (1999). Rapid Pole-to-Pole Oscillation of a Protein Required for Directing Division to the Middle of the *Escherichia Coli*. *Proceedings of the National Academy of Sciences*. 96, 4971-4976.
20. Szeto T.H., Rowland S.L., Rothfield L.I., et al. (2002). Membrane Localization of MinD is Mediated by a C-terminal Motif that is Conserved Across Eubacteria, Archaea, and Chloroplasts. *Proceedings of the National Academy of Sciences*. 99, 15693-15698.
21. Lutkenhaus J., and Sundaramoorthy M. (2003). MinD and Role of the Deviant Walker A Motif, Dimerization and Membrane Binding in Oscillation. *Molecular Microbiology*. 48, 295-303.
22. Hu Z., Saez C., and Lutkenhaus J. (2003). Recruitment of MinC, an Inhibitor of Z-Ring Formation to the Membrane in *Escherichia Coli*: Role of MinD and MinE. *Journal of Bacteriology.* 185, 196-203.
23. Szeto J., Ramirez-Arcos S., Raymond C., et al. (2001). Gonococcal MinD Affects Cell Division in *Neisseria Gonorrhoeae* and *Escherichia Coli* and Exhibits a Novel Self-Interaction. *Journal of Bacteriology*. 183, 6253-6264.
24. Hu Zonglin and Lutkenhaus Joe, (2003). A Conserved Sequence at the C-terminus of MinD is Required for Binding to the Membrane and Targeting MinC to the Septum. *Molecular Microbiology*. 47, 345-355.
25. Szeto T.H., Rowland S.L., Rothfield L.I., et al. (2002). Membrane Localization of MinD is Mediated by a C-terminal Motif that is Conserved Across Eubacteria, Archaea, and Chloroplasts. *Proceedings of the National Academy of Sciences*. 99, 15693-15698.
26. Taghbalout A., Ma L., and Rothfield L. (2006). Role of MinD-Membrane Association in Min Protein Interactions. *Journal of Bacteriology*. 188, 2993-3001.
27. Hu Z. and Lutkenhaus J. (2000). Analysis of MinC Reveals Two Independent Domains Involved in Interaction with MinD and FtsZ. *Journal of Bacteriology*. 182, 3965-3971.
28. Szeto T.H., Rowland S.L., and King G.F. (2001). The Dimerization Function of MinC Resides in a Structurally Autonomous C-Terminal Domain. *Journal of Bacteriology*. 183, 6684-6687.

29. Lackner L.L., Raskin D.M., and De Boer P.A.J. (2003). ATP-Dependent Interactions Between *Escherichia coli* Min Proteins and the Phospholipid Membrane In Vitro. *Journal of Bacteriology*. 185, 735-749.
30. Ma L., King G.F., and Rothfield L. (2004) Positioning of the MinE Binding Site on the MinD Surface Suggests a Plausible Mechanism for Activation of the *Escherichia Coli* MinD ATPase During Division Site Selection. *Molecular Microbiology*. 54, 99-108.
31. Hu Z. and Lutkenhaus J. (2001). Topological Regulation of Cell Division in *E.coli*: Spatiotemporal Oscillation of MinD Requires Stimulation of its ATPase by MinE and Phospholipid. *Molecular Cell*. 7, 1337-1343.
32. Shih Y.L., Le T., and Rothfield L.I. (2003). Division Site Selection in *Escherichia Coli* Involves Dynamic Redistribution of Min Proteins Within Coiled Structures that Extend Between the Two Cell Poles. *Proceedings of the National Academy of Sciences*. 100, 7865-7870.
33. Cytrynbaum E.N., and Marshall B.D.L. (2007). A Multistranded Polymer Model Explains MinDE Dynamics in *E. coli* Cell Division. *Biophysical Journal*. 93, 1134-1150.
34. Lutkenhaus J. (2007). Assembly Dynamics of the Bacterial MinCDE System and Spatial Regulation of the Z Ring. *Annual Review of Biochemistry*. 76, 539-562.
35. William M. (2001). Bacterial Cell Division: A Moving MinE Sweeper Boggles the MinD. *Current Biology*. 11, 395-398.
36. Krstic V., Maglica Z., Paljetak H.C., et al. (2006). Min-Proteins Oscillations in *E. coli*: Three-Dimensional Off-Lattice Stochastic Reaction-Diffusion Model. *Journal of Statistical Physics.* 128, 5-20.
37. Kruse K., Howard M., and Margolin W. (2007). An Experimentalist's Guide to Computational Modelling of the Min System. *Molecular Microbiology*. 63, 1279-1284.
38. Meinhardt H., and de Boer P.A.J. (2001). Pattern Formation in *Escherichia coli*: A Model for the Pole-to-Pole Oscillations of Min Proteins and the Localization of the Division Site. *Proceedings of the National Academy of Sciences*. 98,14202-14207.
39. Huang K.C., Meir Y., and Wingreen N.S. (2003). Dynamic Structures: Spontaneous Formation of MinE Rings and MinD Polar Zones. *Proceedings of the National Academy of Sciences*. 100, 12724-12728.
40. Ivanov V., and Mizuuchi K. (2010). Multiple Modes of Interconverting Dynamic Pattern Formation by Bacterial Cell Division Proteins. *Proceedings of the National Academy of Sciences*. 107, 8071-8078.
41. Kleckner N. (2010). Mesoscale Spatial Patterning in the *Escherichia coli* Min System: Reaction-Diffusion Versus Mechanical Communication. *Proceedings of the National Academy of Sciences*. 107, 8053-8054.
42. Hayashi I., Oyama T., and Morikawa K. (2001). Structural and Functional Studies of MinD ATPase: Implications for the Molecular Recognition of the Bacterial Cell Division Apparatus. *The EMBO Journal*. 20, 1819-1828.

43. Cordell S.C., and Lowe J. (2001). Crystal Structure of the Bacterial Cell Division Regulator MinD. *FEBS Letters*. 492, 160-165.
44. Sakai N., Yao M., Itou H., et al. (2001). The Three-Dimensional Structure of Septum Site-Determining Protein MinD from Pyrococcus Horikoshi OT3 in Complex with Mg-ADP. *Cell*. 9, 817-826.
45. Wu W., Park K.T., Holyoak T., et al. (2011). Determination of the Structure of the MinD-ATP Complex Reveals the Orientation of MinD on the Membrane and the Relative Location of the Binding Sites for MinE and MinC. *Molecular Microbiology*. 79, 1515-1528.
46. Leonard T.A., Butler P.J., and Lowe J. (2005). Bacterial Chromosome Segregation: Structure and DNA Binding of the Soj Dimer – a Conserved Biological Switch. *The EMBO Journal*. 24, 270-282.
47. Zhou H., Schulze R., Cox S., et al. (2005). Analysis of MinD Mutations Reveals Residues Required for MinE Stimulation of the MinD ATPase and Residues Required for MinC Interaction. *Journal of Bacteriology*. 187, 629-638.
48. Schindelin H., Kisker C., Schlessman J.L., et al. (1997). Structure of ADP.AlF_4^- - Stabilized Nitrogenase Complex and its Implications for Signal Transduction. *Nature*. 38, 370-376.
49. Zhou H., Schulze R., Cox S., et al. (2005). Analysis of MinD Mutations Reveals Residues Required for MinE Stimulation of the MinD ATPase and Residues Required for MinC Interaction. *Journal of Bacteriology*. 187, 629-638.
50. Eng N.F., Szeto J., Acharya S., et al. (2006). The C-Terminus of MinE from Neisseria Gonorhoeae Acts as a Topological Specificity Factor by Modulating MinD Activity in Bacterial Cell Division. *Research in Microbiology* 157, 333-344.
51. Pichoff S., Vollrath B., Turiol C., et al. (1995). Deletion Analysis of Gene minE which Encodes the Topological Specificity Factor of Cell Division in *Escherichia Coli*. *Molecular Microbiology*. 18, 321-329.
52. Ma L.Y., King G.F., and Rothfield L. (2003). Mapping the MinE Site Involved in Interaction with the MinD Division Site Selection Protein of *Escherichia Coli*. *Journal of Bacteriology.* 185, 4948-4955.
53. Hu Z., Gogol E.P., Lutkenhaus J. (2002). Dynamic Assembly of MinD on Phospholipid Vesicles Regulated by ATP and MinE. *Proceedings of the National Academy of Sciences*. 99, 6761-6766.
54. Ghasriani H., Ducat T., Hart C.T., et al. (2010). Appropiation of the MinD Protein-Interaction Motif by the Dimeric Interface of the Bacterial Cell Division Regulator MinE. *Proceedings of the National Academy of Sciences*. 107, 18416-18421.
55. King G.F., Rowland S.L., Pan B., et al. (1999). The Dimerization and Topological Specificity Functions of MinE Reside in a Structurally Autonomous C-Terminal Domain. *Molecular Microbiology*. 31, 1161-1169.

56. Zhang Y., Rowland S., King G., et al. (1998). The Relationship Between Hetero-Oligomer Formation and Function of the Topological Specificity Domain of the *Escherichia coli* MinE Protein. *Molecular Microbiology*. 30, 265-273.
57. Shih Y.L., Fu X., King G.F., et al. (2002). Division Site Placement in *E. coli*: Mutations that Prevent Formation of the MinE Ring Lead to Loss of the Normal Midcell Arrest of Growth of Polar MinD Membrane Domains. *The EMBO Journal*. 21, 3347-3357.
58. King G.F., Shih Y.L., Maciejewski M.W., et al. (2000). Structural Basis for the Topological Specificity Function of MinE. *Nature Structural Biology*. 7, 1013-1017.
59. Kang G.B., Song H.E., Kim M.K., et al. (2010). Crystal Structure of Helicobacter Pylori MinE, a Cell Division Topological Specificity Factor. *Molecular Microbiology*. 76, 1222-1231.
60. Ramos D., Ducat T., Cheng J., et al. (2006). Conformation of the Cell Division Regulator MinE: Evidence for Interactions between the Topological Specificity and Anti-MinCD Domains. *Journal of Biochemistry*. 45, 4593-4601.
61. Hsieh C.W., Lin T.Y., Lai H.M., et al. (2009). Direct MinE-Membrane Interaction Contributes to the Proper Localization of MinDE in *E. coli*. *Molecular Microbiology*. 75, 499-512.
62. Tapsall J.W. (2005). Antibiotic Resistance in Neisseria Gonorhoeae. *Clinical Infectious Diseases*. 41, S263-S268.
63. Corbin B.D., Yu X.C., and Margolin W. (2002). Exploring Intracellular Space: Function of the Min System in Round-Shaped *Escherichia coli*. *The EMBO Journal*. 21, 1998-2008.
64. Ramirez-Arcos S., Szeto J., Dillon J.R., et al. (2002). Conservation of Dynamic Localization among MinD and MinE Orthologues: Oscillation of Neisseria Gonorrhoeae Proteins in *Escherichia Coli*. *Molecular Microbiology*. 46, 493-504.
65. Szeto J., Acharya S., Eng N.F., et al. (2004). The N Terminus of MinD Contains Determinants Which Affect its Dynamic Localization and Enzymatic Activity. *Journal of Bacteriology*. 186, 7175-7185.
66. Szeto J., Ramirez-Arcos S., Raymond C., et al. (2001). Gonococcal MinD Affects Cell Division in Neisseria Gonorrhoeae and *Escherichia Coli* and Exhibits a Novel Self-Interaction. *Journal of Bacteriology*. 183, 6253-6264.
67. Papadopoulus J.S., and Agarwala R. (2007). COBALT: Constraint-Based Alignment Tool for Multiple Protein Sequences. *Bioinformatics*. 23, 1073-1079.
68. Waterhouse A.M., Procter J.B., Martin D.M.A., et al. (2009). Jalview Version 2: A Multiple Sequence Editor and Analysis Workbench. *Bioinformatics*. 25, 1189-1191.
69. Weiss James N. (1997). The Hill Equation Revisited: Uses and Misuses. *The FASEB Journal*. 11, 835-841.
70. Voet D., and Voet J.G., (2004). *Biochemistry.* John Wiley and Sons Inc.

71. Yang J.T., and Doty P. (1956). The Optical Rotary Dispersion of Polypeptides and Proteins in Relation to Configuration. *Journal of the American Chemical Society*. 79, 761-775.
72. Kelly S.M., Jess T.J., and Price N.C. (2005). How to Study Proteins by Circular Dichroism. *Biochemica et Biophysica Acta*. 1751, 119-139.
73. Johnson W.C. (1988). Secondary Structure of Proteins Through Circular Dichroism Spectroscopy. *Annual Review of Biophysics and Biophysical Chemistry*. 17, 145-166.
74. Johnson W.C. (1990). Protein Secondary Structure and Circular Dichroism: A Practical Guide. *Proteins: Structure, Function and Bioinformatics*. 7, 205-214.
75. Greenfield N.J. (2006). Using Circular Dichroism Spectra to Estimate Protein Secondary Structure. *Nature Protocols*. 1, 2876-2890.
76. Whitmore L., and Wallace B.A. (2004). Dichroweb: An Online Server for Protein Secondary Structure Analyses from Circular Dichroism Spectroscopic Data. *Nucleic Acids Research.* 32, 668-673.
77. Lobley A., Whitmore L., and Wallace B.A. (2002). Dichroweb: An Interactive Website for the Analysis of Protein Secondary Structure from Circular Dichroism Spectra. *Nucleic Acids Research*. 18, 211-212.
78. Sreerama N., and Woody R.W. (2000). Estimation of Protein Secondary Structure from Circular Dichroism Spectra: Comparison of CONTIN, SELCON, and CDSSTR Methods with an Expanded Reference Set. *Analytical Biochemistry*. 287, 252-260.
79. Lees J.G., Miles A.J., Wien F., et al. (2006). A Reference Database for Circular Dichroism Spectroscopy Covering Fold and Secondary Structure Space. *Bioinformatics*. 22, 1955-1962.
80. Louis-Jeune C., Andrade-Navarro M.A., and Perez-Iratzeta C. (2012). Prediction of Protein Secondary Structure from Circular Dichroism using Theoretically Derived Spectra. *Proteins: Structure, Function and Bioinformatics.* 80, 374-381.
81. Correia J.J., and Detrich H.W. (2008). *In Vitro Techniques*. Academic Press.
82. Warren W.S. (2000). *The Physical Basis of Chemistry*. Academic Press.
83. Claridge T.D.W., (1999). *High Resolution NMR Techniques in Organic Chemistry*. Amsterdam: Pergamon.
84. Pavia D.L., Lampman G.M., and Kriz G.S. (2000). *Introduction to Spectroscopy*. Brooks Cole 3rd Edition.
85. Wider G., and Wuthrich K., (1999). NMR Spectroscopy of Large Molecules and Multimolecular Assemblies in Solution. *Current Opinion in Structural Biology*. 9, 594-601.
86. Clore G.M., and Gronenborn A.M., (1998). NMR Structure Determination of Proteins and Protein Complexes Larger than 20 kDa. *Current Opinion in Chemical Biology*. 2, 564-570.

87. Krueger-Koplin R.D., Sorgen P.L., Krueger-Koplin S.T., et al. (2004). An Evaluation of Detergents for NMR Structural Studies of Membrane Proteins. *Journal of Biomolecular NMR*.17, 43-57.
88. Kanelis V., Forman-Kay J.D., and Kay L.E. (2001). Multidimensional NMR Methods for Protein Structure Determination. *IUBMB Life*. 52, 291-302.
89. Qureshi T., and Goto N.K. (2012). Contemporary Methods in Structure Determination of Membrane Proteins by Solution NMR. *Topics in Current Chemistry*. 326,123-185.
90. Sanders C.R., and Sonnichsen F. (2006). Solution NMR of Membrane Proteins: Practice and Challenges. *Magnetic Resonance in Chemistry*. 44, S24-S40.
91. Avanti Polar Lipids Inc. (Accessed 2012). http://www.avantilipids.com.
92. Andersson A., and Maler L., (2005). Magnetic Resonance Investigations of Lipid Motion in Isotropic Bicelles. *Journal of the American Chemical Society*. 21, 7702-7709.
93. Whiles J.A., Deems R., Vold R.R., et al. (2002). Bicelles in Structure-Function Studies of Membrane Associated Proteins. *Bioorganic Chemistry*. 30, 431-442.
94. Diller A., Loudet C., Aussenac F., et al. (2009). Bicelles: A Natural 'Molecular Goniometer' for Structural, Dynamic, and Topological Studies of Molecules in Membranes. *Biochimie*. 91, 744-751.
95. Marcotte I, and Auger M. (2005). Bicelles as Model Membranes for Solid-and Solution-State NMR Studies of Membrane Peptides and Proteins. *Concepts in Magnetic Resonance.* 24, 17-37.
96. Seddon A.M., Curnow P., and Booth P.J. (2004). Membrane Proteins, Lipids and Detergents: Not Just a Soap Opera. *Biochimica et Biophysica Acta*. 1666, 105-117.
97. Le Maire M., Champiel P., and Moller J.V. (2000). Interaction of Membrane Proteins and Lipids with Solubilizing Detergents. *Biochemica et Biophysica Acta*. 1508, 86-111.
98. Sambrook J., Fritsch E.F., and Maniatis T. (1989). *Molecular Cloning: A Laboratory Manual.* Cold Spring Harbour Laboratory Press. Cold Spring Harbor, New York.
99. Laemmli U.K. (1970). Cleavage of Structural Proteins During the Assembly of the Head of Bacteriophage T4. *Nature*. 227, 680-685.
100. Smith P.K., Krohn R.I., Hermanson G.T., et al. (1985). Measurement of Protein Using Bicinchoninic Acid. *Analytical Biochemistry*. 150, 76-85.
101. Wiechelman K.J., Braun R.D., and Fitzpatrick J.D. (1988). Investigation of the Bicinchoninic Acid Protein Assay: Identification of the Groups Responsible for Color Formation. *Analytical Biochemistry*. 175, 231-237.
102. Geladopoulos T.P., Sotiroudis T.G., and Evangelopoulos A.E. (1991). A Malachite Green Colorimetric Assay for Protein Phosphatase Activity. *Analytical Biochemistry.* 192, 112-116.
103. Feng J., Chen Y., Pu J., et al. (2011). An Improved Malachite Green Assay of Phosphate: Mechanism and Application. *Analytical Biochemistry*. 409, 144-149.
104. Itaya K., and Ui M. (1965). A New Mircromethod for the Colorimetric Determination of Inorganic Phosphate. *Clinica Chemica Acta*. 14, 361-366.

105. Wu H., Su K., Guan X., et al. (2010). Assessing the Size, Stability, and Utility of Osotropically Tumbling Bicelle Systems for Structural Biology. *Biochemica et Biophysica Acta*. 1798, 482-488.
106. Kay L.E., Keifer P., and Saarinen T. (1992). Pure Absorption Gradient Enhanced Heteronuclear Single Quantum Correlation Spectroscopy with Improved Sensitivity. *Journal of the American Chemical Society*. 114, 10663-10665.
107. Delaglio F., Grzesiek S., Vuister G.W., et al. (1995). NMRPipe: A Multidimensional Spectral Processing System Based on UNIX Pipes. *Journal of Biomolecular NMR*. 6, 277-293.
108. Johnson B.A., and Blevins R.A. (1994). NMRView: A Computer Program for the Visualization and Analysis of NMR Data. *Journal of Biomolecular NMR*. 4, 603-614.
109. Hart C.T., (2009). *Functional and Structural Studies of the Anti-MinCD Domain of MinE*. University of Ottawa.
110. Laura Mcleod, personal communication. 2012.
111. Goto N.K., and Ducat T. (2010). ^{1}H,^{13}C, ^{15}N Chemical Shift Assignments for the Neisseria Gonorrhoeae MinE Regulator of Cell Division Septum Placement. *Biomolecular NMR Assignment*. 4, 227-229.
112. Parker W., and Song P. (1992). Protein Structures in SDS Micelle-Protein Complexes. *Biophysical Journal*. 61, 1435-1439.
113. Baxter N.J. and Williamson M.P. (1997). Temperature Dependence of 1H Chemical Shifts in Proteins. *Journal of Biomolecular NMR*. 9, 359-369.
114. Park K.T., Wu W., Lovell S., et al. (2011). The Min Oscillator Uses MinD-Dependent Conformational Changes in MinE to Spatially Regulate Cytokinesis. *Cell*. 146, 396-407.
115. Shih Y-L., Huang K-F., Lai H-M., et al. (2011). The N-Terminal Amphipathic Helix of the Topological Specificity Factor MinE is Associated with Shaping Membrane Curvature. *Plos One*. 6, 1-12.
116. Dimitrova M.N., Matsumura H., Terezova N., et al. (2002). Binding of Globular Proteins to Lipid Membranes Studied by Isothermal Titration Calorimetry and Fluorescence. *Colloids and Surfaces B: Biointerfaces*. 24, 53-61.
117. Mazor S., Regev T., Mileykovskaya E., et al. (2008). Mutual Effects of MinD-Membrane Interaction: I Changes in the Membrane Properties Induced by MinD Binding. *Biochemica et Biophysica Acta*. 1778, 2496-2504.
118. Mileykovskaya E., Fishov I., Fu X., et al. (2003). Effects of Phospholipid Composition on MinD-Membrane Interactions in Vitro and in Vivo. *Journal of Biological Chemistry*. 278, 22193-22198.
119. Brown D.A., and London E. (1998). Functions of Lipid Rafts in Biological Membranes. *Annual Review of Cell and Developmental Biology*. 14, 111-136.
120. Renner L.D., and Weibel D.B. (2011). Cardiolipin Microdomains Localize to Negatively Curved Regions of *Escherichia coli* Membranes. *Proceedings of the National Academy of Sciences*. 108, 6264-6269.

121. Rahman M.M., Kolli V.S.K., Kahler C.M., et al. (2000). The Membrane Phospholipids of Neisseria meningitides and *Neisseria gonorrhoeae* as Characterized by Fast Atom Bombardment Mass Spectrometry. *Microbiology*. 146, 1901-1911.
122. Ghasriani H. and Goto N.K., (2011). Regulation of Symmetric Bacterial Cell Division by MinE. *Communicative and Integrative Biology*. 4, 101-103.

Appendix

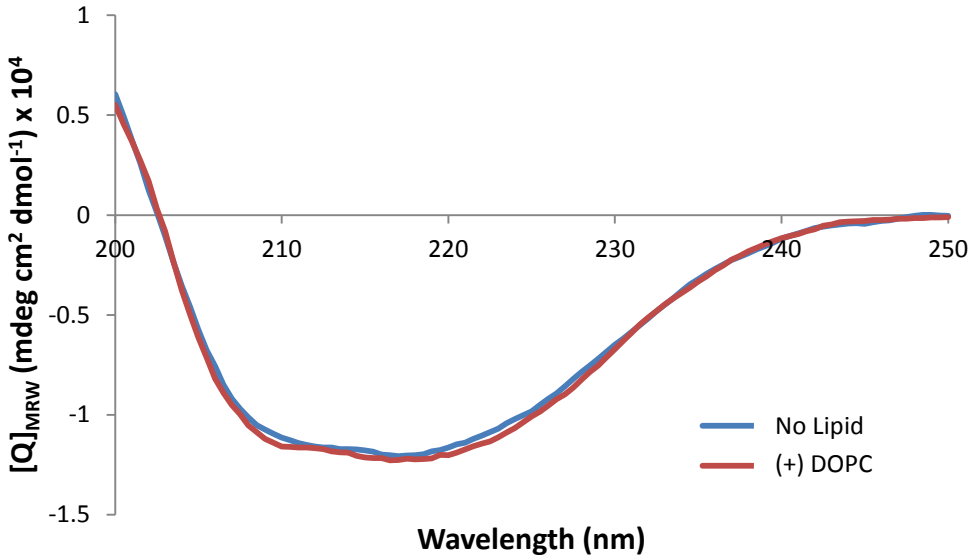

Figure A1: CD Spectra of MinE E46A in the Presence and Absence of DOPC. Solutions contained ~15 µM MinE in 10 mM Tris with/without 0.5 mg/mL DOPC at pH 8.0. The spectrum shows that there is no interaction between MinE E46A and DOPC.

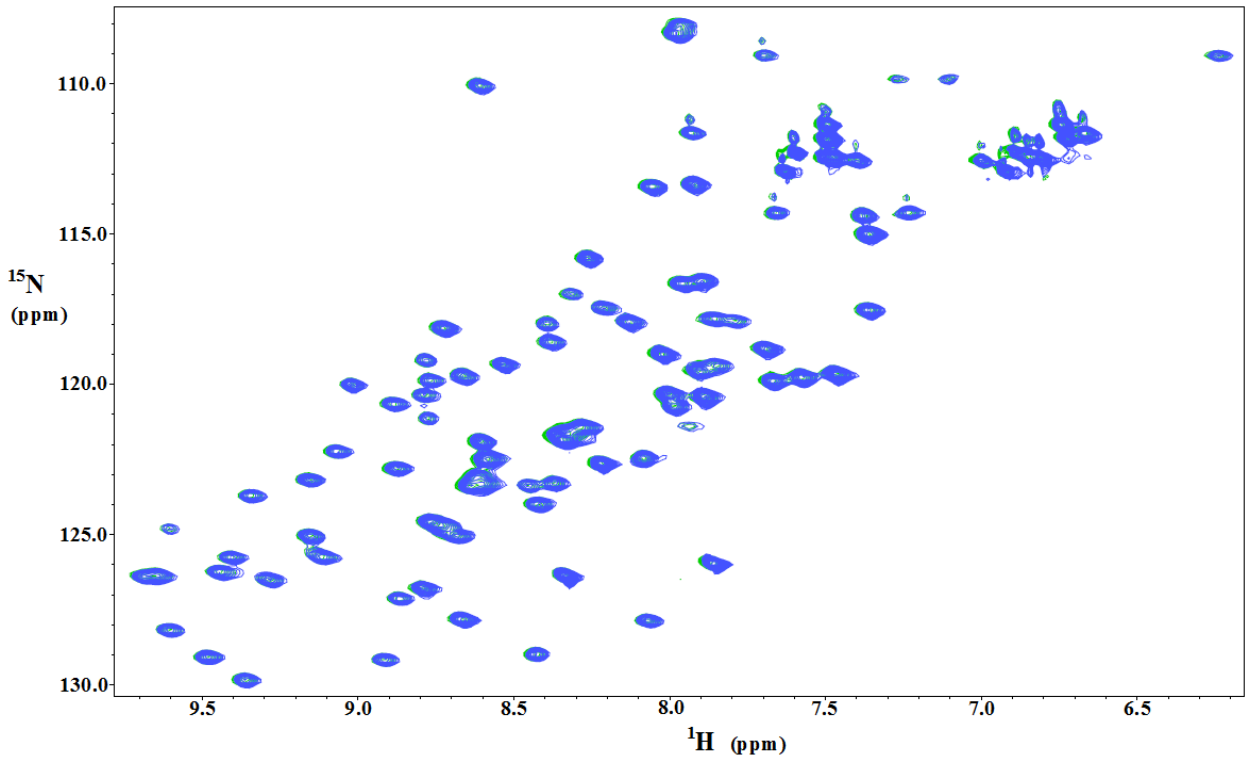

Figure A2: HSQC Spectrum of MinE E46A in the Presence of a Low Concentration of *E. coli* Lipids. 0.45 mM E46A at pH 7.5 with 0.06% (w/v) *E. coli* lipids is shown in blue, superimposed on the reference spectrum in green.

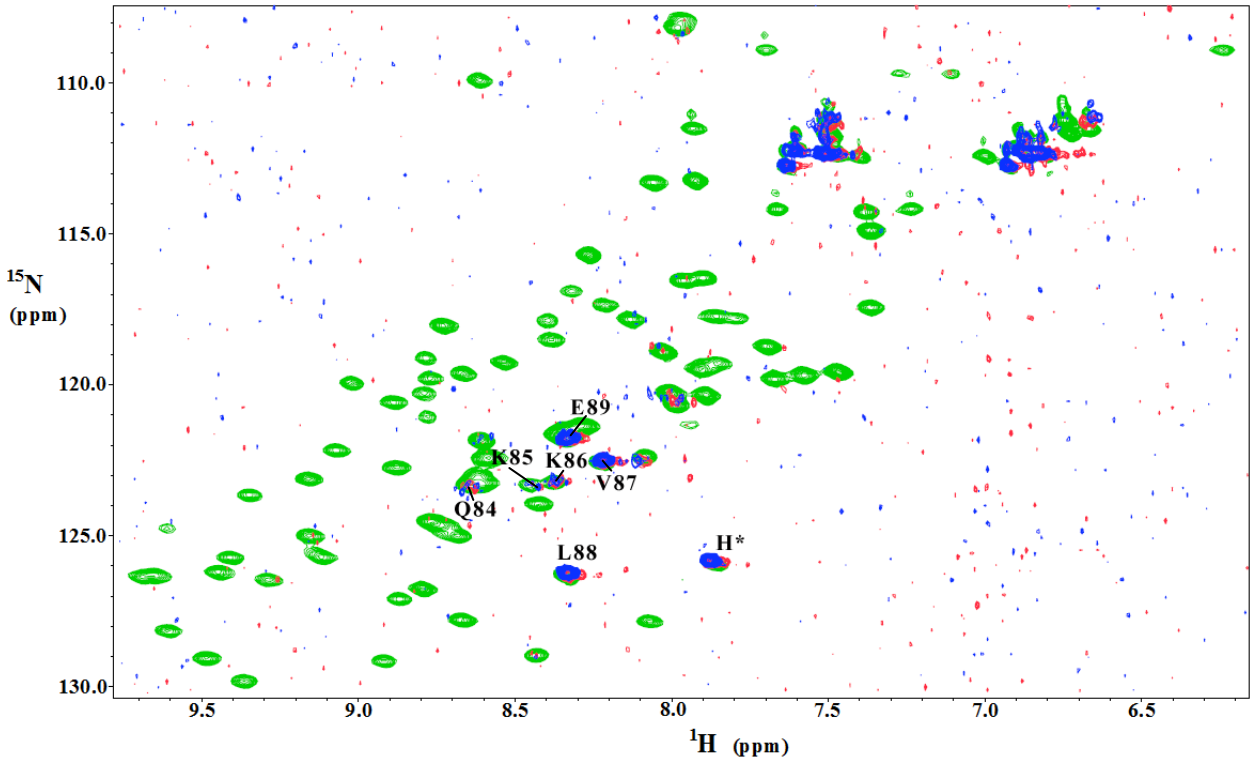

Figure A3: MinE E46A Interacts with Bicelles Containing DMPC and DHPC (C6 and C7). 0.30 mM MinE E46A at pH 7.5 in the presence of 80 mM DMPC/DHPC(C7) in blue, overlayed with a spectrum acquired for 100 mM DMPC/DHPC(C6) in red.

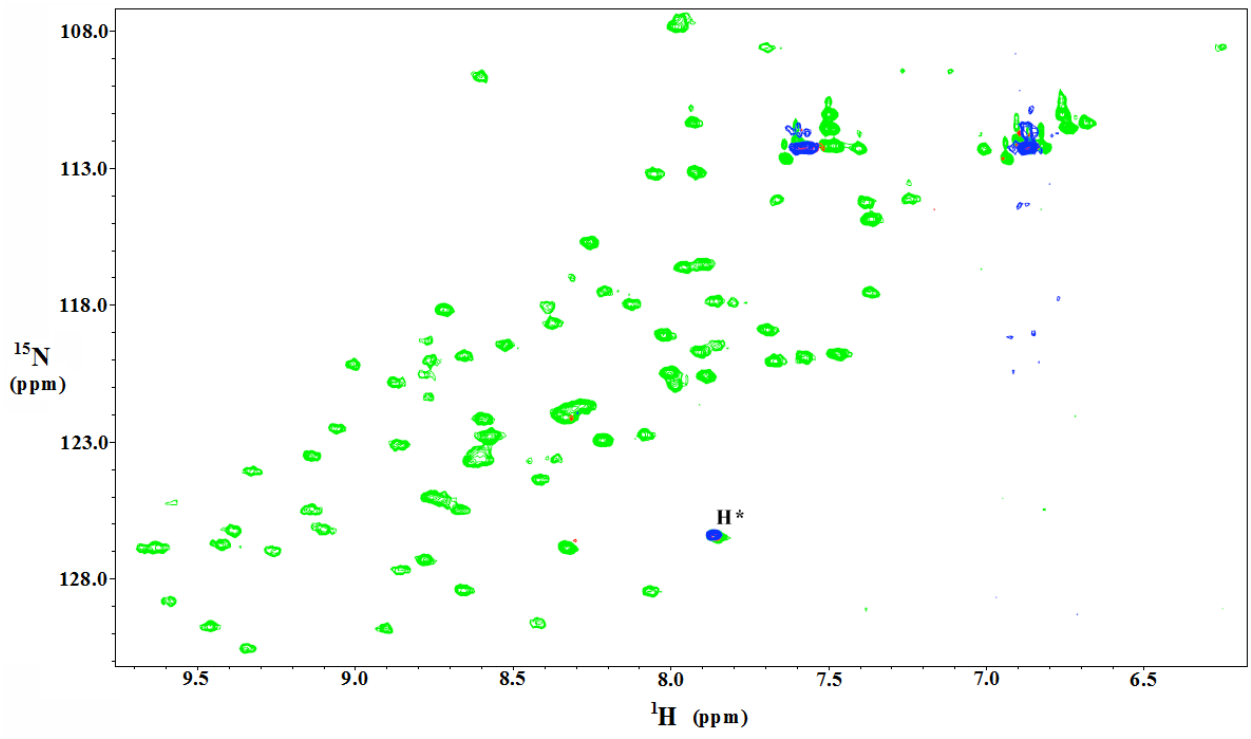

Figure A4: HSQC Spectra of MinE E46A with Fos-12 and Fos-16. 0.25 mM E46A at pH 7.5 with 10 mM Fos-12 (red) or 25 mM Fos-16 (blue) superimposed on the reference spectrum (green).